UAVs with a Passive Rotating Spherical Shell for Exploration of Infrastructure and Disaster Sites

TOHOKU UNIVERSITY

Graduate School of Information Sciences

UAVs with a Passive Rotating Spherical Shell for Exploration of Infrastructure and Disaster Sites

(インフラ点検や災害対応のための受動回転球殻を有する飛行ロボットの研究)

A dissertation submitted for the degree of Doctor of Philosophy

(Information Science)

Department of Applied Information Sciences

by

Carl John SALAAN

July 7, 2017

UAVs with a Passive Rotating Spherical Shell for Exploration of Infrastructure and Disaster Sites

Carl John SALAAN

Abstract

Unmanned aerial vehicle or UAV is an aircraft without a human pilot onboard. UAVs are developed primarily to take the place of manned aircraft in a mission where it is too dangerous for the human to engage. Likewise, a couple of advantages of using the UAVs attracted the researchers to focus on them that include higher mobility than ground robots and can fly above the ground. They are now one of the emerging technology with promising applications to improve the quality of life of the modern society. They have various usage for civilian purposes in the field of agriculture, industry, environment, infrastructure and disaster response. In the area of infrastructure inspection and disaster response, they are becoming very attractive because of their unique capabilities.

Many incidents of collapsed infrastructures that killed several people and created a negative impact on the economy are one of the motivation to develop a UAV system that can perform an efficient and immediate method of inspection to prevent any serious problem. For instance, the part of the ceiling of Sasago tunnel had collapsed which killed nine people, and two others were injured. It is found out that the main reason is due to the degradation of infrastructure. Periodic and immediate inspection of infrastructures like visual checking of cracks and non-destructive testing on the internal condition of structure could avoid any undesirable event. Likewise, looking for a solution on how to save human lives without risking the lives of human rescuers during destructive calamities such as earthquake and tsunami is another motivation. The main problem is that almost all disaster sites are inaccessible by human rescuer as they are dangerous and cluttered. But, the robots especially the flying robot or UAV can take over some of the roles of human rescuers on accessing the disaster sites and perform visual and physical interaction task.

The surrounding of most infrastructure and disaster sites, however, is cluttered and unknown that could make it difficult for the UAV to perform the mission or worst case, it might fail the mission. The cluttered environment is the primary challenge that most researchers are trying to solve and provide an efficient system under a severe condition. One of the main problems is that UAVs are vulnerable to falling plainly because of its exposed propellers. There are methods to avoid the obstacle such as obstacle avoidance and control strategy when losing propeller(s); however, they are not enough to handle the situation in the complex-structured sites. These areas have a lot of blind spots where it too difficult for the operator to control. Also, external disturbances are likely to exist that may exceed the UAV's control response. Two independent research group introduced a novel approach to solving the problem of accessing cluttered environment. They separately presented a concept of passive rotating spherical shell mechanism to be added in the UAV that will protect and keep the UAV significantly stable during a collision with obstacles.

The general objective of this study is to develop two type of system: a UAV with a passive rotating spherical shell for visual exploration and a UAV with two passive rotating hemispherical shells for physical interaction that can be used for infrastructure inspection and disaster response. The focused are design optimization of the system, introduction of a new concept, and utilization of the mentioned systems to a practical application.

The 2^{nd} Chapter of this dissertation presents the design optimization of the UAV with a passive rotating spherical shell for visual exploration and one of its practical application. This system has already been introduced by past researchers but focused mainly on the concept of the mechanism. In this study,

an appropriate and optimal design with the consideration of important parameters and conditions based on the certain complex environment is proposed to make it effective in an actual mission. The plan is to improve the performance of the existing UAV with a passive rotating spherical shell so it can be applied in a real mission.

For the optimization part, the specific aims are to maximize the flight capability of the UAV, minimize the weight of the system, and reduce the effect of air drag. The main components of the UAV such as motors, propellers, and battery were reselected to its optimal value to maximize the flight capability without compromising the size of the spherical shell. The spherical shell component specifically the joint was redesigned to reduce the effect of air drag by applying the concept of an efficient aerodynamic shape. During the design process, the strength and weight of the component were also considered not to get compromised. Moreover, the spherical shell structure was reselected to minimize the weight and further reduce the air drag without compromising the strength of the spherical shell.

The increase of the payload capacity and flight time compared to the previous system is the result of the positive outcome of the reselection of UAV's main components. The computational fluid dynamic (CFD) simulation and wind-tunnel experiment revealed a significant reduction of drag force compared to the previous system. Likewise, the actual flight experiment verified the positive performance of the new system in the presence of strong wind. Changing the structure of the spherical shell from 2V geodesic to fullerene type was able to reduce the weight significantly and brought a small contribution to lessening the drag. In general, the new system has improved its payload capacity, flight time, and ability to fly against the strong wind while maintaining the size of the spherical shell as part of the mission requirement before the actual visual inspection of the bridge as compared to the previous system.

For the application part, a close visual bridge inspection is proposed as the practical mission. The main purpose of the close visual inspection of the bridge is to check for any damages such as cracks and rust. The situation in the bridge is precisely a good test condition because of the existence of the complex structure and the frequent presence of strong wind. Prior to the actual mission, the bridge requirement and condition are determined. The required diameter of the spherical shell is determined based on the open gap of the bridge structure. The possible location of damages is being studied to provide an appropriate visual system. In the actual field, the first objective is to fly and traverse into the complicated and narrow part of the bridge to verify its performance. The second objective is to capture close images in the different part of the bridge at the different position. Finally, the people who are the expert on managing the bridge evaluated the performance of the system to further determine the effectiveness of the system in an actual mission on a harsh and complex environment.

Before the actual inspection of the bridge, the simulated bridge inspection verified the advantage of passive rotating spherical shell showing no significant disturbance on the UAV's flight attitude and demonstrating the performance of the visual system to capture images on the different section. In an actual visual inspection, the mission was successfully implemented. The visual system was able to obtain images from various areas in the real bridge experiment. The images include a part of the main girder, floor slabs, and bridge shoe, and bridge corner. The use of the UAV with passive rotating spherical shell along with a visual system has shown to be effective for close visual bridge inspection by satisfying the essential mission requirements. The majority of the evaluators (bridge management people) verified that the system only requires a few improvements before its final operation.

The 3^{rd} Chapter of this dissertation presents a new concept of UAV with two passive rotating hemispherical shells for physical interaction and one of its practical application. The idea was brought from the fact that the UAV with the passive rotating spherical shell cannot be completely utilized for physical interaction. The passive rotating spherical shell will eventually cause a self-collision. Any attempt to access the outside of the shell will disturb the rotation of the spherical shell and will compromise the stability of the UAV. One way to address the problem without discarding the idea of passive rotating spherical shell mechanism, considering its immense advantages for a complex environment application, is to cut the spherical shell into two hemispherical shells. As a result, it will provide a gap for the manipulator to access outside the shell without affecting the rotation of the two hemispherical shells. The protection offered by the spherical shell is maintained and retained two-degree of passive rotation enough to secure better stability for the UAV.

The first step to realizing the new concept was to determine the valuable part of the gap unaffected by the passive rotation of the two hemispherical shells. Finding out the usable gap is necessary to know what kind of physical interaction configuration as well as the possible movement of the manipulator. On the other hand, the different rotations of the two hemispherical shells depending on the point of contact of disturbance are analyzed. The cutting of the spherical shell, however, resulted to deformation and deflection. Thus, thorough structural analysis and appropriate mechanical design were implemented. The final step was to develop a prototype and perform a flight experiment to validate the capabilities of the new system such as able to fly over the obstacle and able to manipulate without disturbing the rotation of the two hemispherical shells.

Based on the analysis, the location of the valuable part of the gap is along the roll axis (front-back side) of the UAV. It was determined that the appropriate configuration of physical interaction is a frontal type, a perfect setting for the expected practical application. The deformation and deflection were resolved. In particular, the deflection was minimized by introducing the trusses. Several flights affirmed the capabilities of the new system.

A hammer test using the UAV with two passive rotating hemispherical shells is proposed as practical application. For infrastructure inspection, this system is important to determine damage structures that are not visible on the outer surface, for example, hollow space in the concrete wall due to deterioration. The system as well is intended for the target environment that is too cluttered for an ordinary UAV like a complex-structured bridge or partially damaged building. The challenge is to maintain a stable hovering position of the UAV and keep a close distance to the target structure while performing a hammer testing so it can provide useful data from the sensors, such as impact force and sound, needed for further evaluation. Extra subsystems are added to achieve the objective, such as the horizontal actuator and hammer guide. Then the overall system is developed and tested to verify its performance.

The integration of UAV with two passive rotating hemispherical shells and hammering system was successfully implemented. The idea of horizontal actuator and hammer guide found to be effective to obtain appropriate striking position based on the conducted flight experiment. The flight test verified that the UAV with two passive rotating hemispherical shells is a good platform for physical interaction. Though, several future works are required to make a robust system so it can be used in the actual mission.

The 4^{th} Chapter presents the conclusion of this dissertation. In this study, it showed that the design optimization of the system is an important strategy as a primary reason for the success of the actual mission. The visual inspection of the bridge using the UAV with passive rotating spherical shell affirmed that it could provide safe and efficient visual inspection approach to facilitate human inspector. Moreover, the concept of UAV with two passive rotating hemispherical shells showed to be useful for physical interaction task as demonstrated using the hammer testing application. This new concept as an initial approach for physical interaction in a complex environment can lead to several works in the future. In general, it was concluded that both UAV with a passive rotating spherical shell for visual inspection and UAV with two passive rotating hemispherical shells for physical interaction are significant for exploration of a complex environment such as infrastructure and disaster site.

Contents

Contents v

List of Figures vii

List of Tables xi

1 Introduction 1

1.1 Motivation . . . 2
1.2 General Objectives . . . 3
1.3 Fundamental Knowledge About the UAV . . . 5
1.4 Target Environment . . . 9
1.5 Background of PRSS Mechanism . . . 11
1.6 Summary of Main Contributions of this Dissertation . . . 17

2 UAV for Visual Exploration in a Complex Environment 19

2.1 Introduction . . . 19
2.2 Objectives of this Chapter . . . 25
2.3 Significance of the Study . . . 26
2.4 Related Literature . . . 26
2.5 Improving the Performance of Existing System . . . 28
2.5.1 Initial PRSS UAV and the Issues . . . 28
2.5.2 General Approach . . . 29
2.5.3 Minimizing the Weight . . . 31
2.5.4 Improving the Flight Capability of the UAV . . . 35
2.5.5 Minimizing the Drag Force . . . 38
2.5.6 The Newly Improved System . . . 48
2.6 Close Visual Bridge Inspection Using UAV with a Passive Rotating Spherical Shell . . . 50
2.6.1 Bridge Inspection and the Issues . . . 50
2.6.2 Bridge Condition and Requirements . . . 51
2.6.3 Test Flight Replicating Actual Bridge Conditions . . . 57
2.6.4 Actual Experiment: Accessing the Complex Part of the Bridge . . . 62

2.6.5 Acquiring Images on Critical Parts of the Bridge 65
2.6.6 Comparison with the Previous System 69
2.6.7 Evaluation of Highway Management Professionals 72
2.7 Chapter Conclusions 73

3 UAV for Physical Interaction in a Complex Environment 75
3.1 Introduction 75
3.2 Objectives of this Chapter 80
3.3 Significance of the Study 81
3.4 Related Literature 81
3.5 UAV with Two Passive Rotating Hemispherical Shells 83
3.5.1 General Concept 83
3.5.2 Rotation Analysis of the Hemispherical Shells 85
3.5.3 Analysis for Physical Interaction 85
3.5.4 Structural Analysis and Mechanical Design 87
3.5.5 Experimental Prototype and Test Flight 92
3.6 Hammer Test (HT) Using UAV with Two Passive Rotating Hemispherical Shells 97
3.6.1 Background of HT, Initial work and the Issues 97
3.6.2 General Concept 98
3.6.3 Hammer Test System: Design and Analysis 99
3.6.4 System Prototype and Flight Experiment 103
3.7 Chapter Conclusion 110

4 General Conclusions 113
4.1 Individual Contributions 114
4.1.1 Optimization of Existing UAV with a Passive Rotating Spherical Shell 114
4.1.2 Close Visual Bridge Inspection using the UAV with a Passive Rotating Spherical Shell 114
4.1.3 UAV with Two Passive Rotating Hemispherical Shells for Physical Interaction on Complex Environment 115
4.1.4 Hammering Test using the UAV with Two Passive Rotating Hemispherical Shells 116
4.2 Conclusive Remarks on UAV for Visual Exploration of Infrastructure and Disaster Site 116
4.3 Conclusive Remarks on UAV for Physical Interaction of Infrastructure and Disaster Site 117

Bibliography 121

List of Figures

1.1 New improved UAV with a passive rotating spherical shell fly under the bridge for visual inspection. 4
1.2 UAV with two passive rotating hemispherical shells with attached simple manipulation system for physical interaction. 5
1.3 UAV classification based on wing type [Source: Ghazbi, 2016]. 8
1.4 Quadrotor configuration: Left is the cross configuration and right is the plus configuration.[Source: Ghazbi, 2016]. 9
1.5 Complex structure of the bridge showing multiple braces and narrow available passages. 10
1.6 Bridge with high elevation. 10
1.7 Condition in partially damaged building. 11
1.8 Two main components of a passive rotating spherical shell mechanism. . . 12
1.9 The first spherical drone and its spherical structure. 13
1.10 Procedure in generating a geodesic structure from icosahedron. 13
1.11 Common geodesic division: 2V (left), 3V (center) and 4V (right). 14
1.12 Three-axis gimbal system configuration: typical (left) and configuration suited for quadrotor UAV (right), Source: Mizutani, 2015. 15
1.13 Key advantages of passive rotating spherical shell mechanism, Source: Mizutani, 2015. 16

2.1 Drag coefficient comparison between circular and square body shape of rod. Source: Sadraey, 2009. 23
2.2 Drag coefficients for various aerodynamic shape Source: Anderson, 2011. . 23
2.3 Initial system prototype [Mizutani, 2015]. 28
2.4 Principal forces acting on the UAV. 30
2.5 3D models of 2V geodesic domes. 32
2.6 Transformation of 3V geodesic to fullerene structure. 32
2.7 Drop test for the part of spherical shell. 33
2.8 Actual drop test set-up. 34
2.9 Proposed brushless motor for the new UAV. 35
2.10 Estimated battery's weight versus the flight time. 36

2.11 Clearance or gap between the UAV, gimbal and spherical shell. 37
2.12 New UAV redesigned to provide additional payload and flight endurance. . 38
2.13 Different views of the flat-plate (large-drag type) joint 38
2.14 Different views of streamline body or air-foil (low-drag type) joint 39
2.15 Cut plot showing the overall mesh and refined mesh in the boundary of the spherical shell components. 40
2.16 Computational geometry and boundary conditions 40
2.17 Drag force of two joints for different wind speed and sideslip angle (β). Note: A, P, F, B means airfoil, flat-plate, front side, back side, respectively. 41
2.18 Flow trajectory of airfoil joints showing a smaller wake region. 42
2.19 Flow trajectory of flat-plate joints showing large wake region. 42
2.20 Drag force of 3.5 mm cylindrical carbon rod of 100 mm length for different wind speed and β. 43
2.21 Isoline of cylindrical rod showing the wake at 9 m/s, t = 8 sec. 44
2.22 Drag force of the spherical shells for different wind speed 44
2.23 Isoline cut plot of 2V geodesic structure spherical shell showing large wake at flat-plate joint 45
2.24 Isoline cut plot of fullerene structure spherical shell showing smaller wake at airfoil joint 45
2.25 Drag force distribution of joints and connections at 9 m/s wind speed for spherical shell. 46
2.26 2m x 2m Low-speed Wind tunnel 46
2.27 Numerical results of drag force from wind tunnel experiment 47
2.28 Newly improved UAV with a passive rotating spherical shell. 49
2.29 Breakdown of various type of bridges in Japan's national road system. . . . 52
2.30 A cross-sectional view of concrete (left) and steel (right) type girder bridges. 52
2.31 Distribution of the main girder spacing for concrete girder bridges. 53
2.32 Distribution of the main girder spacing for steel girder bridges. 53
2.33 Breakdown of damage occurrence in a girder-type bridge. 54
2.34 Common damage location in a girder-type bridge. 55
2.35 Visual system set-up. 55
2.36 Air unit of the visual system. 56
2.37 Ground unit of the visual system. 56
2.38 Mock-up structure simulating the actual bridge structure. 57
2.39 An example of an actual test flight (right). 58
2.40 Flight attitude (pitch) on horizontal collision at different flight speeds. . . . 59
2.41 Flight attitude (roll) on horizontal collision at different flight speeds. . . . 59
2.42 Flight attitude when the UAV crosses a structure at 0.7 m/s. 60

2.43 Flight attitude during vertical collision shows no significant disturbance at 0.6 m/s 60
2.44 Captured images at 0 degree camera tilt using the image test material. . . 61
2.45 Captured images at 45 degree camera tilt using the image test material. . . 61
2.46 Captured images at 90 degree camera tilt using the image test material. . . 62
2.47 Steel girder bridge with a large number of steel bracing including k-type bracing in the crossbeam. 63
2.48 Crossing the steel k-type brace underneath the bridge. 63
2.49 Image of the PRSS UAV as it moves while in contact with the floor slab. . 64
2.50 Image of the PRSS UAV as it moves while in contact with the main girder web-plate. 64
2.51 Images from different camera angles. 66
2.52 Images on different parts of the main girder including the web-plate, and tensile bolts in and outside the bridge. 67
2.53 Images of the floor slab main and overhang where cracks normally develop. 67
2.54 Images of the bridge shoe and bridge corner. 68
2.55 Steel girder bridge with channel-type bracing. 68
2.56 Captured images of test material attached to the floor slab of the bridge (left) and image of the PRSS UAV moving close to the test material (right). 69
2.57 Actual flight of old system at Ushigeo Bridge in Sendai. 70
2.58 Wind speed during the actual flight experiment of the old system. 71
2.59 Wind speed during the actual flight experiment of the new system. 71

3.1 Basic structure of the Omni-ball [Source: Tadakuma, 2007]. 77
3.2 Illustation of three possible physical interaction configurations [Source: Peschel, 2012]. 78
3.3 General concept of UAV with two passive rotating hemispherical shells. . 83
3.4 Significant gap unaffected by rotation of hemispherical shells. 84
3.5 Postures of hemispherical shells (HS) with corresponding center of gravity's orientation. 84
3.6 Motion of two hemispherical shells during disturbances. 85
3.7 Positioning of manipulation system along roll axis. 86
3.8 Hemispherical shell structure. 87
3.9 Deflection of hemispherical shell (HS) due to weak support. 88
3.10 Proposed trusses and secondary bearing to minimize deflection of hemispherical shell (HS). 89
3.11 Calculation of the reaction force on the truss. 89
3.12 Estimated deflection of bearing due to internal clearance. 90
3.13 Simulation to determine the deflection caused by HS's own weight. 91

3.14 Internal mechanical structure of proposed system. 92
3.15 Experimental prototype. 93
3.16 Simple manipulation system model with sample object to grabbed. 94
3.17 Sequence of images for the system with manipulation system model as it crosses the obstacle. Labels A, B, and C are the system, obstacle, and object to be grabbed, respectively. 95
3.18 Flight attitude of the UAV during collisions with obstacle taken using motion capture system. 96
3.19 Sequence of images for simple grabbing task using the manipulation system model. 96
3.20 Initial study of hammering test of structure using multicopter, Source: Yano, 2014. 98
3.21 Proposed hammer test using UAV with two passive rotating hemispherical shells. 99
3.22 Block diagram of the proposed hammering system. 100
3.23 Hammering device provided by external company. 101
3.24 Concept of fixed space to provide appropriate striking. 102
3.25 Striking force versus distance. 102
3.26 Rollers to avoid excessive friction on the surface. 103
3.27 Checking the RPM of horizontal actuator through digital tachometer. . . 104
3.28 Aerodynamic simulation to verify the noninterference of horizontal actuator's airflow. 104
3.29 UAV with two passive rotating hemispherical shells attached with hammering system. 105
3.30 Flight experiment of UAV with two passive rotating hemispherical shells attached with hammering system. 106
3.31 A 75-second hammering action without horizontal actuator. 107
3.32 Closest distance from the wall for without horizontal actuator. 107
3.33 A 75-second hammering action with horizontal actuator activated. 108
3.34 Closest distance from the wall with the horizontal actuator activated. . . 109
3.35 Appropriate hammering posture as a result of adding horizontal actuator. 109

List of Tables

1.1 UAV classification based on MTOW 7

2.1 Specification of the initial PRSS UAV 28
2.2 Relationship between dome parameters and the radius of the circumscribed sphere. 31
2.3 Drop test result. 34
2.4 Estimated weight of two spherical shell for Rc = 0.5 m. 35
2.5 Estimated power consumption of all the components 36
2.6 Initial and the new UAV specification. 37
2.7 Flow simulation conditions 39
2.8 Comparison and specification of the new and old system. 49
2.9 NGRSI requirements for visual bridge inspection robot. 51
2.10 Comparison of flight time for old and new system on actual experiment . . 70
2.11 Third party evaluation result. 72

3.1 Deflections for different conditions 90

Chapter 1

Introduction

Unmanned aerial vehicles or UAVs are now one of the emerging technology with promising applications to improve the quality of life of the modern society. It has various uses for civilian purposes in the field of agriculture, industry, environment, infrastructure and disaster response. In past few decades, they are mostly applied for reconnaissance and mapping. Likewise, ongoing research about UAV with physical interaction also increased. A couple of advantages of using the UAVs attracted the researchers to focus on them that include higher mobility than ground robots and can fly above the ground. Likewise, the UAV esp. multirotor can hover in a specific place making easy for the UAV to acquire relevant information through the attached sensor (e.g. camera).

It is also becoming interesting to be used for infrastructure inspection and search and rescue operation because of the several advantages. In infrastructure inspection, the use of UAV can help speed up and reduce the cost of the operation. Most infrastructures are elevated that may require scaffolding for the human inspector to reach the target and perform the inspection. Using UAV, it may not need any scaffoldings. In disaster response, the UAVs can be very useful in the operation. They are helpful in situation where the operation may risk the life of the human rescuer. Likewise, the UAVs are probably more effective in the situation where the access point or path are too difficult for mobile ground robot. For the past few decades, many people in academia as well as in the industries are working on UAV for infrastructure inspection and search and rescue operation in disaster sites.

The surrounding of most infrastructure and disaster sites, however, is cluttered and unknown that could make it difficult for the UAV to perform the mission or worst case, it might fail the mission. This is the main challenge that most researchers are trying to solve and provide an efficient system under difficult condition. One of the primary problems is that UAVs are vulnerable to falling plainly because of its exposed propellers. So far, most UAVs available in the market are designed to fly in an open space distant

from any obstacle. There are methods to avoid the obstacle such as obstacle avoidance and control strategy when losing propeller(s); however, they are not enough to handle the situation in the complex infrastructure and disaster sites. These areas have a lot of blind spots where it too difficult for the operator to control. Also, external disturbances (e.g. wind gust) are likely to exist that may exceed the UAV's control response. In 2014, two independent research group introduced a significant approach to solving the problem of accessing cluttered environment. They separately presented a concept of passive rotating spherical shell mechanism to be added in the UAV that will protect and keep the UAV significantly stable during a collision with obstacles. The UAV and spherical shell are connected by way of three degree-of-freedom (3 DOF) gimbal system. In this way, the spherical shell can rotate freely in pitch, roll, and yaw axis during disturbances without significantly affecting the UAV's attitude.

1.1 Motivation

The motivation for this paper stems from the desire to develop mechanisms for the UAV that can be used for infrastructure inspection and disaster response. It started with the concern of many incidents of collapsed infrastructures that killed several people and created a negative impact on the economy. For instance, the part of the ceiling of Sasago tunnel had collapsed which killed nine people and two others were injured [1]. It is found out that the main reason is the structure started to degrade. Periodic checking of infrastructures could avoid such undesirable event.

Likewise, there is a fast growing number of aged bridges in the different part of Japan. Based on the report of MLIT, the number of old bridges will grow 67% by 2033 [2]. This will cause a huge problem if most of the vital infrastructure collapses. The need to perform an inspection of the infrastructures in all part of Japan is becoming the priority of Japanese government to perform the necessary action if required. However, they are facing another serious problem, the human workforce of Japan decreases as a result of shrinking population [3]. Moreover, the Japanese government is looking for a solution that could lead to a much safer, faster and low cost of operation. The best alternative is to use a robot to facilitate human operator. The flying robots are a great option because of its several advantages than another type of robots.

In the field of disaster response, it started with the need to find a solution on the many incidents of destructive calamities such as earthquake and tsunami on how to save human lives. The first 72 hours of response is critical to help save survivors who are still trapped in the disaster site. Similarly, an immediate response to halt any ongoing operation of power plants in the midst of disaster and obtain valuable samples for further analysis are

substantial. One main challenge though is that almost all disaster sites are inaccessible by human rescuer as they are dangerous and cluttered. However, the robots can take over some of the roles of human rescuers on accessing the disaster sites and perform the necessary task.

The future goal is to develop an unmanned aerial system that can perform a physical task (for example: manipulating the safety valve or grabbing sample) in a cluttered and dangerous environment such as in damaged nuclear power plant. This desire is also to answer the problem of mobile ground robot accessing disaster sites by replacing them with an unmanned aerial system to perform the task. For example, the robot Quince was used to perform both visual inspection (recording video) and physical interaction (taking sample) in the damaged Fukushima nuclear power plant after the Great Tohoku earthquake. The problem is that the Quince was not able to complete its task as it got stuck in the stairs because of the obstacle [4]. In the case of the UAV, it presumes to fly over the obstacle and continue its task. The use of UAV is very promising that today many people in academia as well as in the industry do the research to find a solution in the midst of increasing cases of natural and human-made calamities. It is the author's desire to develop a different type of mechanisms for the UAV so it can be used for the two important tasks; visual exploration, and physical interaction.

1.2 General Objectives

The primary objective is to develop a robust system for visual exploration by improving the existing UAV with a passive rotating spherical shell. This is because of the past researchers [5] [6] are, for the most part, focused only on the concept of the passive rotating spherical shell. There is no appropriate design yet that could allow such concept to be used in a real complex environment considering several conditions. As for now, Mizutani et. al initiated work on the general design strategy for UAV with a passive rotating spherical shell so it can be applied in a complex environment. This will be the basis for optimizing the existing system as it already identified some of the important design points based on the general problems in the actual field. Other relevant parameters are expected to be added to ensure that the system will work well in the actual field. The additional goal is to perform an actual visual inspection using the passive rotating spherical shell to verify the performance of the system once it is improved. Several experiments are expected to be conducted in the field to obtain adequate information. The improvement and the implementation of UAV with a passive rotating spherical shell in the actual field will be discussed in Chapter 2. As a brief look at Chapter 2, Fig. 1.1 shows the improved UAV with a passive rotating spherical shell fly under the bridge.

The second objective is to develop a new mechanism that would allow physical inter-

Figure 1.1: New improved UAV with a passive rotating spherical shell fly under the bridge for visual inspection.

action for the UAV while the features from the previous mechanism such as protection by the spherical shell and passive rotation are retained. The interest is to find a solution to solve the flaw of the passive rotating spherical shell mechanism regarding physical interaction. As a preliminary remark, the latter mechanism is effective only for remote sensing, especially for visual exploration. In the former system, the presence of spherical shell, as well as the gimbal system, have no negative impact in acquiring data such as images. For example, images captured by the on-board camera blocked by the spherical shell and gimbal can be processed to obtain the clear output. For physical interaction, however, it is not the same case. The passive rotation will limit any attempt to access outside of the spherical shell. Any attempt will likely cause self-collision and may result in the unstable flight of UAV, or the worst case is it will cause falling. Physical interaction is an important task for infrastructure inspection and disaster response. For example, it can be used to take or manipulate sample object in a destructed nuclear plant (which is likely cluttered environment) while keeping the operator away from danger. Also, it can check the condition of infrastructure by physical interaction such as non-destructive hammer test. The main challenge is to develop a system that can perform physical interaction while keeping the spherical shell as the protective mechanism and its passive rotation. The general idea is to cut the spherical shell into two separated hemispherical shells which provide a gap for interaction with the environment. The additional goal is to implement the new concept with a real physical interaction application. Chapter 3 discussed the novel UAV with two passive rotating hemispherical shells as shown in Fig.

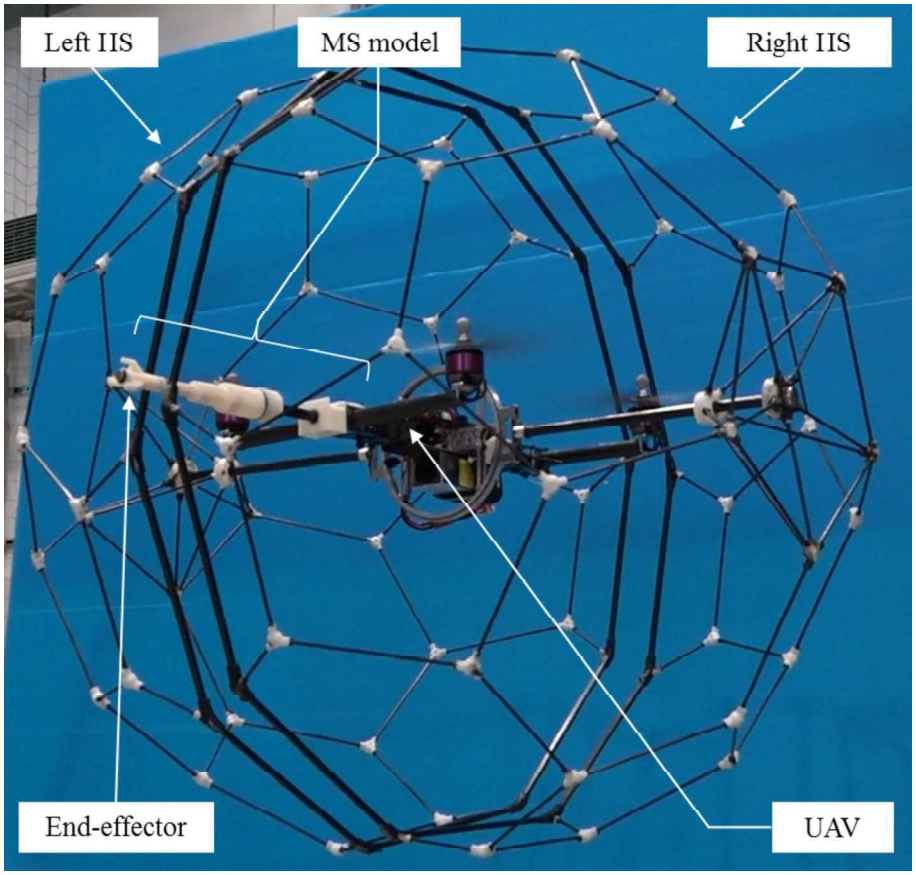

Figure 1.2: UAV with two passive rotating hemispherical shells with attached simple manipulation system for physical interaction.

1.2 and one of its application.

1.3 Fundamental Knowledge About the UAV

Unmanned aerial vehicle or UAV is defined as an aircraft without a human pilot onboard. UAV is a subcomponent of an unmanned aerial system or UAS. The UAV can be operated with various degrees of autonomy: either under remote control by a human operator or autonomously, by onboard computers [7]. UAVs are developed primarily to take the place of manned aircraft in a mission where it is too dangerous for human.

UAVs have been around much longer than most people realize. The first autonomous flying machine has been credited to Archytas the Tarantine as the first documented unmanned aerial vehicle in the history. It is alleged that Archytas' pigeon flew about 200 m before falling to the ground, once all energy was used. During the same era, the Chinese were also the first to document the idea of a vertical flight aircraft. The earliest version consisted of feathers at the end of the stick. The stick was spun between the hands to generate lift before it is released. Over the years, the Chinese experimented with other

types of flying machines. In fact, there are historical records of a wooden hawk that was used for reconnaissance around 450 BC, as well as a kite in the shape of a crow, which was used during the Ming Dynasty to bomb enemy positions. Several centuries later, Leonardo Da Vinci, in 1483, designed a aircraft capable of hovering, called aerial screw or air gyroscope [8]. During World War I, both the Navy and the Army experimented with unmanned aerial torpedoes and flying bombs. In 1911, just eight years after the advent of manned flight, Elmer Sperry, inventor of the gyroscope, became intrigued with the application of radio control to aircraft. Advancements in radio furthered development and fielding of radio-controlled aircraft. The successful demonstrations of aircraft against capital ships off the Virginia Capes in June 1921 stressed the need for the development of radio-controlled target drones for use in fleet training exercises. In the brinks of World War II, the United States continued their efforts to perfect radio control of aircraft, primarily as weapons delivery and guided missile platforms. In May 1942, CNO Admiral Ernest King directed that a program is initiated to expedite the development and use of target drones as guided missiles in combat [9]. Unmanned aircraft development in the follow-on Cold War years shifted dramatically toward reconnaissance and decoy missions [10]. The first reconnaissance drone introduced was the SD-1. It was remotely operated, carried a camera, performed a 30 min flight, and returned to base and recovered with a parachute. However, the Ryan Model 147, used in the 1960s and 1970s, can be considered as the first unmanned aircraft based on a modern definition of UAV [8]. Today, the UAV systems have evolved to various and different designs from traditional fixed-wings to rotor-type UAV, ducted fan, and flapping-wings.

Different classification schemes have been introduced to categorize existing systems as there is no general classification to fit all existing UAV. Mean takeoff weight (MTOW), size, and capabilities are some of the metrics used to classify the UAV. Based on Dalamagkidis [11], the mean takeoff weight is a good metric to classify aircraft for regulatory purposes since it correlates well with the expected kinetic energy imparted at impact. It is also considered as the primary factor affecting the safety of operations as mentioned by several groups [12] [13] [14]. Table 1.1 shows one of the UAV classification based on MTOW.
Likewise, Austin also listed a UAV category based on air vehicle type [15]. The following are listed below with definitions:

1. HALE High altitude long endurance. Over 15000 m altitude and 24+ hr endurance. They carry out extremely long-range (trans-global) reconnaissance and surveillance and increasingly are being armed. They are usually operated by Air Forces from fixed bases.

2. MALE Medium altitude long endurance. 5000 to 15000 m altitude and 24 hr

Table 1.1: UAV classification based on MTOW

Category No.	Name	MTOW
0	Micro	Less than 1 kg
1	Mini	Up to 1 kg
2	Small	Up to 13.5 kg
3	Light/ultralight	Up to 242 kg
4	Normal	Up to 4,332 kg
5	Large	Over 4,332 kg

endurance. Their roles are similar to the HALE systems but generally operate at somewhat shorter ranges, but still in excess of 500 km. and from fixed bases.

3. TUAV Medium Range or Tactical UAV with range of order between 100 and 300 km. These air vehicles are smaller and operated within simpler systems than are HALE or MALE and are operated also by land and naval forces.

4. Close-Range UAV used by mobile army battle groups, for other military/naval operations and for diverse civilian purposes. They usually operate at ranges of up to about 100 km and have probably the most prolific of uses in both fields, including roles as diverse as reconnaissance, target designation, NBC monitoring, airfield security, ship-to-shore surveillance, power-line inspection, crop-spraying and traffic monitoring, etc.

5. MUAV or Mini UAV relates to UAV of below a certain mass (yet to be defined) probably below 20 kg, but not as small as the MAV, capable of being hand-launched and operating at ranges of up to about 30 km. These are, again, used by mobile battle groups and particularly for diverse civilian purposes.

6. Micro UAV or MAV. The MAV was originally defined as a UAV having a wingspan no greater than 150 mm. This has now been somewhat relaxed but the MAV is principally required for operations in urban environments, particularly within buildings. It is required to fly slowly, and preferably to hover.

7. NAV Nano Air Vehicles. These are proposed to be of the size of sycamore seeds and used in swarms for purposes such as radar confusion or conceivably, if camera, propulsion and control sub-systems can be made small enough, for ultra-short range surveillance.

Another classification is based on the type of wing of the aircraft as shown in Fig. 1.3. They are mainly classified into three groups: the fixed wing, rotary wing, and the flapping wing. Fixed-wing UAVs are most used for long-distance, long-range and high-altitude missions. The wing is used to generate lift using vehicle's forward airspeed and

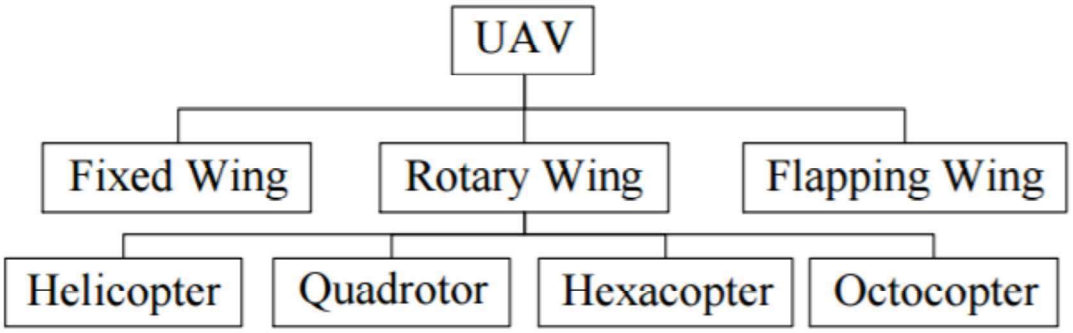

Figure 1.3: UAV classification based on wing type [Source: Ghazbi, 2016].

the shape of the wings. They are useful for scientific applications such as meteorological reconnaissance and environmental monitoring [16]. Meanwhile, the flapping-wing UAVs are designed based on the way birds or insect fly. The wings are required to flap similar to the biological counterpart. The recent interest in flapping-wing, especially for the micro aerial vehicle, has been motivated by the notion that flapping wings may offer some unique aerodynamic advantages over a fixed wing and rotary wing [17]. However, most of the studies of this type are still under development. On the other hand, the rotary wing UAVs are the most widely used type than fixed and flapping wings in the academia as well as in industry. They are also called Vertical Take-off and Landing (VTOL) rotorcraft. They are particularly useful in a mission which requires hovering flight. Today, rotary wing UAVs have been exploited for a variety of applications that include reconnaissance, industrial and agricultural inspection, and search-and-rescue operations. They differ from the fixed and flapping wing as their set of wings, or so-called propellers were from as rotor mounted on a spinning shaft to generate thrust. The most widely used type of rotor UAV is the quadrotor. This is because of various characteristics of quadrotor such as high maneuverability, small size, and easy control. Throughout this paper, the quadrotor UAV is used as the fundamental component of the UAV system.

As presented by Ghazbi et. al, the quadrotors are small, agile vehicles that can be controlled by the rotational speed of the four rotors. The position of rotors arrangements relative to the body coordinate system causes two different types of quadrotor configurations: the cross configuration and the plus configuration shown in Fig. 1.4. An x-configuration quadrotor is considered to be more stable in comparison to the + configuration, which is a more acrobatic structure. The four rotors are aligned such that the rotors on opposite ends rotate in the same direction and the other two in the opposite direction. The quadrotor has six degrees of freedom, three translational and three rotational movements. As the number of system inputs is lower than the number of outputs, quadrotors are classified under a under-actuated category. The flying mechanism of the

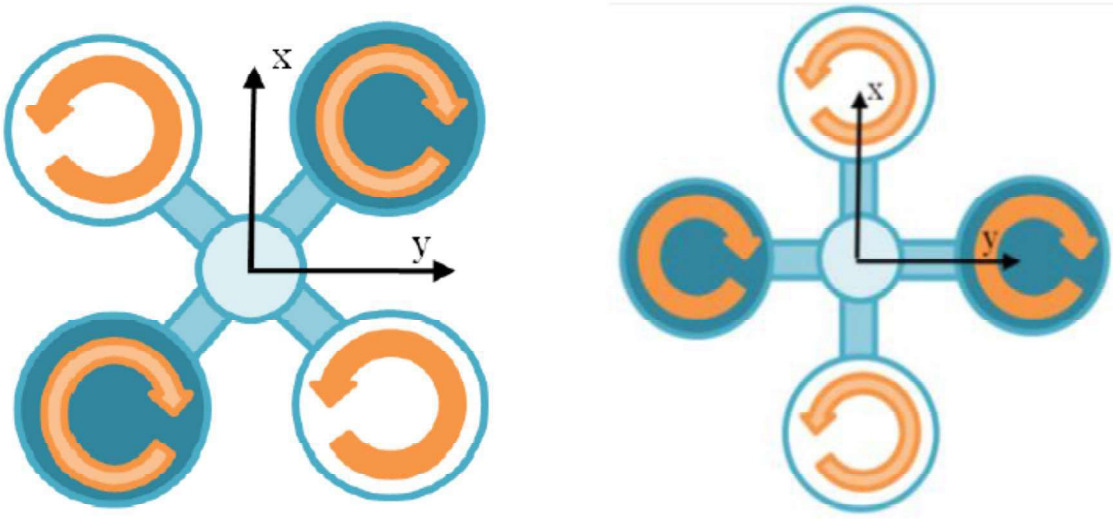

Figure 1.4: Quadrotor configuration: Left is the cross configuration and right is the plus configuration.[Source: Ghazbi, 2016].

vehicle is simple. The quadrotor rotates on three axes by simply adjusting the angular velocity of each rotor in relation to the other three. If half of the rotors rotate clockwise and the other half rotate counter clockwise at the same speed, the net yaw is zero. A difference in speeds between the two pair motors creates a net yaw. Different speeds in opposite motors create a net roll or pitch. Forward (backward) motion is maintained by increasing the (decreasing) speed of the front (rear) rotor while reducing the (increasing) rear (front) rotor speed simultaneously which means changing the pitch angle. Left and right motion are accomplished by changing the roll angle in the same way.

1.4 Target Environment

The target places of this study are infrastructure and disaster site. The situation on these type of environment is cluttered or complex, difficult to access, have a narrow passage, and unsafe for the human to engage. In infrastructure like the bridge, the structures are purposely designed to be complex as shown in Fig. 1.5. For instance, the presence of many braces of the bridge is mainly to stabilize the main girders during construction, to contribute to the distribution of load effects and to provide restraint to compression flanges or chords where they would otherwise be free to buckle laterally [18]. As a result, it only leaves small passages. Likewise, other bridge structures are difficult to access due to high elevation as shown in Fig. 1.6 and may require costly scaffolding to reach the target when doing the inspection. Scaffolding as temporary support is sometimes dangerous for human inspector because it has the chance to collapse.

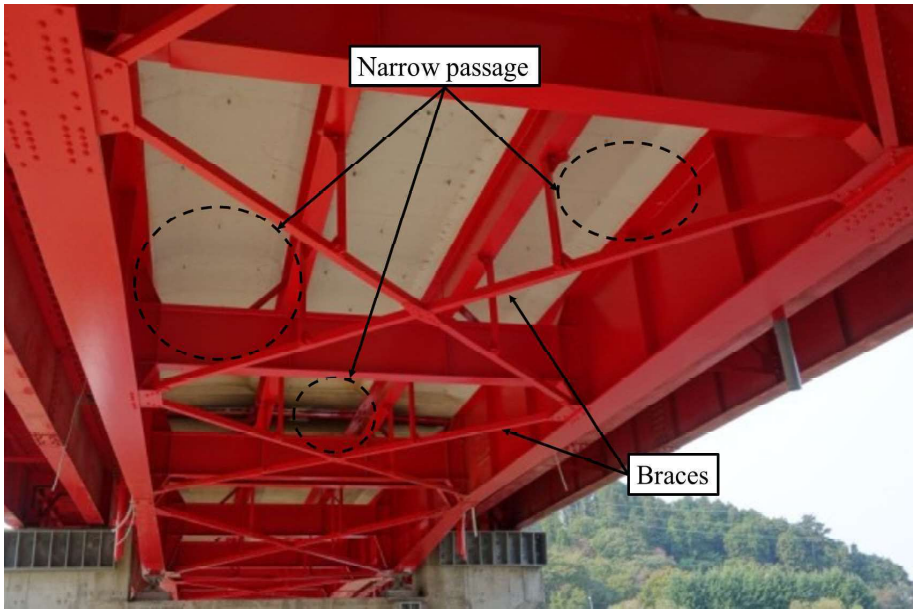

Figure 1.5: Complex structure of the bridge showing multiple braces and narrow available passages.

The situation in disaster site has an almost similar case in infrastructure site. In particular, the partially damaged building will leave a small and limited number of passages as the destructive earthquake or strong typhoon hits the site as shown in Fig. 1.7. Moreover, the condition of the most disaster area is too dangerous for a human rescuer to enter as it may have the chance to collapse totally. Thus in the case of serious exploration, these

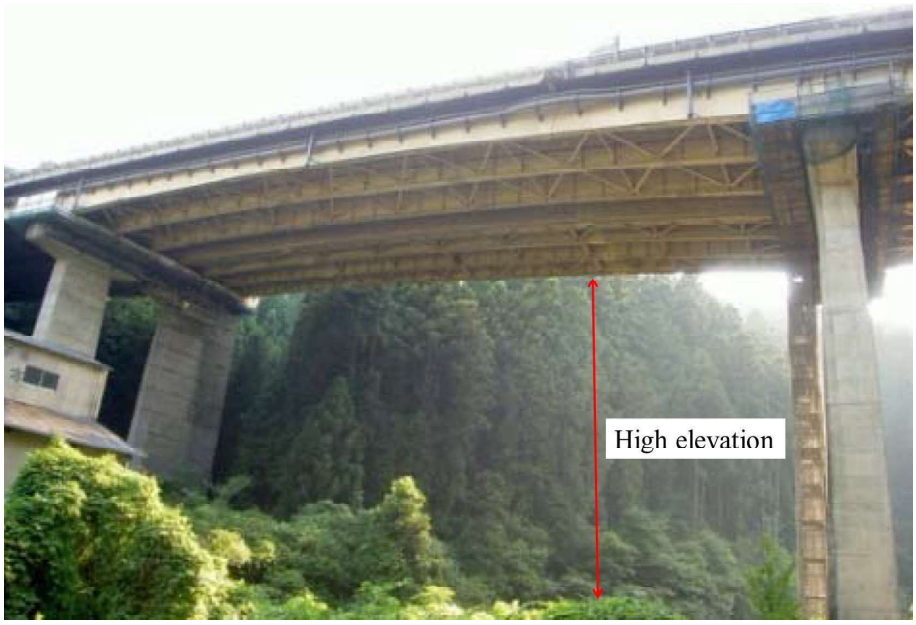

Figure 1.6: Bridge with high elevation.

Figure 1.7: Condition in partially damaged building.

sites require flying robot with a special mechanism to help facilitate human inspector or rescuer without risking their lives.

1.5 Background of PRSS Mechanism

The passive rotating spherical shell (PRSS) mechanism was introduced by two independent group of researcher [5] [6] to mainly address the problem of flying in a complex environment by small UAVs. The general issue is that during the mission (ex. search or inspection), the UAV will likely encounter unavoidable obstacle of a damaged building or complex parts of an infrastructure as it performs close observation. This may result to the falling of the UAV and will fail the entire mission. A distant exploration to the target object or structure may not satisfy the essential requirements of a certain mission. Close observation is necessary as it will allow on-board sensors to gather sufficient and valuable information. Moreover, it is hard for human operator to control the UAV by avoiding the obstacle as there is some unseen area by the operator on the target environment. In the past decades, there are several proposed control methods to avoid contact with obstacles [19] [20] [21] [22], but there remain potential risks such as with obstacles that cannot be handled by the sensor that may exceed the UAV's control response. Control methods to deal with propeller loss by collision have also been proposed [23] [24], but contact with the propeller would cause significant damage to the UAV or the inspection target. Thus, the idea is to add a passive mechanism that will protect the UAV and react to the unavoidable obstacle during the collision but kept the UAV stable.

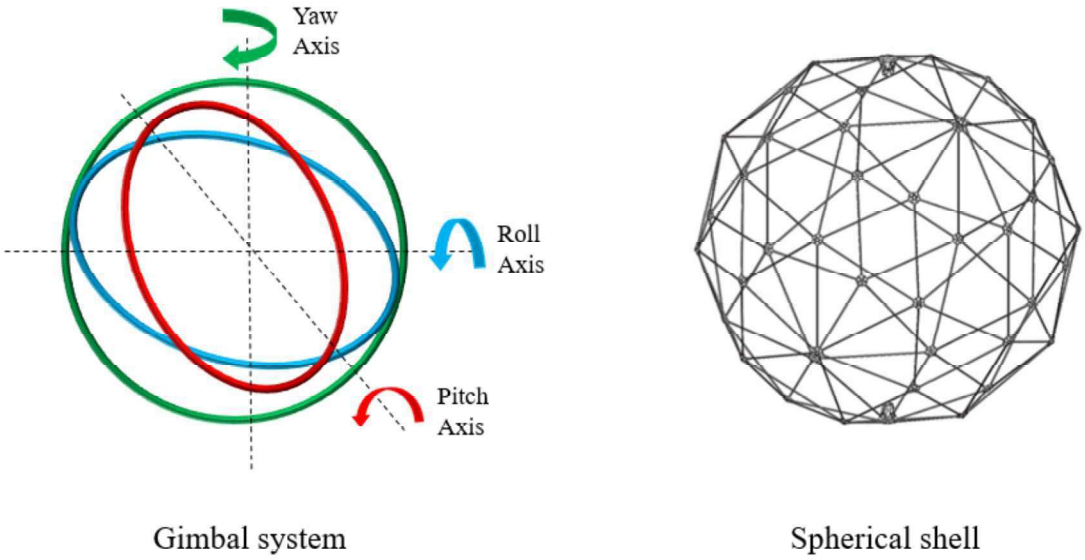

Figure 1.8: Two main components of a passive rotating spherical shell mechanism.

The passive rotating spherical shell mechanism consists of two main components, the gimbal system, and spherical shell, as shown in Fig. 1.8 left and right, respectively. The spherical shell as the outer frame serves as the protecting mechanism to keep the UAV, especially its propellers, distant from the obstacle. The world first flying spherical drone was developed by Japanese ministry of defense for military purposes [25] as shown in Fig. 1.9. The spherical drone can fly down to narrow space and bounce along the ground without significant damage because of its spherical shield. It also has a large opening for the air to flow freely. For the past decade, several types of research [26] [27] [28] have come out to expand the concept and value of the spherical drone. Until recently, a more resilient UAVs with spherical shell have been developed. At the same time, the structure of the spherical shell has evolved to a more efficient design. The preceding structure can be selected if the primary concerns are only the strength and air flow. In a real mission, other parameters (e.g. weight) are necessary. The geodesic structure is considered as a good option as it can offer a positive outcome for the strength of the spherical shell, air flow, weight, landing and rolling performance and other parameters. Geodesic was first designed after the World War I by Walther Bauersfeld. However, it was R. Buckminster Fuller popularized, patented [29] and named its geodesic. A geodesic is generated from icosahedrons, which are regular polyhedrons closest to a sphere. A procedure can be followed to generate a geodesic form. First, each face of the icosahedron is subdivided into small triangles as shown in Fig. 1.10, left. Then, the triangles are projected onto a circumscribed sphere as shown in Fig. 1.10, center. Finally, the geodesic structure

Figure 1.9: The first spherical drone and its spherical structure.

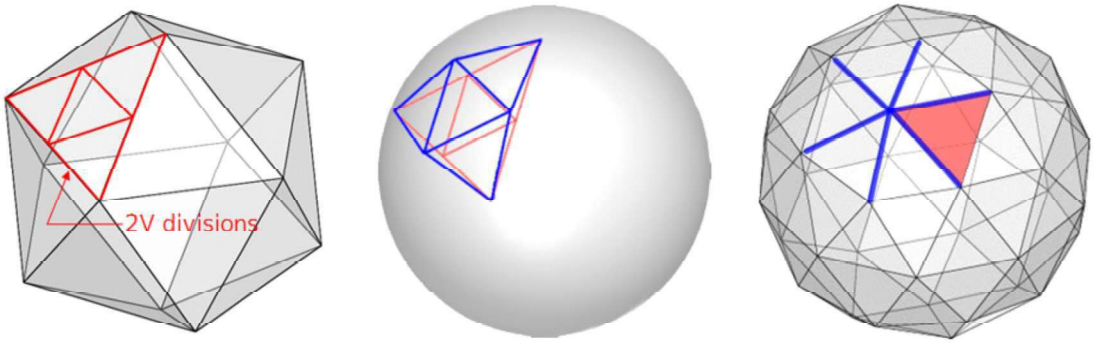

Figure 1.10: Procedure in generating a geodesic structure from icosahedron.

is completed by connecting the vertices of the triangles as shown in Fig. 1.10, right. The icosahedron can generate several divisions or category for geodesic structure represented by nV. Each face of the icosahedron is subdivided into n^2 triangles by nV divisions.

Fig. 1.11 shows the common division of geodesic structure. Each division has a different total length of the connections, the size of the triangle, and sphericity or roundness of the spherical shell. It means that these parameters will have the distinct impact for each division. As the number of division increases, the total number of connection required to create a whole spherical shell also increases. In actual design, this implies that the higher division will be much heavier. In a situation where the payload is limited, the upper division should be avoided. However, more connections would also mean a much

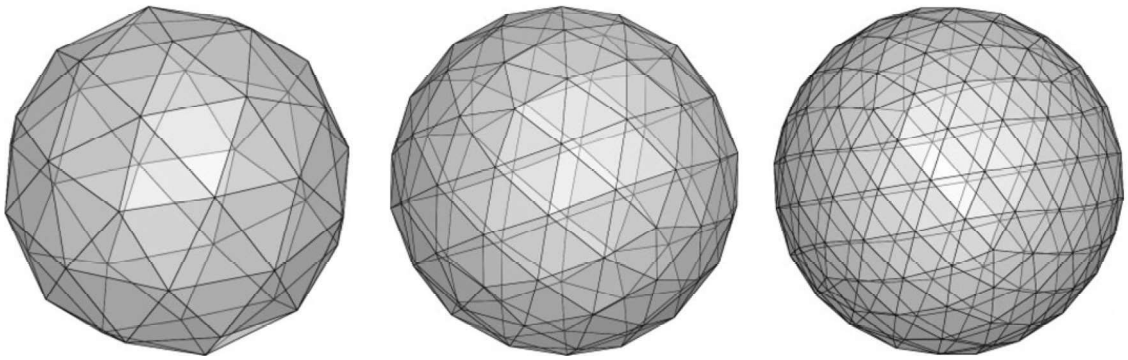

Figure 1.11: Common geodesic division: 2V (left), 3V (center) and 4V (right).

tougher spherical shell as each connection will serve as a truss. Second, as the number of division increases, the size of the triangle decreases. In actual design, this will affect the maintainability of the UAV inside the spherical shell. As the triangle gets smaller, it is hard to maintain (e.g. remove the UAV for repair or install additional components using bare hands) the UAV. Subsequently, the smaller triangle means a smaller space for air to flow. Excessive air drag to the body of the spherical shell will affect the flight performance of the system. Lastly, as the number of division increases, the roundness of the spherical shell approaches to a perfect sphere. Ideally, a perfect sphere will result to a smooth rolling of the spherical shell to any surfaces. However, as the roundness approaches a sphere, it is hard to let it stay in the same position during takeoff or landing. Each division has its advantages and disadvantages. It is necessary to select the appropriate division that best suits the mission condition and requirements.

The gimbal system is another critical component of passive rotating spherical shell mechanism. It is responsible for the passive rotation of the spherical shell in a given degree of freedom. Because of the gimbal system, the spherical shell can freely and randomly rotate especially during a collision with an obstacle while keeping the UAV stable. A single gimbal is defined as a pivoted support that allows rotation of a certain object about an axis. The gimbal was first reported in ancient time by Greek inventor Philo of Byzantium [30] describing an eight-sided ink pot which uses a series of concentric metal rings to keep the pen in its position no matter which way the pot is turned [31]. The dry compass developed in 1570 suspended in gimbals is considered as an early modern device known using a gimbal system. Today, the most common gimbal system is a set of three gimbals connected providing freedom of rotation in pitch, roll, and yaw such as shown in Fig. 1.8 (left). Gimbal system has several useful applications such as for navigation, space propulsion, and photography. As an application to ship and submarines, a gimbal system allows the inertial navigation system to remain stable in inertial space as the

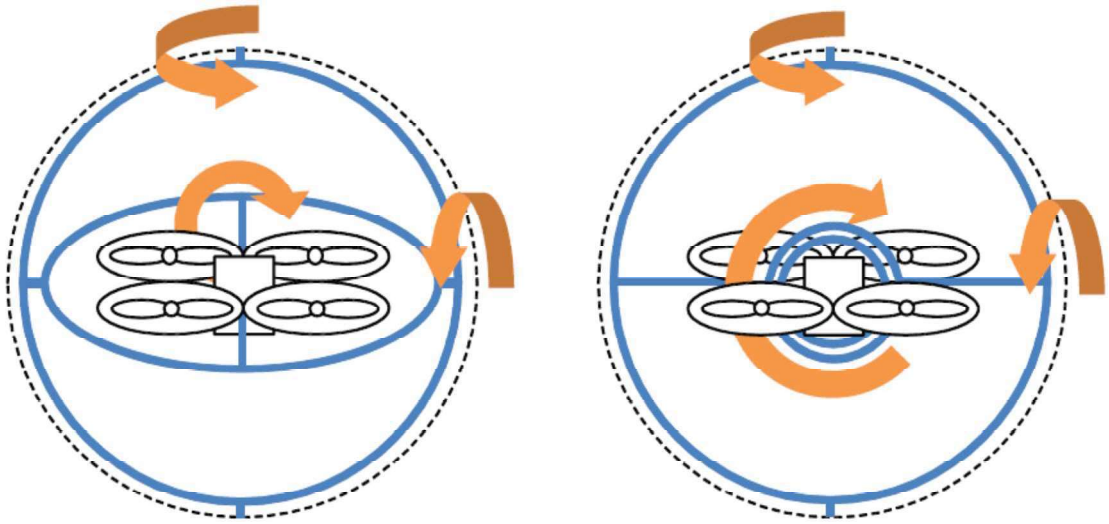

Figure 1.12: Three-axis gimbal system configuration: typical (left) and configuration suited for quadrotor UAV (right), Source: Mizutani, 2015.

ship or submarine is disturbed in pitch, roll and yaw axes. For photography, the gimbal system is used as part of stabilization system supporting the camera operator without camera vibration during shooting. Recently, the gimbal system is used to help stabilize the UAV during disturbances together with another mechanism. The gimbal system intended for passive rotating spherical mechanism can be configured depending on the type of a hovering UAV. Mizutani et. al presented the two configurations of gimbal system: the typical gimbal configuration and the gimbal configuration well-suited for quadrotor UAV as shown in Fig. 1.12. The structure of the new gimbal system configuration differs from the typical configuration regarding the gimbal design. The inner gimbal ring is shrunk to a much smaller gimbal ring but still on the same connection with the other two gimbals. The main purpose is to make it more compact and lightweight [32].

As discussed by Mizutani et. al, the passive rotating spherical shell mechanism offers three key advantages [32]. First, in the event of a collision with an obstacle, only the spherical shell is disturbed and rotated while the attitude of the UAV is not significantly affected. As a result, the UAV can continue its stable flight as shown in Fig. 1.13 (a). Second, the UAV can be moved into contact with the surface by using the spherical shell itself like a wheel. As a result, it can obtain a close and smooth view along the surface of the target as shown in Fig. 1.13 (b). Finally, the UAV can takeoff and land on uneven or bumpy terrain since it is possible to adjust the attitude of the UAV inside the spherical shell as shown in Fig. 1.13 (c).

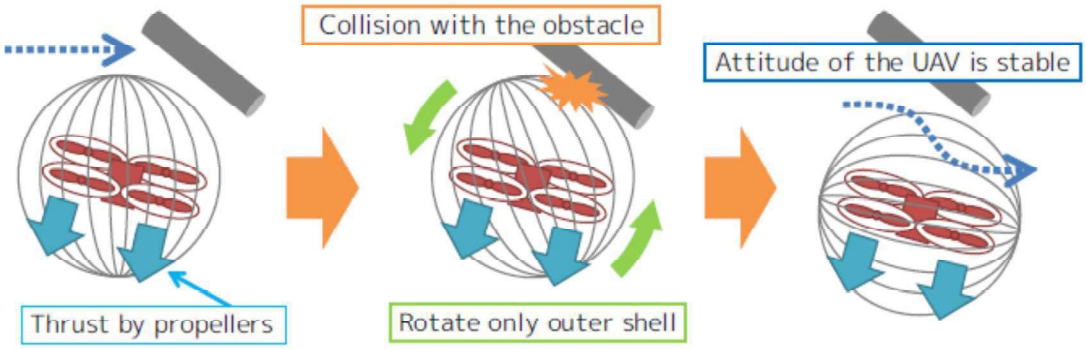

(a) High flight stability during collision

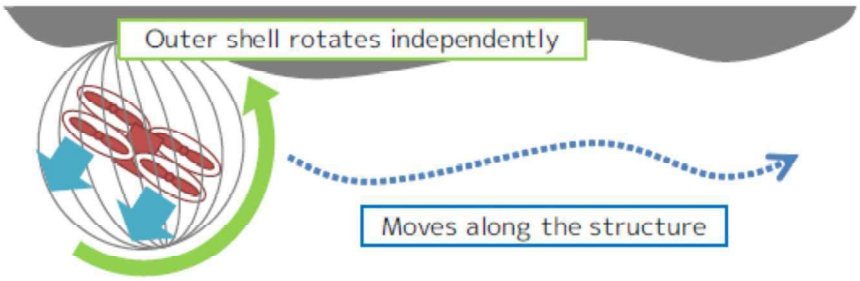

(b) Traveling along the structure

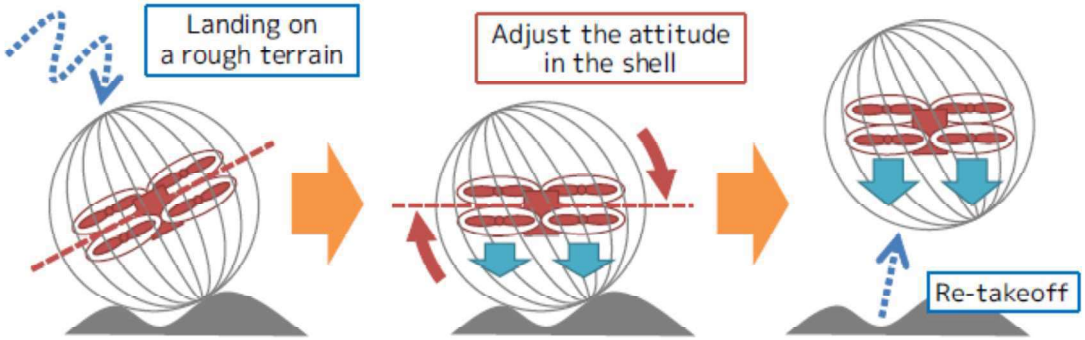

(c) Landing on and re-takeoff from rough terrain

Figure 1.13: Key advantages of passive rotating spherical shell mechanism, Source: Mizutani, 2015.

1.6 Summary of Main Contributions of this Dissertation

The following are the main contributions of this dissertation. To the author's knowledge these are original contributions in the field of unmanned aerial vehicle. The detailed contributions of individual chapters is included in Chapter 5.

1. In Chapter 2.5, a design optimization of the existing UAV with a passive rotating spherical shell was presented. The study focused on maximizing the flight capability of the UAV, improving the payload by reducing the weight of components, and minimizing the external disturbances specifically the drag force. The novel concept lies within the design of the spherical shell components and appropriate selection of shell structure responsible for the improvement of payload and reduction of drag force. Subsequently, the design process continuously considered the important design points in a real complex environment and further consider another serious condition in the actual field which is the presence of erratic wind. This study contributed a novel design technique for an unmanned aerial system to be applied for exploration in a complex and harsh environment.

2. In Chapter 2.6, an application of UAV with a passive rotating spherical shell was introduced. The study involves an actual close visual inspection of the various bridges in Japan. The study is in preparation for nationwide maintenance of all aged bridges in Japan. The function of the UAV with a passive rotating spherical shell is to completely replace the dangerous and time-consuming task of a human bridge inspector. The main objective at the time of inspection is to acquire images in the various part of the complex-structured bridge. This study is expected to be valuable to the infrastructure management people as this will provide a safe, fast, and low-cost operation.

3. In Chapter 3.5, a new concept of passive rotating spherical shell mechanism that would allow physical interaction while the UAV is protected and kept stable was introduced. The idea of cutting the spherical shell to provide gap while maintaining the protective spherical shell and at least retain two axes of passive rotation is the novel part of the study. This new concept will serve as prime research of physical interaction on a complex environment. This concept can be extended to several studies to come up with a robust system that can be used in a real mission.

4. In Chapter 3.6, an application of physical interaction using the UAV with two passive rotating hemispherical shells was introduced. The UAV is attached with a hammering system for interaction with the environment while the two passive rotating hemispherical shells mechanism will allow the system to be used in a complex

infrastructure. The hammer test is used to check the condition of structure especially the concrete. In infrastructure inspection, this study will serve as an initial effort to realize a complete system that can facilitate human inspector on performing hammer test on complex-structured site. This study is expected to provide safe, fast and low-cost operation infrastructure inspection. Also, this study can also be implemented for other related purposes such as to check the partially damaged building struck by an earthquake.

Chapter 2

UAV for Visual Exploration in a Complex Environment

2.1 Introduction

For the past decades, visual exploration has been one of the major task performed by UAV for an actual mission that includes visual inspection task, reconnaissance, and aerial mapping. Many of these missions have been applied in the disaster situation for visual assessment. This is because the use of unmanned aerial vehicles (UAV) offers a unique possibility to capture visual information in areas which are hard to reach or dangerous for humans [33]. In the field of disaster robotics, the structural inspection has occurred at 7 of the 11 deployments, and reconnaissance and mapping have taken place at six events. UAVs have been used for visual assessment, either through video recording or cameras to capture imagery [34].

The use of UAV provides a safe, low-cost and require a shorter time to acquire visual information on the site distant from the human involved like in search and rescue operation. For example, wilderness search and rescue (WiSAR) requires thousands of hours of search over vast and complex terrains. UAVs may dramatically improve search efficiency. Given a well-coordinated human-UAV interaction specifically the coordination between the UAV and ground search resources, and the UAV technology [35] [36]. UAVs specifically micro UAVs or MAVs, have also been widely studied for industrial inspection tasks [37] [38] [39] to mainly prevent a human operator from dangerous task and those areas difficult to access. For example, aerial service robots for visual inspection of thermal power plant boiler systems have been studied [40]. The use of UAVs has also become increasingly important in collecting imagery in emergency response situation. Traditionally, aerial images to examine large scale damage was done using manned aircraft. However that required a takeoff and landing infrastructure, was very costly and involved a rela-

tively long lead time. Comparatively low-cost drones that offer a more rapidly deployable platform with an ability to fly at lower altitudes and hence, collect higher resolution imagery. For example, one researcher used the UAV and explores semi-automatic surveying techniques to support immediate post-earthquake perishable data collection and damage assessment of cultural heritage sites following the 2014 South Napa Earthquake [41]. Other researcher used small UAVs for infrastructure assessment tasks which include inspecting pavement condition and vegetation encroachment on roadways, debris and tree coverage on railways, and corrosion on bridges and water towers [42].

In the case of a cluttered environment such as disaster sites and damaged infrastructure, it is expected that the area that the UAV can perform visual exploration is very limited. This is because of the primary weakness of the UAV especially for rotor-type UAVs that it is more likely to fall when in contact with the obstacle. Either because there is no protection to the exposed propeller or no passive or active control to maintain stability. In the cluttered environment, it is also difficult to control the system and avoid the obstacles as some spots cannot be detected by the sensor or there are external disturbances that will exceed the control response. One way to solve the problem is to implement a passive rotating spherical shell mechanism to be added on the UAV. This method is already introduced by past researchers [6] [5]. The mechanism comprises of the spherical shell and the gimbal. It provides both protection and maintains good stability for the UAV. The spherical shell protects the exposed propeller not to get contact with the obstacle while the gimbal allows rotation in different axes keeping the UAV stable. However, previous researchers focused mainly on the concept of the mechanism. Appropriate and optimal design by the consideration of critical parameters and constraints based on the cluttered environment will allow it to be effective and successful in an actual mission. Robust design is necessary to complete the mission because if the system fails while on a mission, then the entire mission will fail [15].

Prior to the deployment of the UAV with passive rotating spherical shell in an actual mission, a design strategy was proposed [32]. The design strategy is focused on the area of disaster response and infrastructure inspection. The strategy is summarized as follows:

1. Identify the important design points based on the problems in the actual field.
2. Analyze the spherical shell structure by considering several design parameters and the shape of the shell to balance its sphericity and weight.
3. Verify the strength of the shell against possible impact during a mission.
4. Set the gimbal structure. This mainly depends on the size of the UAV or sensor to be mounted.
5. Finally, a design flow by considering each of the design points.

All possible issues of concern in the area of disaster response and infrastructure inspection

are identified. It is then transform to a more specific details needed to obtain the essential design points.

Payload Design of Small UAVs

The payload design can be considered as one of the core design points as the other points, and some constraints also rely on the payload. For small UAV system like the UAV with passive rotating spherical shell, it not unusual to have a limited payload. As a practical case, Gruber et. al have presented the payload design of small UAVs where it discusses the payload design issues [43]. It stated that designing a small UAV payload involves trade-offs among the core subsystems such as power, sensors, communications, and computer. Decision made for one system will affect the design of another subsystem. While managing the balance, the overall small UAV system constraints of weight and volume must be maintained. Furthermore, it also stated that the requirements of the payload must be defined first before a detailed design can be developed. Some of the questions that should be asked that affect a UAV payload design as mentioned by Gruber et. al are as follows but not limited to:

1. What is the flight duration required for the mission?
2. What is the specific task of the mission?
3. What are the detailed mission subtasks? How large is the search area?
4. What is the maximum distance from the ground station that the UAVs will be operating?
5. What are the target characteristics?
6. What are the allowed frequencies that can be used for communications between the UAV and the ground station?
7. What are the situational awareness requirements of the ground station operator?
8. Will other devices be operated in the same area that can cause communication interference?
9. What are the environmental requirements?

Sizing of the UAV

Maximizing the size of the UAV is also an excellent opportunity to help ease the problem of limited payload. Brandt et. al has presented the sizing and optimization of small UAV [44]. It involves several analyses such as constraint, aerodynamic, weight, and mission analysis to determine the appropriate motor and propeller combination and suitable battery size enough for the entire mission. The thrust to weight or T/W ratio is one of the important parameters that determine the performance of the aircraft [45]. For most flight conditions, an aircraft with a high thrust to weight ratio will also have a high value of excess thrust. High excess thrust results in a high rate of climb. If the thrust to weight

ratio is greater than one and the drag is small, the aircraft can accelerate straight up [46]. T/W is simply the ratio between the sea-level static maximum thrust and maximum takeoff gross weight. The motor and propeller thrust to weight ratio, along with values for η_{motor} and η_{prop} can be obtained by testing several typical motor/prop combinations in a wind tunnel. The weight of the battery depends on the level of its energy density, the efficiency of the motor and propeller, and the total thrust energy which the motor and propeller must provide to overcome the aircraft's drag and to increase the aircraft's mechanical energy by climbing or accelerating. In general, the total thrust energy required will, therefore, depend on the details of the design mission profile [44].

Aerodynamic Consideration

Aerodynamic forces such as lift and drag are the resultant components of the pressure field on a moving body or a body of moving air. Drag is an unwanted force that cannot be avoided but can be minimized. Drag is eventually an enemy of flight, and its cost [47]. Minimizing the drag of is one of the main obligations of aerodynamicists [48]. The effect of viscosity can be seen behind a body as disturbed airflow creating a wake. The wake thickness and intensity are indications of the extent of drag. One way to reduce the drag is to shape the body such that it will result in a thinner wake. The general approach is to make the body in a teardrop shape with the aft end closing gradually, as compared to the blunter front-end shape. The smooth contouring of teardrop shaping is called streamlining, which follows the natural airflow lines around the body. Streamlining is synonymous with speed, and its aerodynamic influence in shaping is revealed in any object in a relative moving airflow [48]. The drag is a function of speed, air density, and its configuration. The effect of drag is represented by the drag coefficient (C_d), plus a reference area that relates to the body. A small drag coefficient means low drag force for a certain body. Each body shape will have a different value of drag coefficient for particular flow as shown in Fig. 2.1 and 2.2. The drag force and related parameters can be measured and evaluated by means computational fluid dynamics (CFD) simulation and wind tunnel experiment.

Computational fluid dynamic (CFD) analysis is a powerful, cost-effective tool for the study of the aerodynamic characteristics of the flow. Through careful selection of the grid geometry and resolution, as well as the computational technique used, the sophistication of the analysis can be tailored to meet the needs of the researcher, while conforming to the imposed time and cost constraints [49]. In many designs and analysis applications, CFD methods are quickly replacing experimental and analytical methods because they offer a quick solution at a cheaper cost. CFD techniques have emerged with the advert of digital computers. Since then, a large number of numerical methods were developed to solve flow

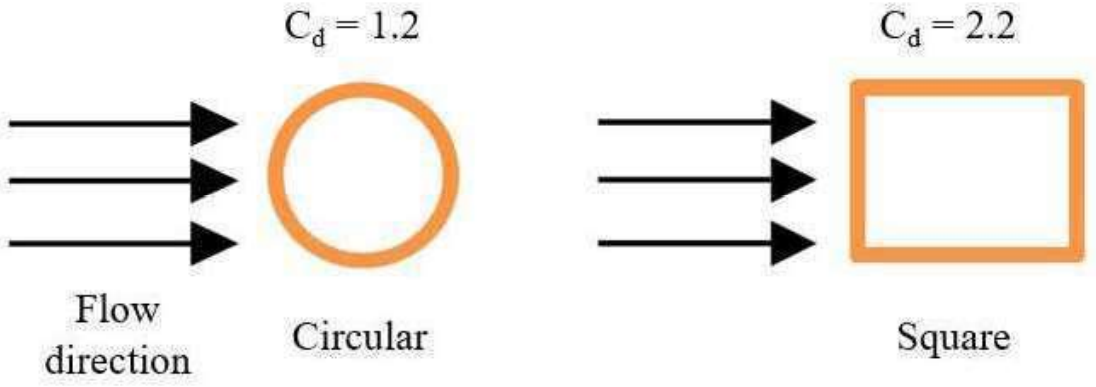

Figure 2.1: Drag coefficient comparison between circular and square body shape of rod. Source: Sadraey, 2009.

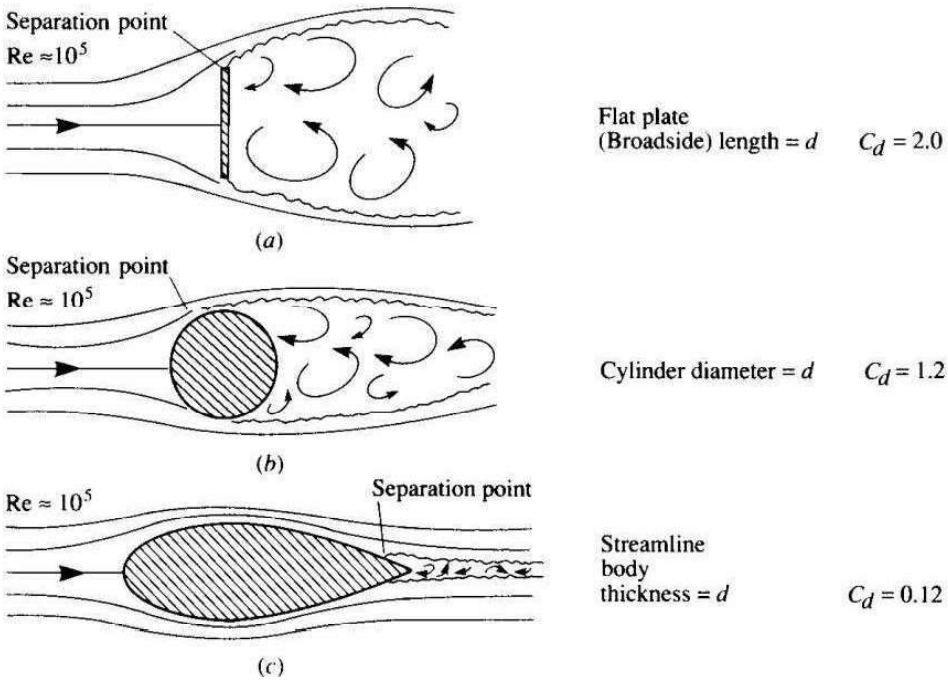

Figure 2.2: Drag coefficients for various aerodynamic shape Source: Anderson, 2011.

problems using this approach [50]. Initially, the physical space through which the flow passes must be divided into some discrete points called a grid. It is then transformed into a computational domain through which the flow solver program can understand and use to perform the numerical calculations. CFD can provide results through both numerical value and visualization. Generally, CFD gives an insight into flow patterns that are difficult, expensive or impossible to study using traditional (experimental) techniques for all desired quantities with high resolution and for virtually any problem and realistic operating conditions [51]. The weakness of the CFD simulation is that the results can be erroneous [52]. Awareness of error sources and ability to control or preclude the error are important [51]. Otherwise, it is good to verify some of the relevant results done in CFD simulation by an actual experiment or wind tunnel testing. A wind tunnel is a tool used in aerodynamic research to study the effects of air moving past solid objects physically. A wind tunnel consists of a tubular passage with the object under test mounted in the middle. Air is made to move past the object by a powerful fan system or other means [53].

Proposal

In this study, it is proposed to improve the system performance of the existing UAV with a passive rotating spherical shell so it can be applied in a real mission. The specific objectives are to maximize the flight capability of the UAV, minimize the overall weight of the system, and reduce the effect of air drag. An appropriate selection of principal components can contribute to the improvement of the system performance. Another idea is to minimize the weight of the system's components, especially the spherical shell. Although it should be noted that any changes need to do on the spherical shell to reduce its weight should not compromise its strength of spherical shell and keep the strength at an acceptable level. Furthermore, external disturbances will likely to exist in a real environment specifically the presence of erratic wind gusts that cause air drag or drag force. This problem cannot be avoided but the system's components, especially the added spherical shell, can be designed with minimal effect on such disturbance. The idea is to apply the concept of an efficient aerodynamic shape to minimize the effect of air drag. It is also proposed to perform an actual mission in a complex environment. This is to primarily verify the performance of the system. Visual inspection of the bridge is the proposed mission. The condition of the bridge is precisely a good test field because of the existence of the complex structure and the frequent presence of erratic wind gusts. The tasks are to fly and traverse into the complex and narrow part of the bridge and to capture close images in the different part of the bridge. To further verify the capability of the system it is then evaluated by the human professionals managing the bridge.

Chapter Outline

In this Chapter, it discusses two main topics: the improvement of the existing UAV with passive rotating spherical shell and the actual visual exploration of the system in complex-structured bridge. The main objectives of this Chapter are enumerated in Chapter 2.2 and specific objectives are further explained in the same Chapter. Furthermore, Chapter 2.3 and 2.4 discusses about the contributions of this study and some of the related studies, respectively. Chapter 2.5 discusses the approach of improvement. The goals are to increase the flight capability, reduce the weight of the system, and minimize the effect of the drag force. Some conditions and constraints were considered to keep the system suitable in an actual complex environment. Chapter 2.6 discusses about the visual inspection conducted in the bridge. The aims are to check the performance of the system in a complex environment and to verify the capability of the system in capturing images on various part of the bridge. Chapter 2.7 concludes and summarizes the result of the improvement of the system and the conducted visual inspection in the bridge.

2.2 Objectives of this Chapter

The main objectives of this chapter are:

1. To improve the flight performance of the existing system that can be applied in a real-world complex environment.
2. To implement a visual exploration on an actual complex-structured bridge to verify the effectiveness of the system.

The first objective can be achieved by maximizing the flight capability of the UAV, minimizing the overall weight of the system, and reducing the effect of external disturbances as specific objectives. The first specific aim is to appropriately select the main components of the UAV such as motors, propellers, and battery to maximize the flight capability of the UAV. The second specific aim is to reduce the weight of the spherical shell without compromising the strength of the spherical shell. The third specific aim is to reselect the spherical shell structure and redesign the components such that it will have a much lesser effect of air drag by applying the concept of an efficient aerodynamic shape.

In the second objective, it is aimed to verify the performance of the system through an actual visual exploration mission in a complex environment. Close visual inspection of the bridge is the proposed mission. Inspection of the bridge is an appropriate task since its main purpose is to check for any damages such as cracks and rusts. Also, the condition of the bridge is precisely a good test field because of the existence of the complex structure and the frequent presence of strong wind. The first specific aim is to fly and traverse into the complex and narrow part of the bridge to verify its performance. The second aim is

to capture close images in the different part of the bridge at various position. The system will be evaluated by the human professionals managing the bridge to further verify the effectiveness of the system in an actual mission on a harsh and complex environment.

2.3 Significance of the Study

There is two main significance of the study of this Chapter. First, this system improvement technique will help other researchers to learn and understand the importance of the design parameters and constraints mentioned in this study so it can be applied in a real-world mission. The technique introduced in this study may contribute for other researchers who will be working on the mechanism for the unmanned aerial vehicle to be used in a complex and harsh environment. Second, given the actual experiment in the bridge, this encourage bridge management and other related areas to consider the utilization of this UAV system further. This UAV system will have a positive impact on infrastructure and other related industries for safe and quick inspection. Besides, a lesson can also be learned by researchers in academia as well as in industry, the harsh conditions in an actual experiment field and how to deal with it.

2.4 Related Literature

Optimization of the unmanned aerial vehicle to make it viable for the actual mission has been vastly exploited for the past decades. In fact, researchers and developers in academia as well as in industry have, mostly, implemented the optimization technique. UAV design, where optimization is a part of it, is a huge area of study and depends mainly on purpose. However, in any part of the vast area of research for UAV design, the primary goal is to make an operational system. In the handbook of unmanned aerial vehicles [54], it importantly includes the UAV Design Principles which presents the basic design principles of UAV and the components that comprise a complete unmanned aircraft system, avoiding in-depth technical details. It aims at creating the overall picture on the UAV functionality and, consequently, to indirectly motivate the reader about the challenges that need to be overcome to make UAVs fully operational, reliable and safe. In an industrial level, the book of Aircraft Design [48], it presents a methodology to aircraft design and aerodynamic considerations. In Unmanned Aerial System book [15], it introduced the complete package of the system design from UAV design and development up to deployment.

Many specific designs have been studied to bring a significant contribution in the field of unmanned aerial vehicle. Several researchers have worked on payload design for small UAVs, mostly to optimized the system and ensure it is fully operational [55] [56] [57] [58]. For example, a design consideration of a small UAV platform carrying medium

payloads was presented [59]. The study focused on the structural components selection that will allow fulfilling the requirements of the project such as the energy consumption, the autonomy of the vehicle and the stable flight. Another, the aerodynamic consideration has been part of aircraft design in the early days. Aerodynamic design primary goal is to make the aerial vehicle efficient. For example, a study on airfoil selection, optimization, and analysis for a solar-powered unmanned aerial vehicle were presented [60]. The paper is a method for obtaining an optimal airfoil for a Solar-powered Unmanned Aerial Vehicle (UAV). Furthermore, evaluation has always been a part of the aerodynamic design which nowadays done through either or both simulation and actual experiment. For example, a study on the aerodynamics of a flying wing UAV with rearward facing stepped wing profile focused on exploring efficient and stable flight was presented [61]. It uses a computational fluid dynamic simulation software to evaluate the subject, the NACA0012 airfoil where both numerical and visual data were presented. On the other hand, a study on low-speed wind tunnel testing for an unmanned aerial vehicle airfoil was performed [62], an example of a conducted actual experiment and evaluation. The study evaluates a specific airfoil's relevant parameters such as lift, drag forces, and pitching moment.

For the past few years, robots have already been introduced for bridge inspection purposes. Mobile robots initially take the role to support human bridge inspector. Lim et. al developed a crack inspection robot for bridge maintenance where the robot collects bridge deck images with a high-resolution camera [63]. Liu et. al presented a line structured light approach for auto bridge inspection based on climbing robot [64] while Wang et. al developed a magnetic climbing robot for steel bridge inspection [65]. However, in just recent years, UAV, specifically rotor-type, becomes popular because of its vast capabilities over the conventional robot being used that includes the ability to hover and able to reach the target point immediately. For example in Japan, the government is fully supportive of the use of UAV for bridge inspection and funded some researcher and developers to build such robots [66]. A Crack Detection System with Unmanned Aerial Vehicles and Digital Image Processing developed by Kim et. al is one clear example [67]. However, a typical UAV is not suitable to be used in a complex environment like the bridge. Recently, two independent group of researchers were able to develop a mechanism for UAV to deal with flying in complex environment [6] [5].

As a summary, there are already vast worked done individually by many researchers in the area of optimization or improvement of the UAV for real mission, visual exploration of a complex environment, and mechanism for UAV suitable of exploring the complex environment. However, there is no research yet have done by resolving the area of concerns altogether so it can be used in an actual mission and a complex environment. The solution for the shortcoming of all the previous researches mentioned is the aim of this study.

2.5 Improving the Performance of Existing System

2.5.1 Initial PRSS UAV and the Issues

The UAV with a passive rotating spherical shell (PRSS UAV) intended for visual exploration on a real mission is initially developed and introduced in the previous paper [32]. The initial system prototype is shown in Fig. 2.3 and its specification is listed in Table 2.1. It uses an off-the-shelf quadrotor UAV called EX450 that weighs 1000 g and has a maximum take-off weight of 2000 g. The diameter of the spherical shell is 894 mm, and it was determined based on the target environment. For a specific case, the PRSS UAV is being used for visual inspection of the bridge in Japan.

Figure 2.3: Initial system prototype [Mizutani, 2015].

Table 2.1: Specification of the initial PRSS UAV

	Specification	Unit
Overall Diameter	894	mm
Max. Takeoff Wt.	2000	g
Available Payload	1000	g
Overall Weight	1956	g
Battery Used @ 11.1 V	3300	mAH

The initial system is designed based on the strategy that considers the condition of a complex environment. However, the existing system was not yet completely optimized, which means that there are still parameters necessary for a real mission that was overlooked. As a result, it causes several problems during the actual mission. Firstly, the existing system does not have enough payload to carry the complete set of visual system that includes but not limited to multiple cameras and transmitter. Furthermore, although the existing system can fly and performed its first mission, it has a very limited flight duration. This is because the existing system uses a low power battery. The cause of the problem can be pointed back to the limited payload that forces the existing system to use a lightweight but low power battery.

Moreover, the actual environment specifically outdoor, will likely to have wind gusts. Although, the system does not need to fly at high speed, unlike fixed wing aircraft, but the strong wind causes significant air drag, specifically on the body of the added spherical shell. Thus, the system needs to increase the flight capability (thrust force) and decrease the effect of air drag force to alleviate the problem. However, the existing system is not capable of compensating the drag because a very small excess thrust of the UAV is left. Likewise, the selection and design of the previous spherical shell did not involve aerodynamic study to minimize the effect of air drag.

2.5.2 General Approach

Based on the issues mentioned above, two sections can contribute to the improvement of the system's flight performance: payload design and aerodynamic consideration. Increasing the flight capability (thrust) and reducing the weight of the system are the objective for the new payload design. The requirements of the payload must be defined first before developing a detailed design [43]. Likewise, aerodynamic design is introduced to minimize the drag force. Those three forces, thrust, weight, and drag, acting on the UAV are illustrated in Fig. 2.4.

Reducing the weight is difficult to implement because the main subcomponents of the system that includes the UAV, gimbal, and spherical shell is already designed to be lightweight. One option to reduce the weight is changing the structure of the spherical shell. However, it is important to take note that the structure of the spherical shell directly affects its strength. The spherical shell is composed of interconnecting structural trusses. Removing some interconnecting trusses will make the spherical shell-less resilient. Thus, it is important to appropriately select an optimal spherical shell structure that has less weight but without compromising the overall strength of the spherical shell.

Increasing the thrust power of the UAV is also challenging because of the limiting factors: weight and size. When designing a high-thrust UAV, it will need a large propeller. The advantage of a large propeller is it has lower disk loading that results in a higher

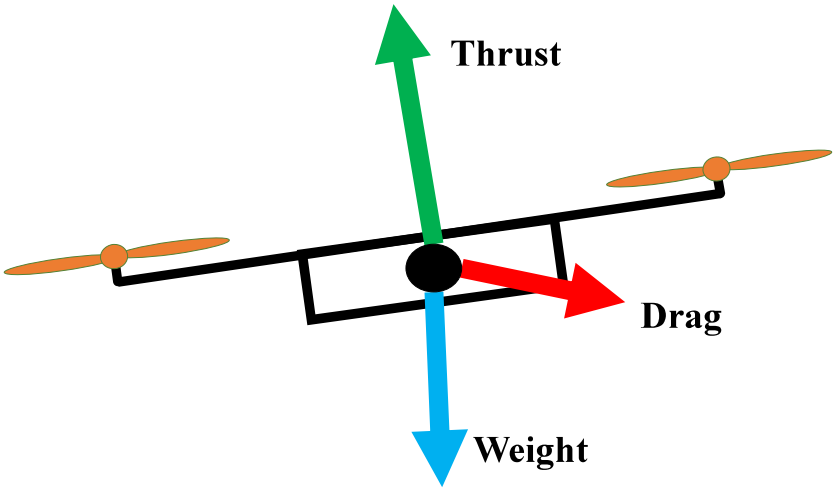

Figure 2.4: Principal forces acting on the UAV.

figure of merit and lowers power consumption than small propellers [68]. However, it will only mean a larger overall diameter of the UAV. It is necessary to limit the size of the UAV because it will also increase the size of the spherical shell. As mentioned in Chapter 2.5.1, the size of the spherical shell is limited to a certain value (depending on the target environment), so it can enter into the narrow path. Subsequently, a high-thrust UAV needs a large (heavy) motor and battery. Thus, it will result in an increase in overall weight. On the other hand, increasing the thrust power of the UAV will increase the flight time. Because the increase of (payload) weight capacity of the UAV would mean it can carry high-powered batteries and thus satisfies the required mission time. Therefore, it is important to select an optimal motor, propeller, and size of the battery without compromising the size of the spherical shell and the overall weight of the system.

Also, the increase of thrust could result into the increase of excess power. For fixed-wing UAV, the excess power is a measure of the aircraft's ability to increase its energy by climbing or accelerating [44]. For rotor-type UAV, this excess power is important to counter the strong and erratic wind gusts in an actual outdoor environment. Although, the excess power will not be a tremendous value since the loading (e.g. the gimbal, spherical shell and visual system components) are the priority for the available thrust.

Reducing the drag force of the spherical shell requires a thorough aerodynamic evaluation. In this study, the drag is the resistance created by the wind to the UAV. The drag force acts in a direction that is opposite to the relative flow velocity [69] and depends on the shape and orientation of a body. As the drag force increase in proportion to the dynamic pressure (q) equals to $\rho V^2/2$ and the projected area of the body (A) in the flow direction, the drag coefficient (C_d) can be calculated as follow:

$$C_d = F_d/(qA) = 2F_d/(\rho V^2 A) \tag{2.1}$$

where, (F_d) is the sum of the pressure force and the viscous force components on the spherical shell surfaces acting in the horizontal direction, and ρ and V are air density and flow velocity, respectively.

Based on the definition of Eq. 2.1, F_d can be written as:

$$F_d = \rho V^2 A C_d / 2 \tag{2.2}$$

Since C_d is a function of Reynolds number (Re) and change in Re has a relatively small effect, then the drag of the spherical shell F_d will eventually increase with the increasing flow velocity V. Subsequently, the projected area of the spherical shell A which depends on the shape of the shell's structure and components will also affect the total drag F_d.

2.5.3 Minimizing the Weight

A geodesic dome structure [29] is used to build a robust spherical shell that is also adopted by Gimball [70] and QBall [71]. Table 2.2 shows the important parameters of a geodesic dome for different divisions where Ri, Rc, Li, Lt, and n represent the radius of the inscribed sphere, radius of the circumscribed sphere, length of each edge or connection, total length of connections, and number of connections, respectively.

The spherical structure primarily consists of joints (vertices) and connectors. The initial system [32] utilized a 2V geodesic structure shown in Fig. 2.5, which requires less material based on Lt but has a good sphericity (Ri/Rc) of 0.93, as listed in Table 2.2. Based on the new objectives: weight and drag reduction, a new structure is selected. A 3V geodesic structure is a good candidate; however, the total length of connections is higher by 52.76 % against the 2V. The idea is to remove some of the connections to form a fullerene structure as shown in Fig. 2.6. As a result, it only requires a shorter length of the connection. The L_t/R_c is equal to 36 which is 48.5 % less connection than the 2V geodesic structure.

However, the strength of the fullerene structure is weaker since it only contains 3-star vertices or so-called joints compared to a 5-star and 6-star in 2V geodesic structure. If

Table 2.2: Relationship between dome parameters and the radius of the circumscribed sphere.

Division	Ri/Rc	(Li × n)/Rc	Lt/Rc	No. Vertices(Form)
1V	0.79	1.05 (30)	31.54	12 (5-star)
2V	0.93	0.55 (60), 0.62 (60)	69.87	12 (5-star)/30 (6-star)
3V	0.97	0.35 (60), 0.4(90), 0.41 (120)	106.73	12 (5-star)/80 (6-star)
4V	0.98	0.25 (60), 0.29 (120), 0.30 (120) 0.31(120), 0.33 (60)	143.20	12 (5-star)/150 (6-star)

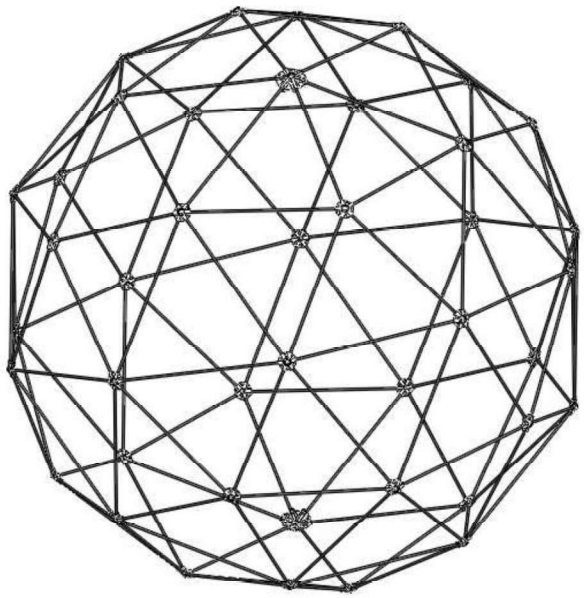

Figure 2.5: 3D models of 2V geodesic domes.

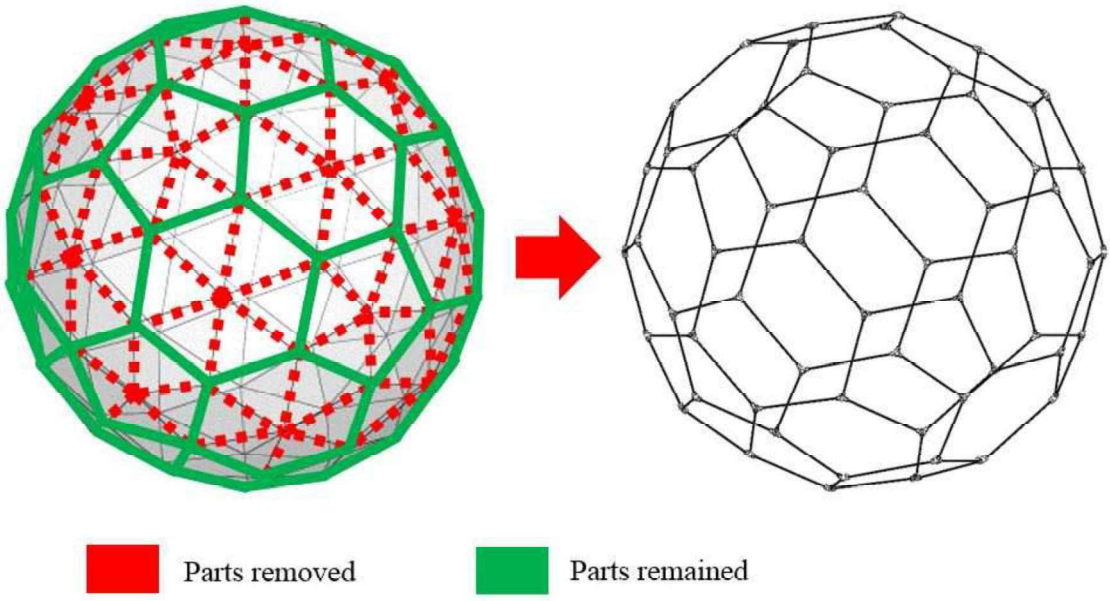

Figure 2.6: Transformation of 3V geodesic to fullerene structure.

the current connectors ($D_O = 3.5$ mm, $D_I = 2$ mm carbon pipe) are used, it will not have enough strength to deal with the impact. Thus, a much tougher carbon fiber connection is selected. The strength depends on the size of the cross-sectional area A_C based on a simple stress formula of any material given in Eq. 2.3. The constraint is to maintain the diameter of the connector while increasing its strength. The 3.5 mm diameter carbon rod is the proposed connector of the new spherical shell.

$$\sigma = Force/A_C \tag{2.3}$$

A drop test was conducted to verify the strength of the components. Drop weight impact testing is a low-velocity testing and the most common test for composite materials [72]. It is the best method for testing the strength of spherical shell parts. In a drop weight test, a certain mass (m) is raised to a known height that will generate an impact equivalent to the expected amount of impact during a collision. The equivalent drop height (h) can be obtained using Eq. 2.4.

$$h = Mv^2/2mg \tag{2.4}$$

,where M is total system mass, v is speed and g is gravitational acceleration

Fig. 2.7 shows the drop test set-up for the spherical shell. To simplify the experiment, only part of the spherical shell or so-called joint assembly (connectors + joints) were tested as this would have a more severe impact effect than would be generated on the spherical shell. The actual drop test set-up is shown in Fig. 2.8. The outcome of the drop

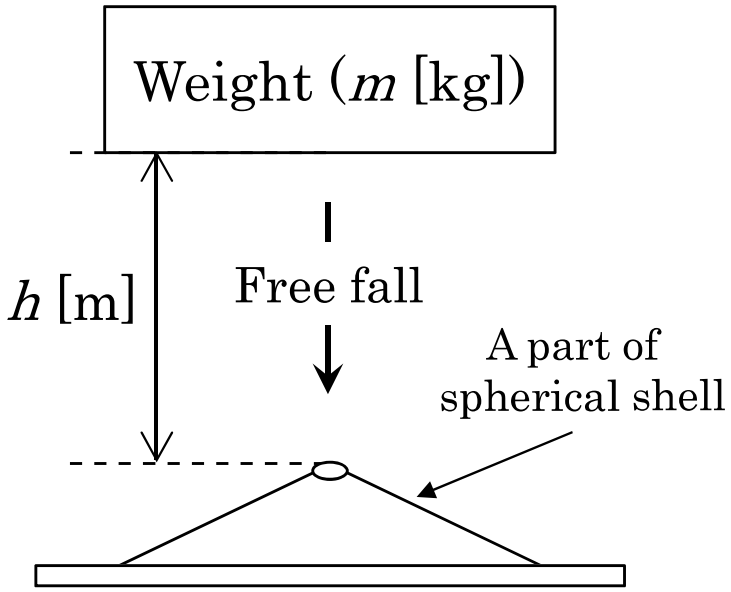

Figure 2.7: Drop test for the part of spherical shell.

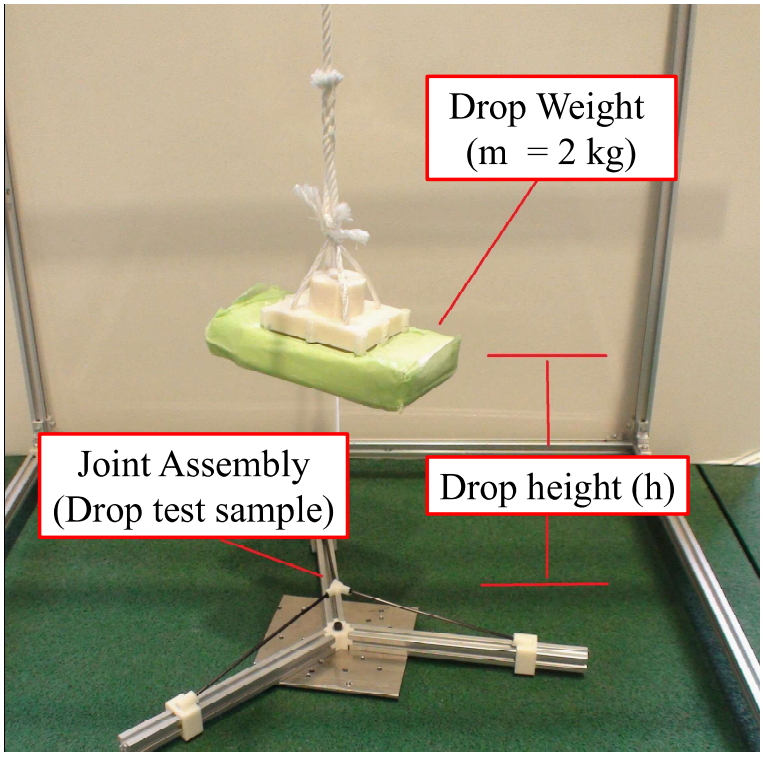

Figure 2.8: Actual drop test set-up.

test was evaluated by clear visible impact damages (CVID).

The maximum flight speed of the UAV is used to calculate the minimum impact requirements for the system during a collision. The estimated maximum flight speed at the full weight capacity of 2.8 kg, when tested, is approximately 1.5 m/s. For a flight speed of 1.5 m/s, the drop height h is equal to 0.16 m. An impact speed of 2 m/s (33 % higher than the maximum flight speed of the UAV), which corresponds to a drop height of approximately 0.3 m was performed to increase reliability.

Table 2.3 displays the result of the drop test. As expected, the previous connector (3.5 × 2 mm carbon pipe) was not able to survive the impact even at the minimum required speed of 1.5 m/s (70 % damage). In contrast, the 3.5 mm carbon rod completely handled the impact up to a flight speed of 2 m/s. In all cases, the ABS plastic joints survived.

Finally, the estimated weight of the two spherical shells is listed in Table 2.4. It shows

Table 2.3: Drop test result.

CFRP material	Collision speed (m/s)	Drop height (m)	No. of samples	No. of damaged samples	Damage (%)
3.5 mm x 2 mm pipe	1.5	0.16	10	7	70
	2	0.3	10	10	100
3.5 mm rod	1.5	0.16	10	0	0
	2	0.3	10	0	0

Table 2.4: Estimated weight of two spherical shell for Rc = 0.5 m.

	2V geodesic	3V geodesic-based fullerene
No. of Joints	42	60
Estimated Weight per Joint	2 g	2 g
Sub-total Weight	84 g	120 g
Total Length of Connections	34.9 m	18 m
Weight Density per Connection	9.5 g/m	11 g/m
Sub-total Weight	331.9 g	198 g
Total Weight	415.9 g	318 g

that the fullerene has 23.54 % less weight than the 2V geodesic structure for $Rc = 0.5$ m.

2.5.4 Improving the Flight Capability of the UAV

As mentioned in Chapter 2.5.1, the initial UAV is an off-the-shelf Zion EX450 quadcopter. It is then redesigned because of the need for additional payload and endurance. The proposed brushless motor is shown in Fig. 2.9. This brushless motor is expected to increase the maximum take-off weight by 40 % from the original capacity of 2000 g. However, this brushless motor is 200 % heavier than the initial motor of 66 g. It also requires 25 to 30 A current rating for the ESC (electronic speed control). The majority of the power is consumed by the four motors of the UAV, taking up to more than 95 % of the total power. If the rated current drawn by the motor is estimated to be half of the maximum rating (30 A), then for the given rated voltage of 11.1 V (3S cell battery), the power consumption of all the motors is 666 W. The estimated power consumption of all the components are listed in Table 2.5.

Figure 2.9: Proposed brushless motor for the new UAV.

Table 2.5: Estimated power consumption of all the components

Component	Voltage (V)	Current (A)	Power (W)
Main Motor	11.1	15	666
Controller	5	0.3	1.5
Guide Light	12	0.025	3.6
Servo Motor	6	-	2.93
Camera Charger	5	1	5
Transmitter	12	0.72	8.64
		Total Power	687.67

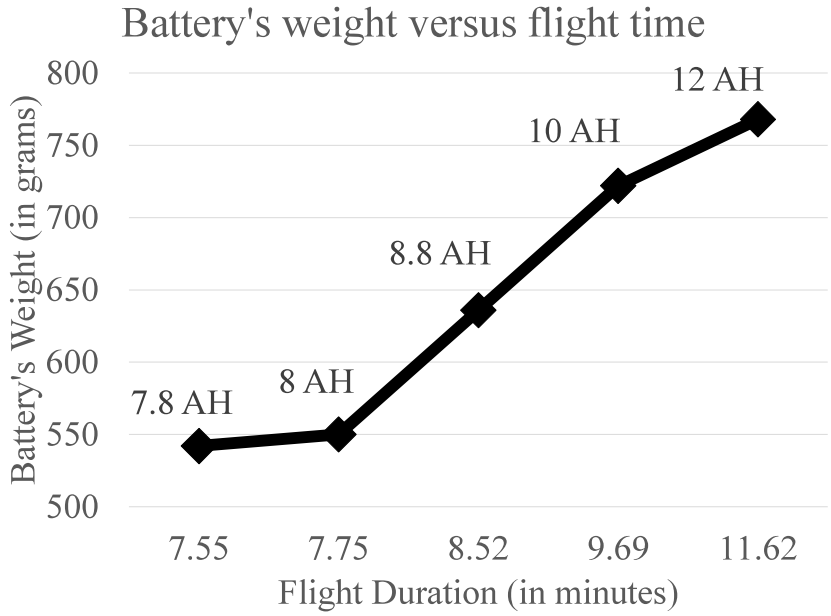

Figure 2.10: Estimated battery's weight versus the flight time.

The flight time of the UAV can be estimated using the total power consumption and the battery rating. As mentioned in Chapter 2.5.2, the size of the battery should be properly selected because even though it will increase the flight time, it will also cause the increase of the overall weight of the system. Fig. 2.10 shows the graph of the flight time versus the weight of each battery. The reserved weight of the battery is 500 to 750 g. The limit is set to ensure other components like gimbal, visual system and spherical shell to be within the weight capacity of the UAV. On the other hand, the estimated flight duration of initial UAV which can only use a maximum battery rating of 3.3 AH due to limited weight is 5 minutes.

The overall diameter of the initial UAV is 704 mm given a 254 mm (10 in.) propeller. As mentioned in Chapter 2.5.2, the size of the UAV should be limited to a certain value because of the limited size of the spherical shell. For the specific mission, the size of the spherical shell is limited to 1000 mm. The size of the UAV is determined based on the

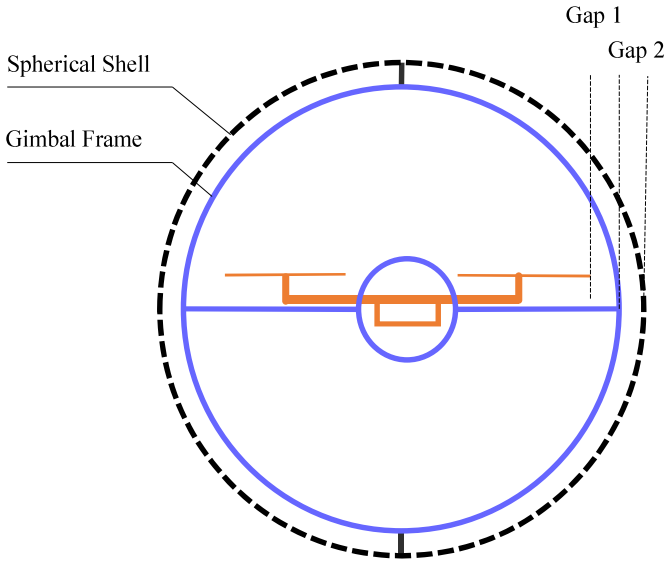

Figure 2.11: Clearance or gap between the UAV, gimbal and spherical shell.

Table 2.6: Initial and the new UAV specification.

	Initial	New	Unit
Propeller Diameter	254	279.4	mm
Overall Diameter	704	730	mm
Overall Weight	1	1.45	kg
Max. Takeoff Wt.	2	2.8	kg
Battery @ 11.1 V	3.3	7.8 to 10	AH
Approx. Flight Time	5	7.6 to 10	min

gap provided between the spherical shell and gimbal, and between the gimbal and the UAV as shown in Fig. 2.11. The safe distance for those gaps is between 50 and 100 mm. This resulted in the size of initial spherical shell equal to 894 mm or about 900 mm. The size of the UAV can still be extended since the spherical shell's limit is 1000 mm. The proposed size of the new propeller is 279.4 mm (11 in.) that is recommended for the new motor. The size of the new UAV is 730 mm while the new spherical shell is 950 mm.

Table 2.6 shows the specification of the initial and the new UAV. The new redesigned rotor-type UAV is shown in Fig. 2.12.

Figure 2.12: New UAV redesigned to provide additional payload and flight endurance.

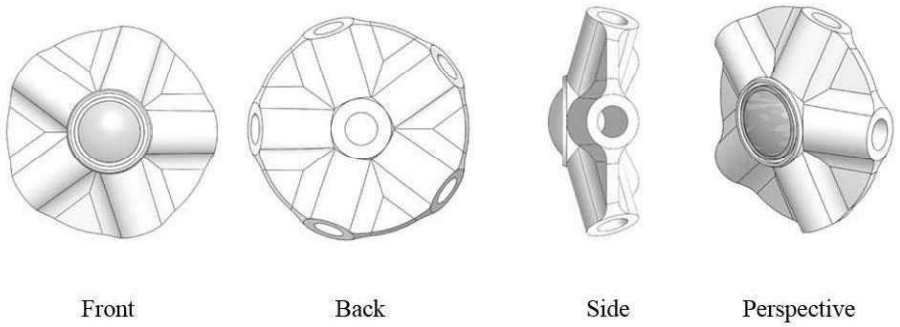

Figure 2.13: Different views of the flat-plate (large-drag type) joint

2.5.5 Minimizing the Drag Force

In this study, the drag effect on the shape of the joints and connections of the spherical shell is considered. The drag force can be minimized by implementing as much as possible efficient aerodynamic shape in all components of spherical shell similar to Fig. 2.2 (b) and (c). For the connection, a cylindrical shape rather than a square shape (both are available in the market) is selected because it can result in a much lower drag based on the drag coefficient comparison between the two shapes as shown in Fig. 2.1. For the joint, the initial design is shown in Fig. 2.13 where the shape is more similar to a flat plate, refer to Fig. 2.2 (a). This type of joint is expected to cause significant air drag especially that the spherical shell is composed of several joints.

Considering the effect of air drag, a new joint design is proposed by applying a streamline or airfoil shape and implement it on the fullerene-type spherical shell. The airfoil shape comes with a variety of design [73] but a simple symmetrical airfoil shape is preferred. This type of airfoil shape has a low drag and produces zero lift force, well-suited for our application. Fig. 2.14 shows the new joint design with the use of airfoil shape.

In this study, the CFD analysis through Solidworks Flow Simulation is implemented. It take advantage of CAD integration since all parts of the spherical shell were designed in Solidworks. In Solidworks flow simulation, the term grid generation is called "meshing". Meshing is vital since it affects the CPU time required, the rate of convergence, and accuracy of the solution. For the simulation of the whole spherical shell, a fine meshes on its boundary and coarse meshes on the rest of the domain is set to optimize the calculation time without affecting the accuracy of the solution. A cut plot of refined mesh in the boundary of the spherical shell is shown in Fig. 2.15.

The simulation inlet velocity flow settings are 4 m/s, 6 m/s, 9 m/s at 1 atm and 293.2 K. Though the velocity settings can be extended to a much higher value but we focused on a realistic value where the UAV with a spherical shell can be applied. The flow simulation conditions are listed in Table. 2.7. The computational geometry and boundary conditions is shown in Fig. 2.16.

First, the simulation for the two different joints (flat-plate and airfoil shape) on various sideslip angle (β) and wind speed is performed. A simulation on cylindrical carbon rod of 100 mm length is also performed. For the whole spherical shell, two separate sets of simulation is conducted. The first set is for the simulation with spherical shell only while the second includes the gimbal mechanism. The second set will be used to verify the wind tunnel experiment for two main reasons. First, it's hard to perform the wind tunnel test without the gimbal mechanism that holds the spherical shell. Second, the gimbal

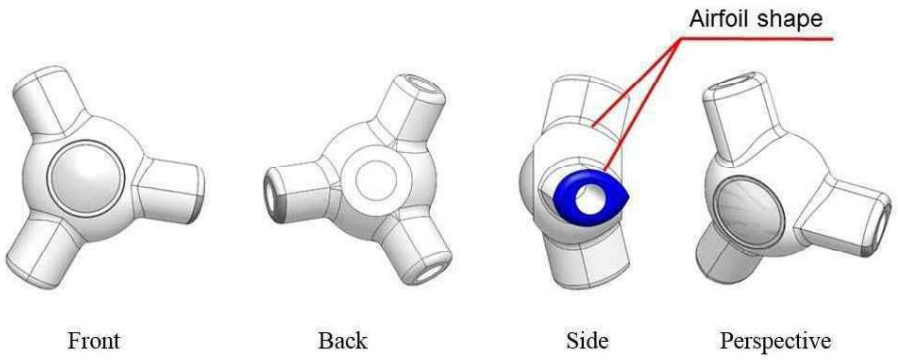

Figure 2.14: Different views of streamline body or air-foil (low-drag type) joint

Table 2.7: Flow simulation conditions

Initial and Ambient Condition		
Pressure	101325	Pa
Temperature	293.2	K
Boundary Condition		
Inlet Velocity	4,6,9	m/s
Body Condition	Non-slip	-

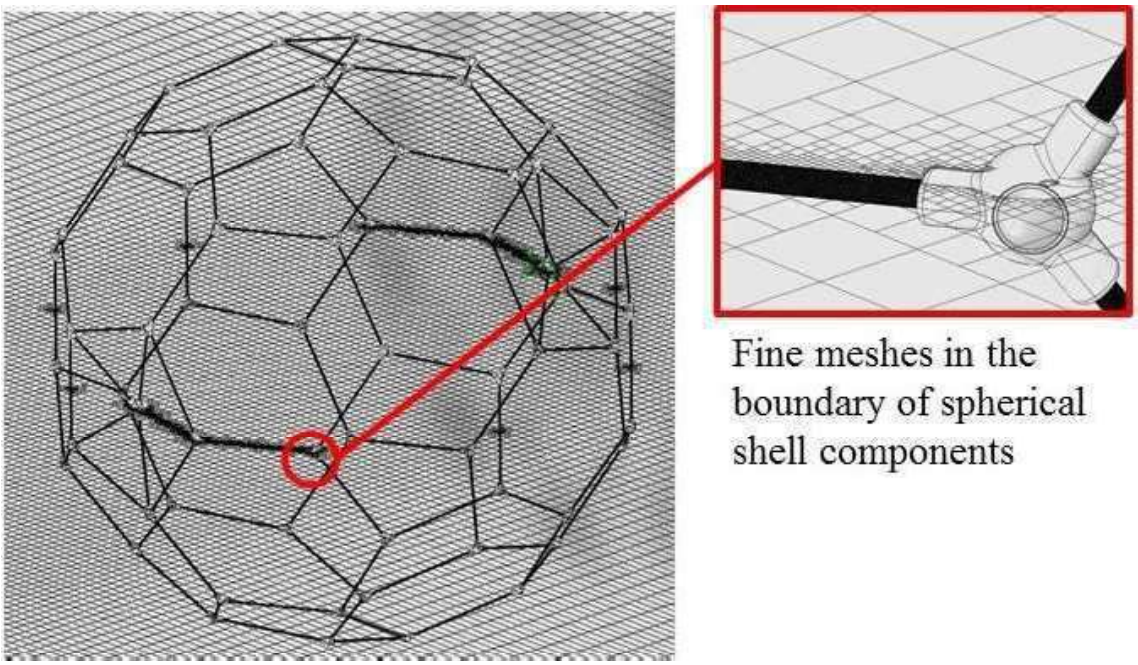

Figure 2.15: Cut plot showing the overall mesh and refined mesh in the boundary of the spherical shell components.

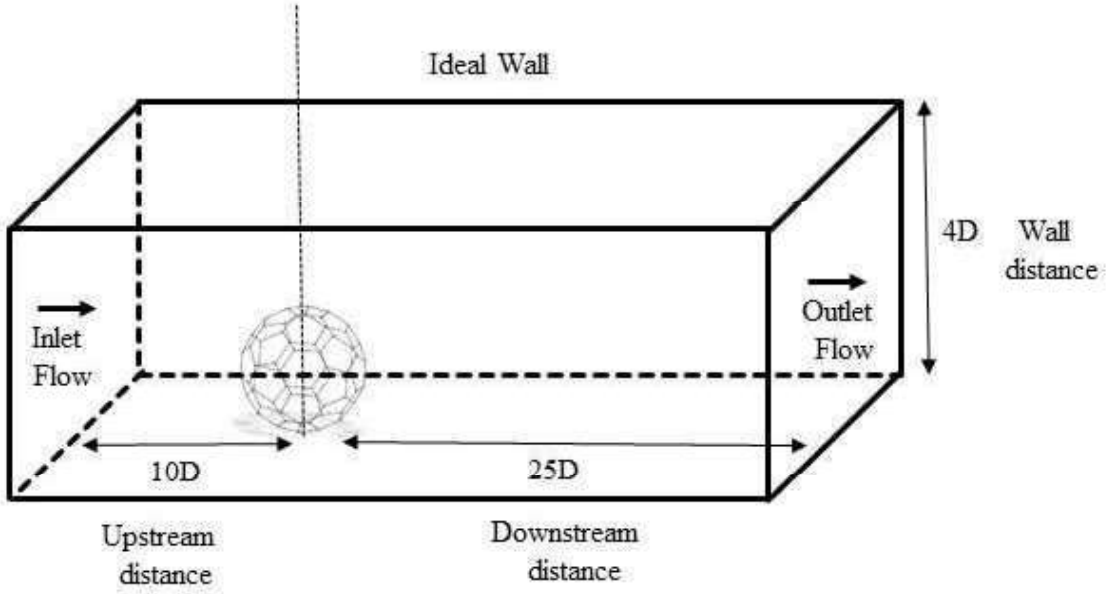

Figure 2.16: Computational geometry and boundary conditions

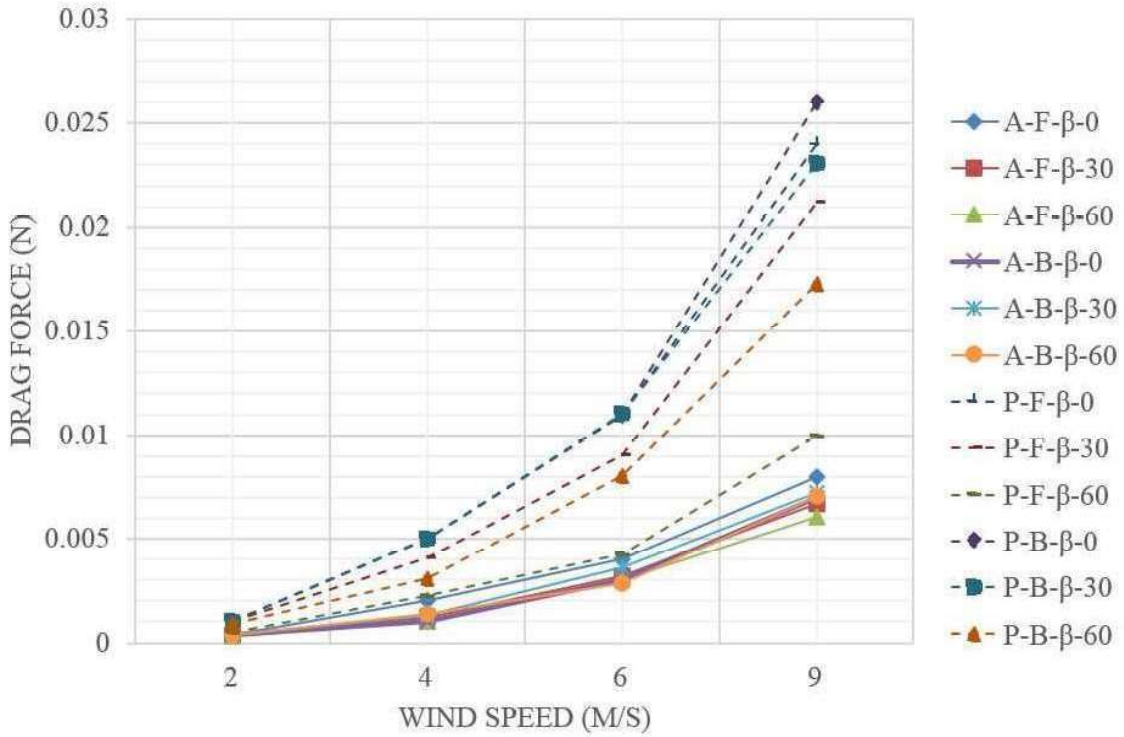

Figure 2.17: Drag force of two joints for different wind speed and sideslip angle (β). Note: A, P, F, B means airfoil, flat-plate, front side, back side, respectively.

for the two shells has a different dimension that would have been directly eliminated to obtain the difference of drag force for the spherical shell only. Only one reference axis is selected for the air to flow since the structure is almost symmetrical and it means that the drag force is approximately equal on the different axis. The yaw axis of rotation of the spherical shell is selected as reference.

After the computational process had been completed, the data were then extracted. Likewise, visualizations were also generated to illustrate its characteristics on the flow of interest. The numerical and visual results of the simulation are presented. Fig. 2.17 shows the results of the flow simulation for the two (2) joints on a different wind speed and β. All dashed lines indicate a flat-plate joints while all solid lines are for the airfoil joints.

Subsequently, the flow trajectories of the velocity for both joints are extracted. In Fig. 2.18, it shows a smaller wake flow region due to the shape of airfoil joint. In Fig. 2.19, it is noticeable that there leaves a large wake slow velocity flow region due to the shape of the flat-plate joint.

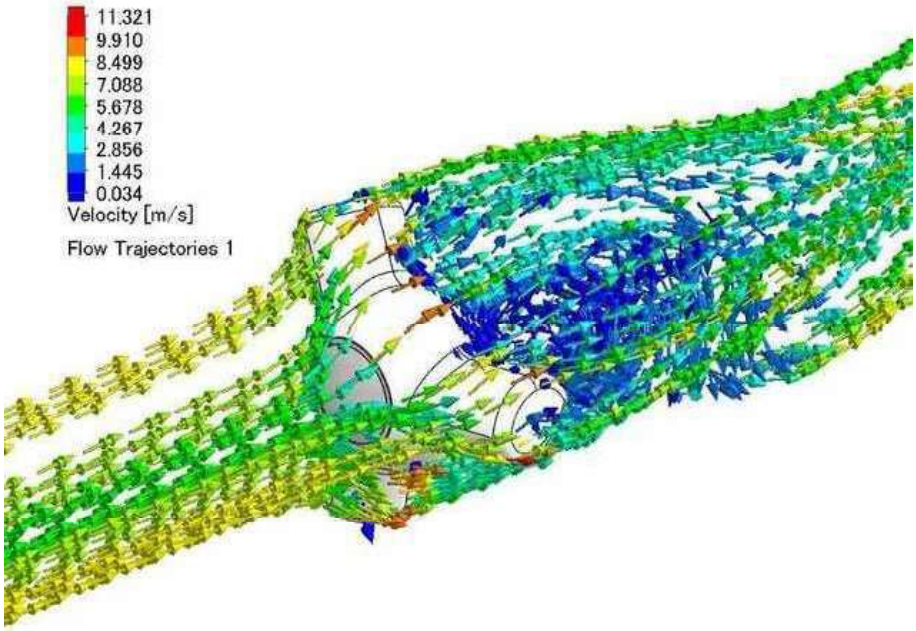

Figure 2.18: Flow trajectory of airfoil joints showing a smaller wake region.

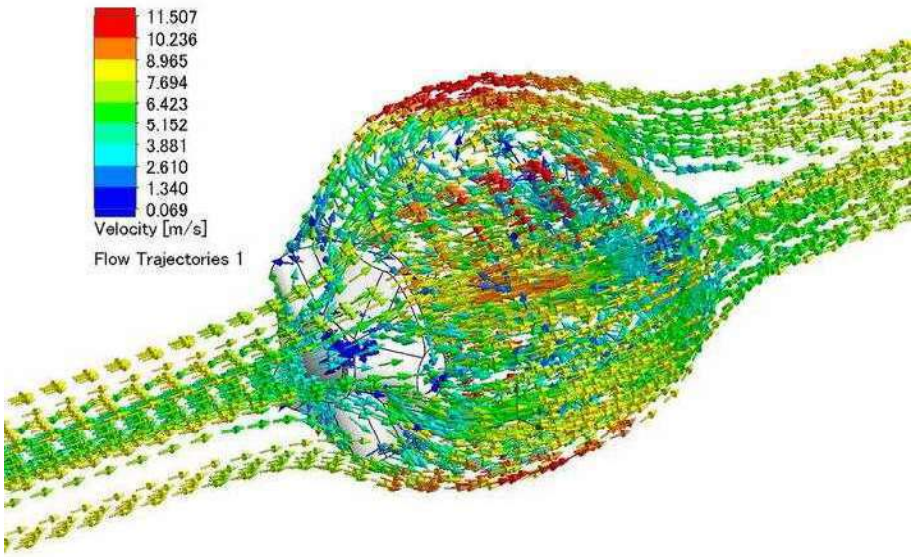

Figure 2.19: Flow trajectory of flat-plate joints showing large wake region.

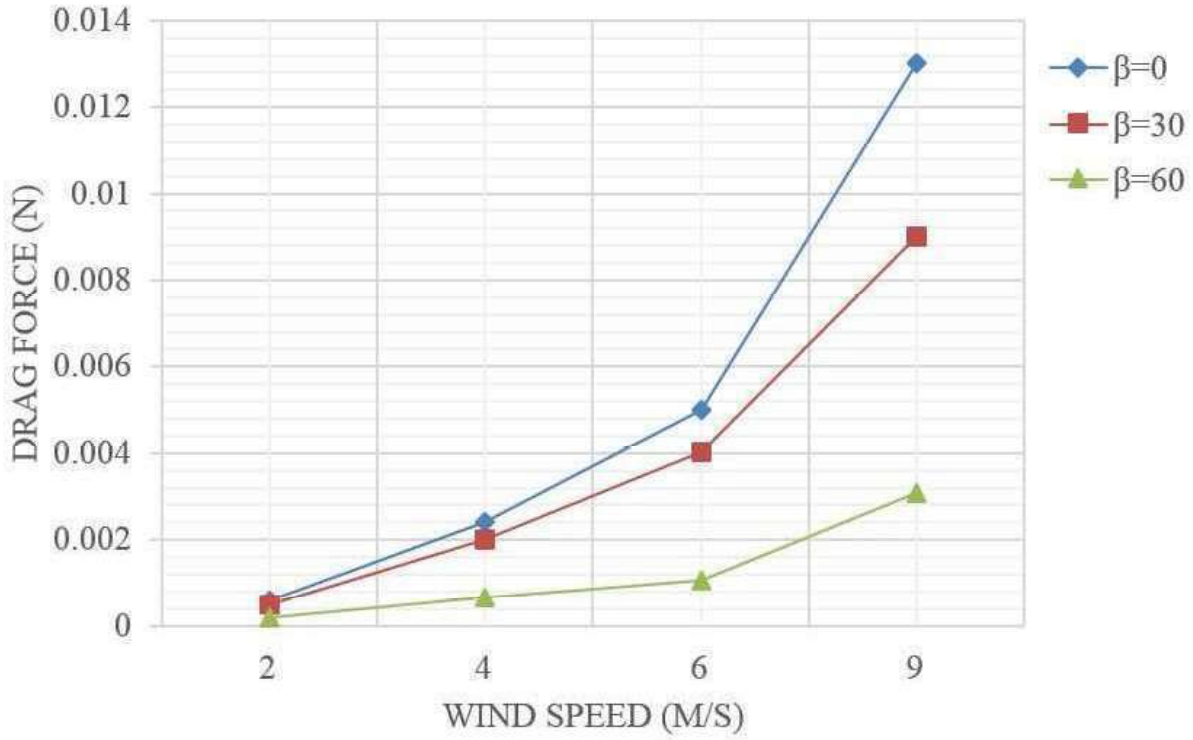

Figure 2.20: Drag force of 3.5 mm cylindrical carbon rod of 100 mm length for different wind speed and β.

The simulation result of drag force for 3.5 mm diameter cylindrical carbon rod of 100 mm length is plotted in Fig. 2.20 for different wind speed. Isoline cut plot of cylindrical rod is shown in Fig. 2.21.

The simulation result of the two spherical shells for various wind speed are also plotted in Fig. 2.22. Visualizations are plotted in Fig. 2.23 and 2.24 showing the wake flow region for the two spherical shells.

The distribution of drag force for the components of the two spherical shells is plotted to determine the contribution of joints and connections as shown in Fig. 2.25.

Although CFD simulation is cost-effective approach to predict the drag force of spherical shell, however it not 100% reliable. Thus, it is much better to perform wind tunnel experiment for validation as it provides more accurate result. A wind tunnel experiment at Chofu Aerospace Center of Japan Aerospace Exploration Agency (JAXA) in Tokyo, Japan is conducted. Their low speed wind tunnel with test section size of 2 m x 2 m (operates at 3 to 60 m/s) have enough testing capability for the dimension of the spherical shell [74]. The entire wind tunnel system is shown in Fig. 2.26.

The experiment focused on conducting test at free stream velocity of 4,6, and 9 m/s. The condition is 1 atm of pressure at 297.15 K. Two sets of experiment were performed to obtain the required output. The first set includes the spherical shell, gimbal, and dummy UAV while the second set includes only the dummy UAV. A small correction was added

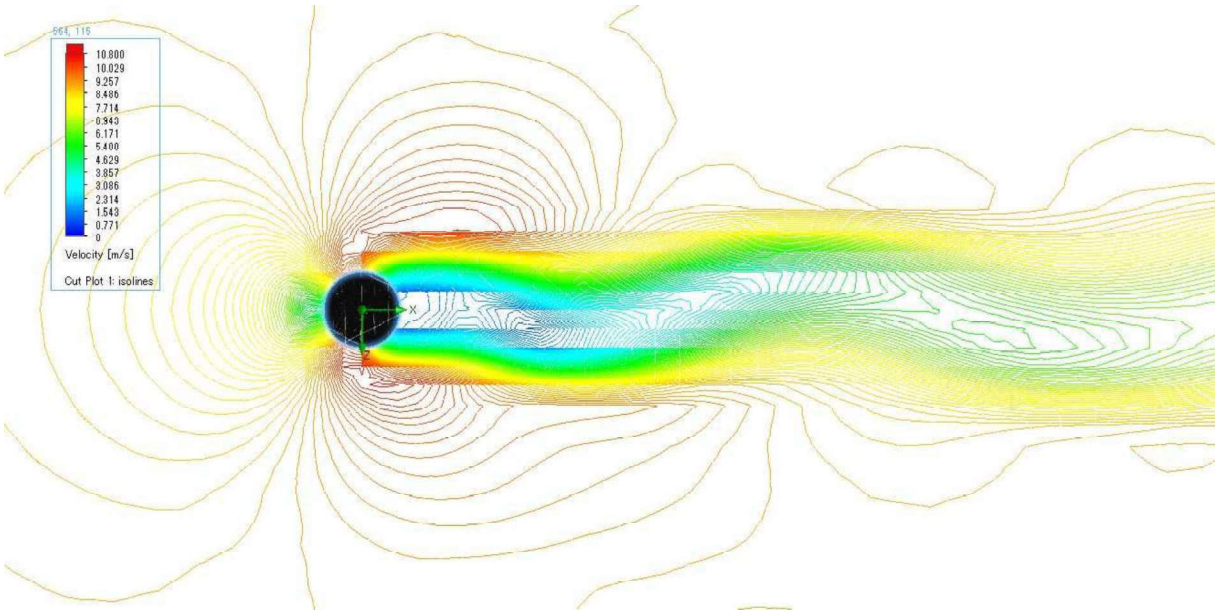

Figure 2.21: Isoline of cylindrical rod showing the wake at 9 m/s, t = 8 sec.

to eliminate the drag force caused by the sting in which the JAXA already have data on it.

After the experiment was completed, the drag force data for different wind speed were extracted for further analysis. Fig. 2.27 shows the data from wind tunnel experiment.

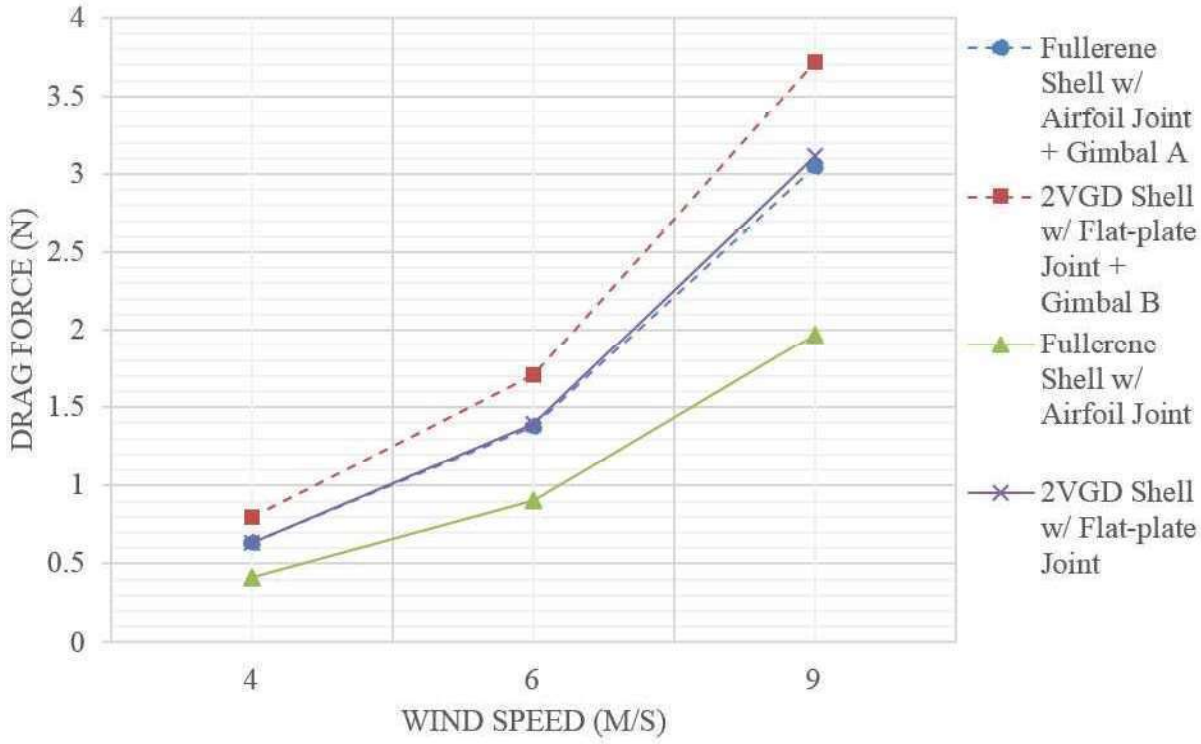

Figure 2.22: Drag force of the spherical shells for different wind speed

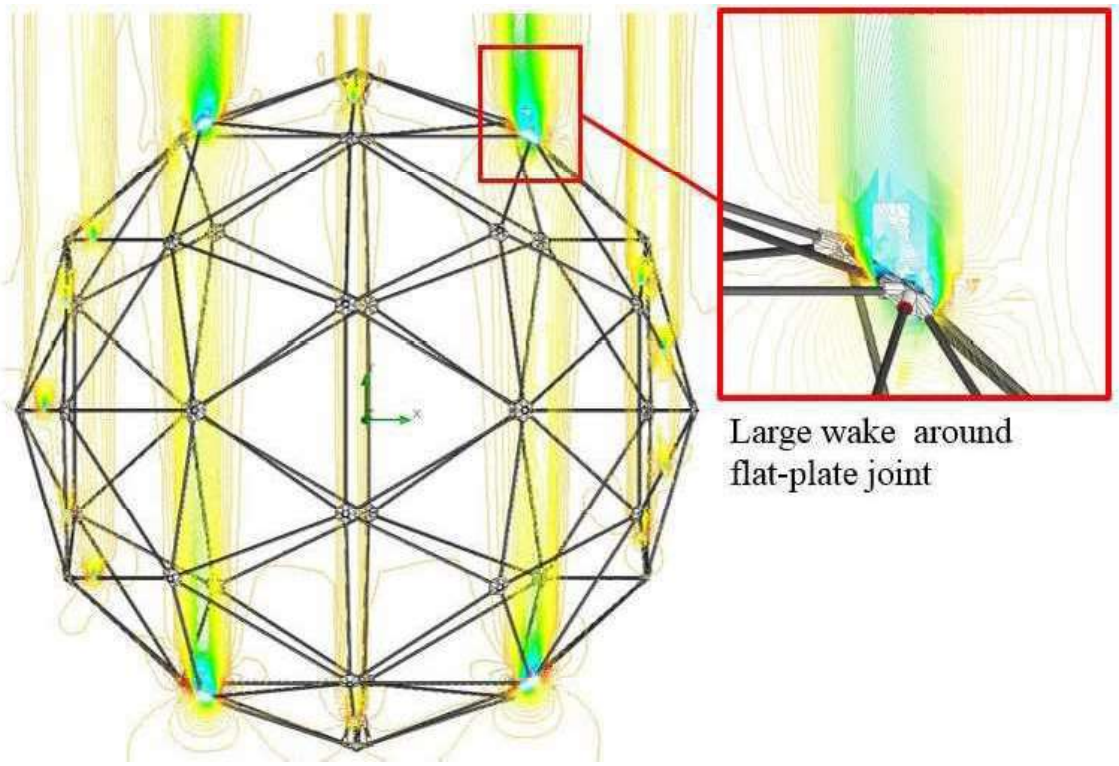

Figure 2.23: Isoline cut plot of 2V geodesic structure spherical shell showing large wake at flat-plate joint

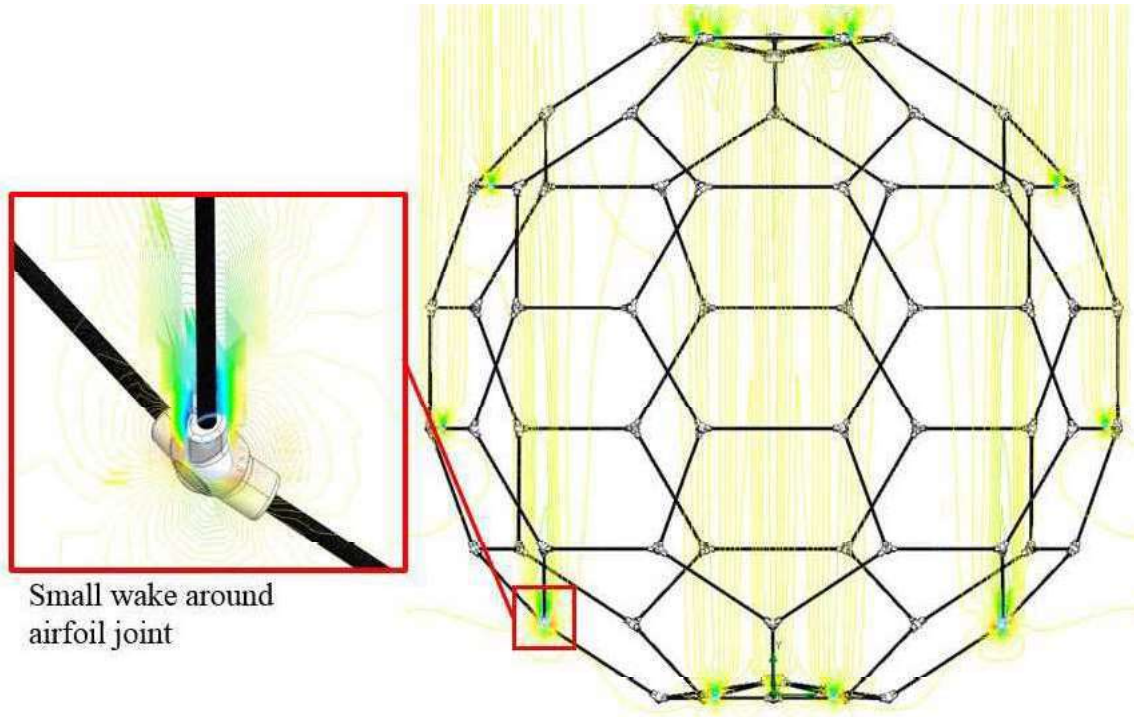

Figure 2.24: Isoline cut plot of fullerene structure spherical shell showing smaller wake at airfoil joint

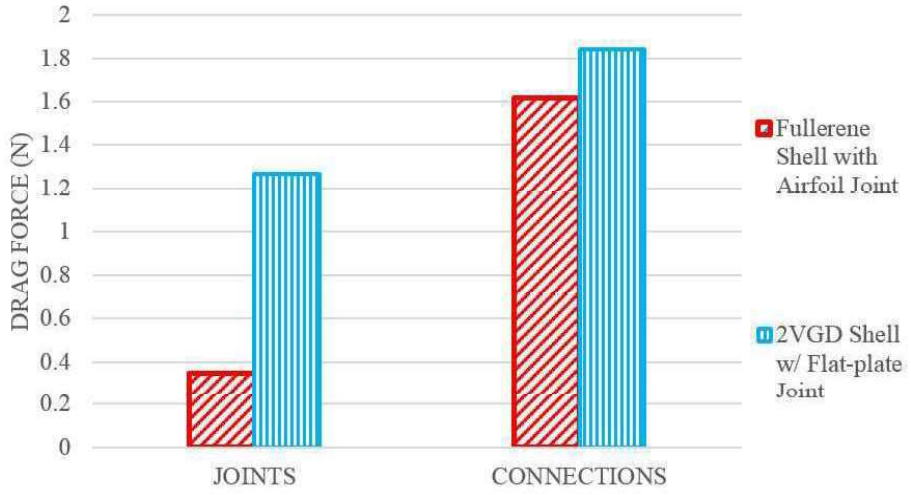

Figure 2.25: Drag force distribution of joints and connections at 9 m/s wind speed for spherical shell.

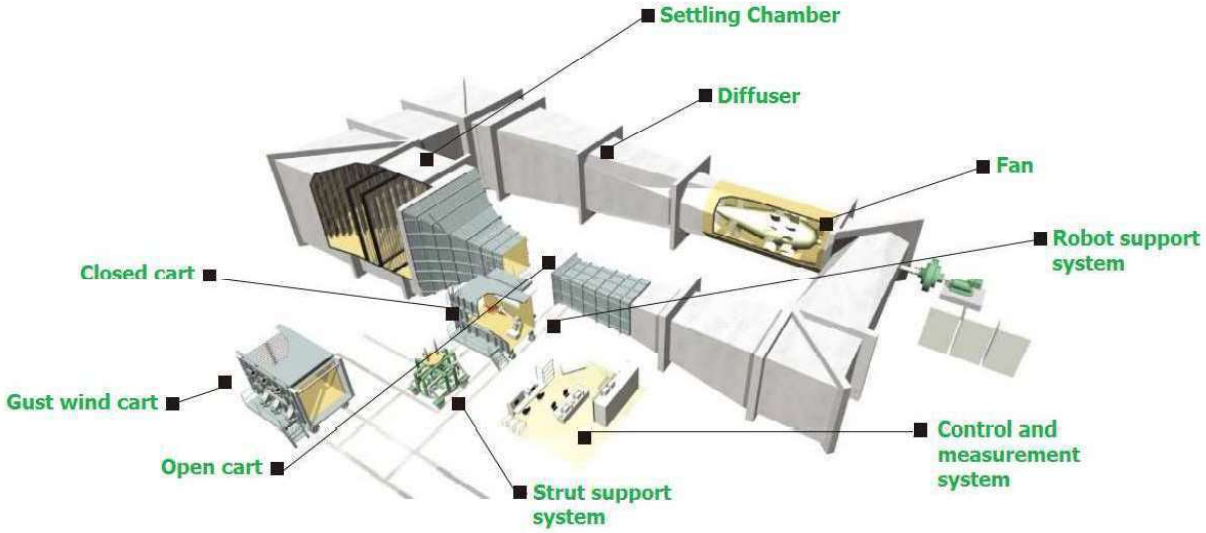

Figure 2.26: 2m x 2m Low-speed Wind tunnel

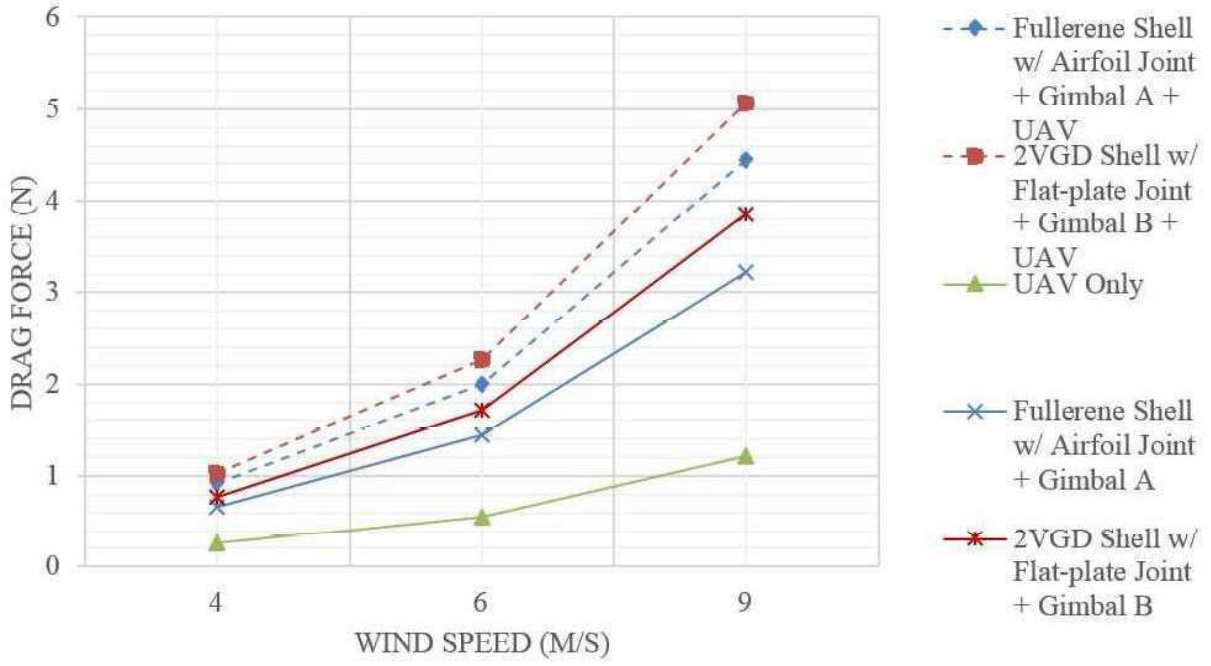

Figure 2.27: Numerical results of drag force from wind tunnel experiment

The spherical shell + gimbal drag force was obtained by subtracting the dummy UAV's drag force.

For the evaluation of the two joints, the simulation result in Fig. 2.17, shows that the drag force of flat-plate decreases as β increases and has a maximum drag force of 0.026 N at 9 m/s hitting the back side with β=0. Meanwhile, the drag force of all airfoil joint is almost constant with low drag values for all β and sides and develop a maximum drag force of 0.008 N at 9 m/s. In an actual spherical shell, the joints are in different orientations which make it difficult to evaluate individually but can be assessed as a whole.

Fig. 2.25 shows the drag distribution of the spherical shell components. All airfoil joints (60 pieces) has a total drag force of 0.3514 N compared to the flat-plate (42 pieces) of 1.2691 N at the wind speed of 9 m/s. Also, the airfoil joints contribution is only 17.88 % for the whole fullerene-type spherical shell. While the flat-plate joints contribution is 40.78 % for the entire 2V geodesic spherical shell.

For the cylindrical carbon rod, the simulation result in Fig. 2.20 shows a maximum drag force of 0.013 N at 9 m/s and decreases as the β decrease. Similarly, the carbon rods as connections are difficult to assess individually because their orientations are unique but the drag force can be determine as a whole.

The total drag force of the connections in Fig. 2.25 are 1.6139 N and 1.8427 N at 9 m/s for fullerene and 2V geodesic structure, respectively. The result indicates that the lesser the total length of the connection, the lower the drag force. Though the orientation of the connection has a large impact on the drag force.

The validity of our simulation results based on the wind tunnel experiment data are

verified. The wind tunnel test only provide drag force data with gimbal mechanism, thus, the simulation results with gimbal mechanism are used for comparison. The simulated drag forces at 9 m/s are 3.0521 N and 3.7172 N while the wind tunnel data are 3.2228 and 3.8501 N for fullerene and 2V geodesic-type spherical shell, respectively.

The percentage error of simulated drag force versus wind tunnel drag force for the two spherical shells are 5.30 % and 3.45 %. These errors are still in acceptable level considering that a small discrepancy in actual and CAD model exist and other computation errors. Other factor is the difference in drag force estimation of the simulation and wind tunnel experiment.

For the spherical shell alone, the simulated drag force at 9 m/s in Fig. 2.22 for fullerene-type with airfoil joint and 2V geodesic with flat-plate joint are 1.9623 N and 3.034 N, respectively. The drag reduction is 1.0717 N or almost equivalent to 1/3 of the 2V geodesic with flat-plate joint. The combination of fullerene structure and airfoil joint reveal that it is very effective in reducing the overall drag force.

Based on the result, the fullerene-type with airfoil joint spherical shell is then utilized in the actual field experiment with the presence of the wind.

2.5.6 The Newly Improved System

Fig. 2.28 shows the newly improved UAV with a passive rotating spherical shell. The final dimension of the spherical shell outer diameter is 950 mm. Its inner dimension of 875 mm provides space for the UAV and gimbal mechanism. The fabricated gimbal mechanism has an inner and outer diameter of the octagonal-shape outer frame that is equivalent to 770 mm and 830 mm, respectively. This dimension provides enough space for the UAV and spherical shell. Lightweight carbon pipe and aluminum were used for the outer and inner gimbals, respectively.

Table 2.8 shows the comparison and specification of the new and initial system. The specification of the old system is revealed in the previous paper [32] [75]. The specification of the new system is based on the 7.8 AH battery rating. The overall weight of the new system is equivalent to 2297 g, which is about 82 % of the maximum take-off weight of the new UAV. This gives an extra payload of 503 g compared to the initial system with only 120 g extra payload. As mentioned in Chapter 2.5.2, the extra payload is necessary for the additional load specifically the camera system needed for visual exploration. Also, extra payload means extra thrust that also means there is an excess power. Excess power is necessary to help for climbing or accelerating especially in the presence of strong winds, this statement is also mentioned in Chapter 2.5.2. The thrust-to-weight ratio (T/W) of the new system is 1.22, higher than the initial system that is equal to 1.06. The T/W determines the performance of the system. The higher is T/W, the better performance for the UAV.

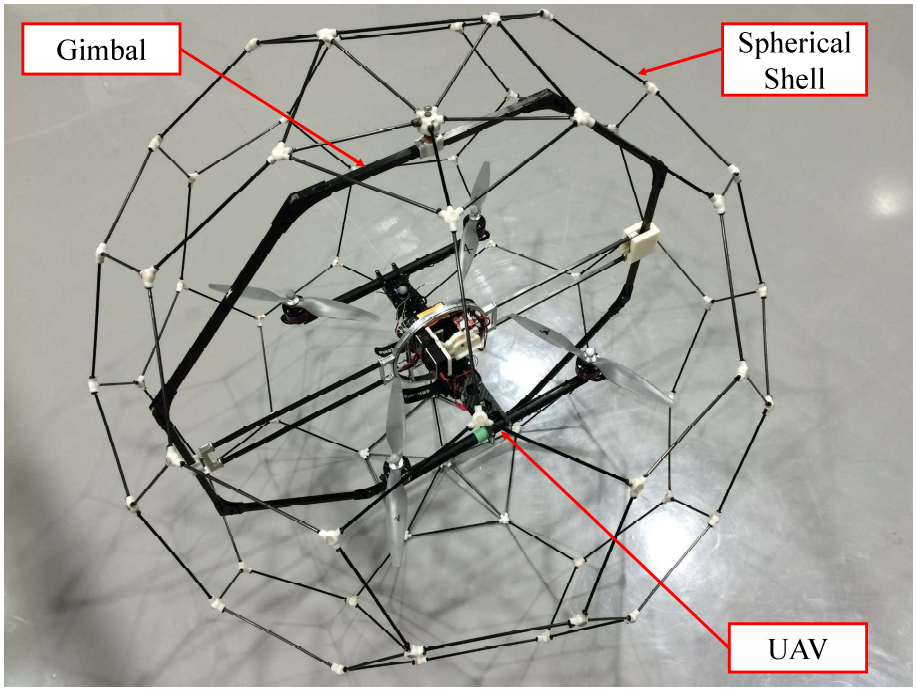

Figure 2.28: Newly improved UAV with a passive rotating spherical shell.

Table 2.8: Comparison and specification of the new and old system.

Initial System	Specification	New System
894 mm	Spherical shell diameter	950 mm
416 g	Spherical shell weight	318 g
1000 g	Weight of UAV including the battery	1450 g
1880 g	Overall weight	2297 g
2000 g	Maximum take-off weight	2800 g
120 g	Extra payload	503 g
1.06	Thrust to weight ratio	1.22

2.6 Close Visual Bridge Inspection Using UAV with a Passive Rotating Spherical Shell

2.6.1 Bridge Inspection and the Issues

A bridge is an important investment in the transportation network that plays a vital role in an economy and is a prerequisite for future growth. Any problems caused by deterioration or damage resulting from a disaster is a serious problem that may result in the collapse of the whole bridge. In Japan, these problems are taken seriously because of the country's tendency to suffer from natural disasters such as earthquakes and tsunamis. Subsequently, Japan is facing a deterioration problem on bridges that is a result of the increasing number of old bridges. As of 2013, there are about 700,000 bridges in Japan and the Ministry of Land, Infrastructure, Transport and Tourism (MLIT) reported that the percentage of bridges over 50 years old is expected to rise from 18% to 43% by 2023 and then to 67% by 2033 [2].

In response, Japan is aiming for a full-scale maintenance that includes the implementation of routine close visual inspection for all the bridges every five years. However, the number of human bridge inspectors in Japan is not sufficient to cover all domestic bridges and will not increase because of safety concern about inspectors, decreasing birthrate, and an aging population. Also, there is an issue that an inspection by a human requires temporary scaffolds that are expensive and take time to construct as well as ladder trucks that often block traffic. Therefore, the Japanese government has launched several programs to facilitate the development of robots for bridge inspection that can check critical parts of a bridge with less time, cost, human inspector, and traffic disruption requirements. For instance, the cross-ministerial Strategic Innovation Promotion (SIP) program has funded developers of bridge maintenance/inspection systems. Also, the implementation of Next Generation Robots for Social Infrastructure (NGRSI) by MLIT has provided opportunities to perform field tests on actual bridges.

In previous years, researchers introduced mobile robots with unique bridge inspection methods [63] [64] [65]. Today, many researchers focus on UAV for bridge inspection, for example, Kim et al., 2015 uses a UAV for crack detection because of its efficient capability to move and collect information above the ground [67]. However, a common UAV without proper protection and a mechanism to maintain stability during unavoidable collisions with an obstacle cannot be used for the close visual inspection of bridges with complex structure because of the high risk of falling.

NGRSI has also released an official requirements for a UAV system that will be used in visual bridge inspection as shown in Table 2.9. The objective of this study that is in-line with the NGRSI project is to satisfy three important requirements for close visual bridge inspection using the UAV. The following requirements are (1) able to access complex parts

Table 2.9: NGRSI requirements for visual bridge inspection robot.

TYPE	STAGE	REQUIREMENTS
Required	Field operation	Use of robots instead of human bridge inspectors
		Acquire data to evaluate the degree of damage (e.g., at least 0.1 mm crack width)
		No scaffolding
		Safe and secure operation
Optional		Access/inspect complex parts of the bridge
		No use of a ladder/inspection truck
		Less affected by external illumination
		Inspection of critical parts of the bridge
	Indoor works	Facilitate in making report on the degree of damage
		Summarization of inspection result
		Improve the accuracy in characterization of damage
	Utility	Ease of transport and deployment
		General use for a wide range of bridge types
		Clear and objective specification of the system performance

of the bridge, (2) able to inspect critical parts of the bridge, and (3) able to acquire images with at least 0.1 mm crack width. However, the third requirement will be obtained based on the sample test image. The acquisition of actual images like cracks or any damages will be performed by the project collaborator. Their focus is to develop robust visual system while this study focuses on acquiring images only.

2.6.2 Bridge Condition and Requirements

The main task is to perform close visual inspection. It is necessary for the PRSS UAV to move into different sections of the bridge efficiently and access narrow paths and spaces. Thus, the size of the spherical shell must be limited according to the available spacing in the bridge. An intensive study of various types of bridge in Japan has been performed to determine the appropriate size of the spherical shell as well as the types of bridges where inspection using PRSS UAV would be suitable.

Fig. 2.29 shows a breakdown of the various type of bridges in Japan's national road network (about 30,000 bridges) [76] . This data shows that an inspection can be performed for 32.7 % of the bridges, which are concrete-type slab bridges and concrete and steel box-girder bridges, regardless of the size of the spherical shell. However, concrete and steel girder bridges, which are respectively 37.2 % and 27.2 % of the bridges, or total of 64.4 % of all bridges (majority of the bridges) require the external diameter of the PRSS UAV to be limited. Fig. 2.30 illustrates the spacing or gaps of concrete and steel girder bridges.

A further study focused on concrete and steel girder bridges to determine the maximum allowable diameter of the spherical shell. Figs.2.31 and 2.32 show a distribution of the

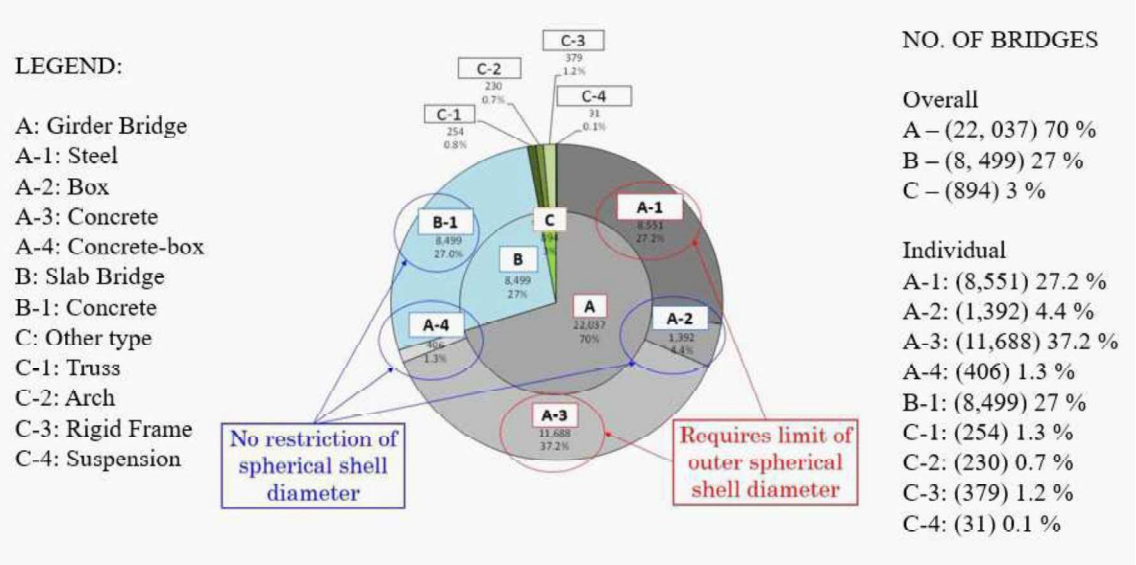

Figure 2.29: Breakdown of various type of bridges in Japan's national road system.

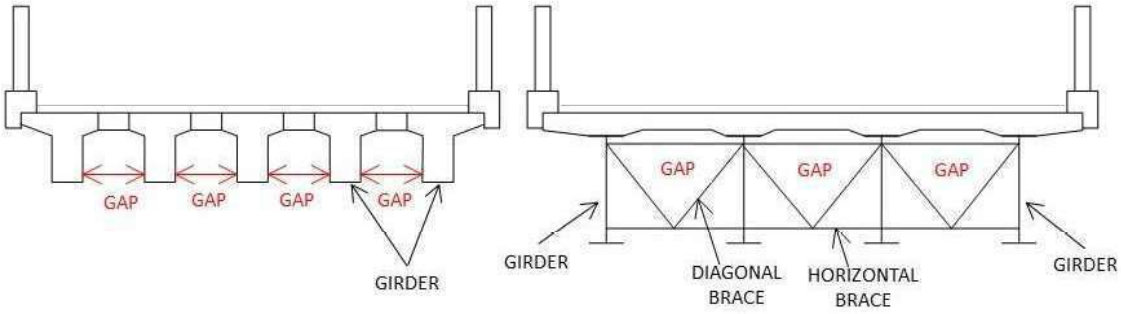

Figure 2.30: A cross-sectional view of concrete (left) and steel (right) type girder bridges.

main girder spacing for concrete and steel girder bridges, respectively [77] [78]. In concrete girder bridges, the main girder spacing of large-scale bridges is between 1.1 and 1.7 m. While, the main girder spacing of small-scale bridges is between 0.6 and 0.8 m. However, small-scale bridges are excluded from consideration of the PRSS UAV design because the elevation of those bridges is low, enough for a human to inspect without any scaffolding.

Similarly, for steel girder bridge, the main girder spacing is between 1.3 and 1.8 m for large-type bridges. Hence, the maximum allowable diameter of a spherical shell for concrete-type and steel girder bridge inspection is 1.1 m and 1.3 m, respectively.

Based on this data, the minimum bridge spacing or maximum diameter for the spherical shell for general use is 1.1 m. However, because of the possible existence of obstructions like piping or other irregularities of the bridge structure, an allowance of about 10 % is added. Hence, the maximum diameter of the spherical shell that can be fabricated is 1 m.

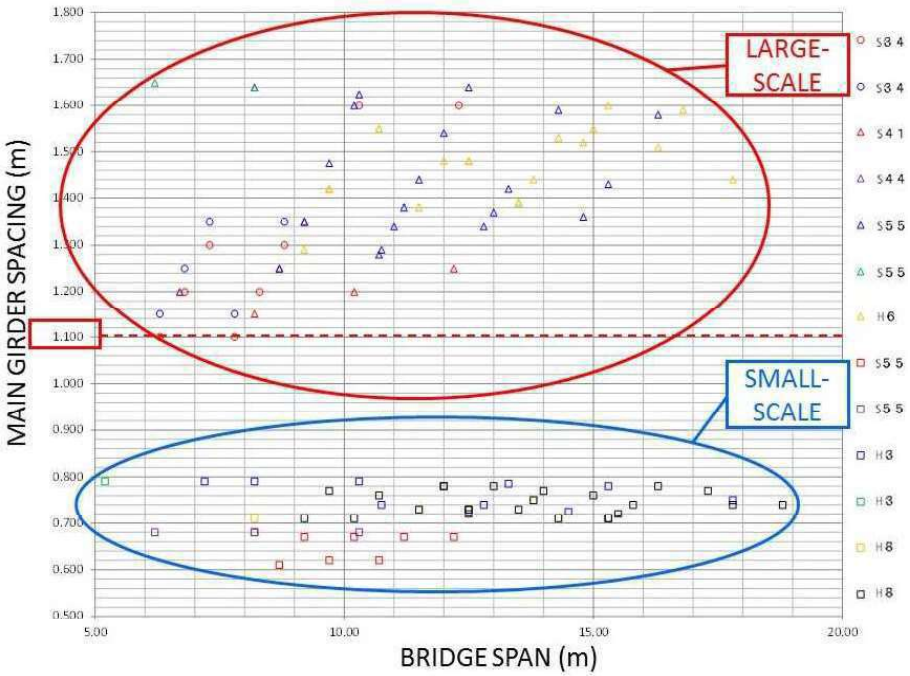

Figure 2.31: Distribution of the main girder spacing for concrete girder bridges.

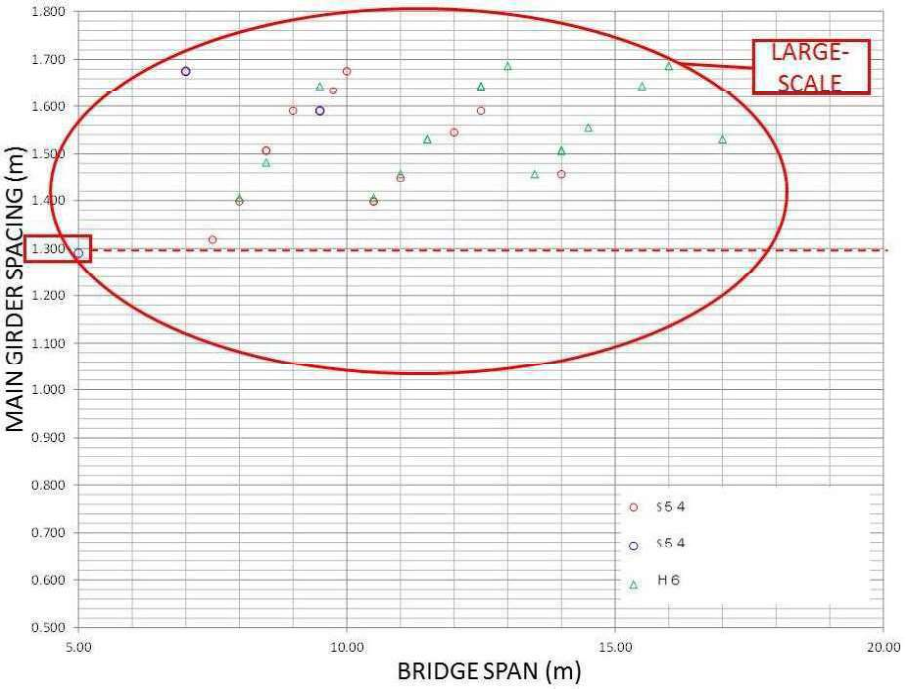

Figure 2.32: Distribution of the main girder spacing for steel girder bridges.

Visual inspection requires a camera to capture images of cracks, corrosions, or any other problem in all critical parts of the bridge. A good image resolution is necessary for better analysis of the bridge condition. Further, the visual inspection should focus on the area where damage regularly develops.

Although it is better to perform inspection all throughout the bridge, determining critical points will speed up the operation. Fig. 2.33 shows a breakdown of damage occurrence points for girder-type bridges based on periodic inspections while Fig. 2.34 shows the specific location of damage (Japan Road Association, 2012), revealing that a large proportion of the damages occurs within the main girders and crossbeams.

A high-resolution camera records all the events during the entire bridge inspection. It is important to provide real-time monitoring from the PRSS UAV's viewpoint for immediate action on significant findings by a bridge inspector. Bridge damages also appears from different angles (at the side, top, or edges), thus this requires a camera that can adjust its position. The camera adjustment should be from 0 to 90 degrees. With the addition of yaw rotation/movement, a full overhead view for our application is enabled.

The visual system set-up is shown in Fig. 2.35. It is categorized into two unit: air and ground. The air unit comprises mainly of the camera, video transmitter, RC signal receiver, servo motor, and a microcontroller while the ground unit includes the video receiver and PC/Tablet. The set-up is similar to widely used on-board camera systems except for the modified camera movement to provide a full overhead view of the

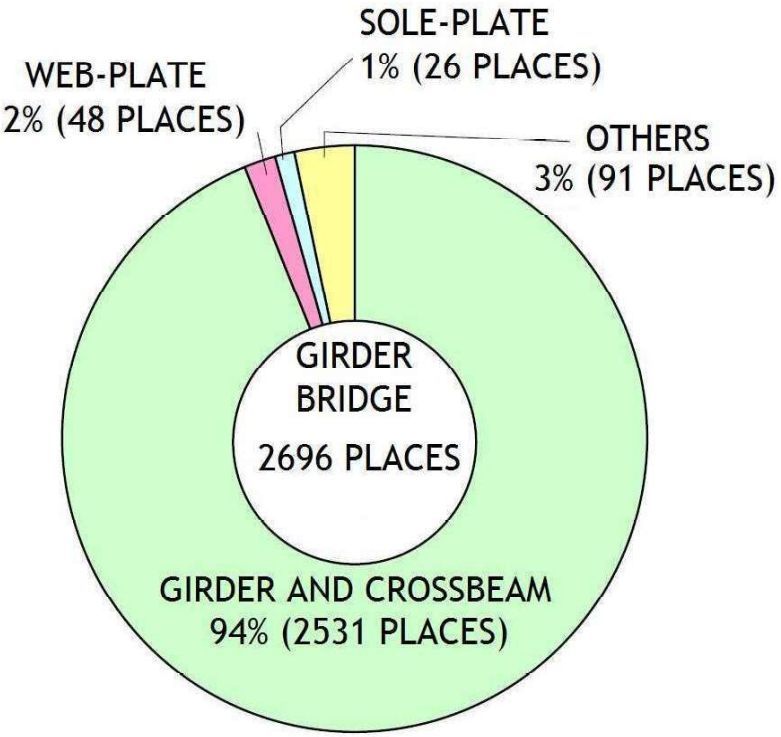

Figure 2.33: Breakdown of damage occurrence in a girder-type bridge.

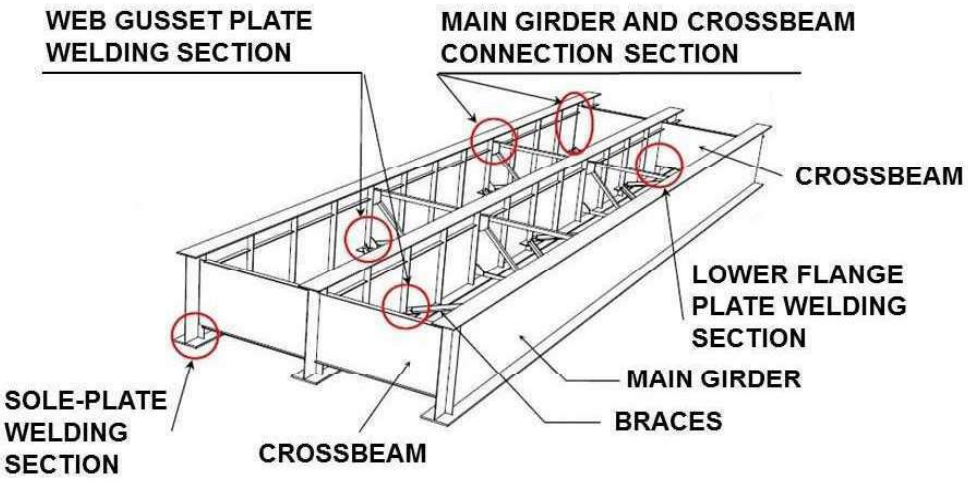

Figure 2.34: Common damage location in a girder-type bridge.

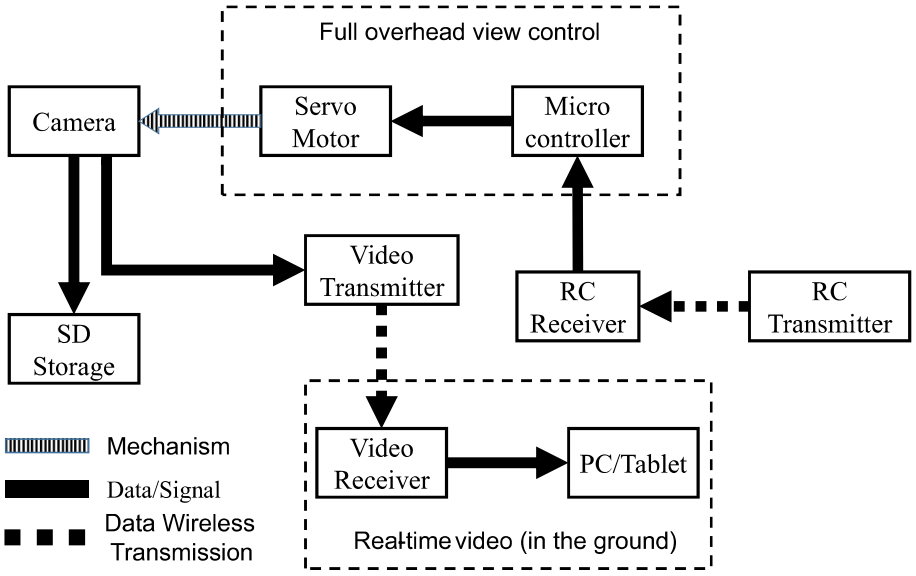

Figure 2.35: Visual system set-up.

bridge structure, an important feature in our bridge inspection task. The system utilizes the lightweight and high-resolution GoPro Hero camera, which is good for indoor and outdoor use [79]. The system also provides a real-time wireless transmission of video from the camera using DJI Lightbridge. A mechanical system was developed for camera tilt while an Arduino Micro, a microcontroller board based on the Atmega32u4, controls the orientation of the camera based on the command sent from the RC transmitter. Figs. 2.36 and 2.37 shows the air and ground units of the visual system. The system has an overall weight of 286 g, 1920×1080 camera resolution, camera proximity distance of 0.5 m, and camera tilt range of 0 to 90 degrees.

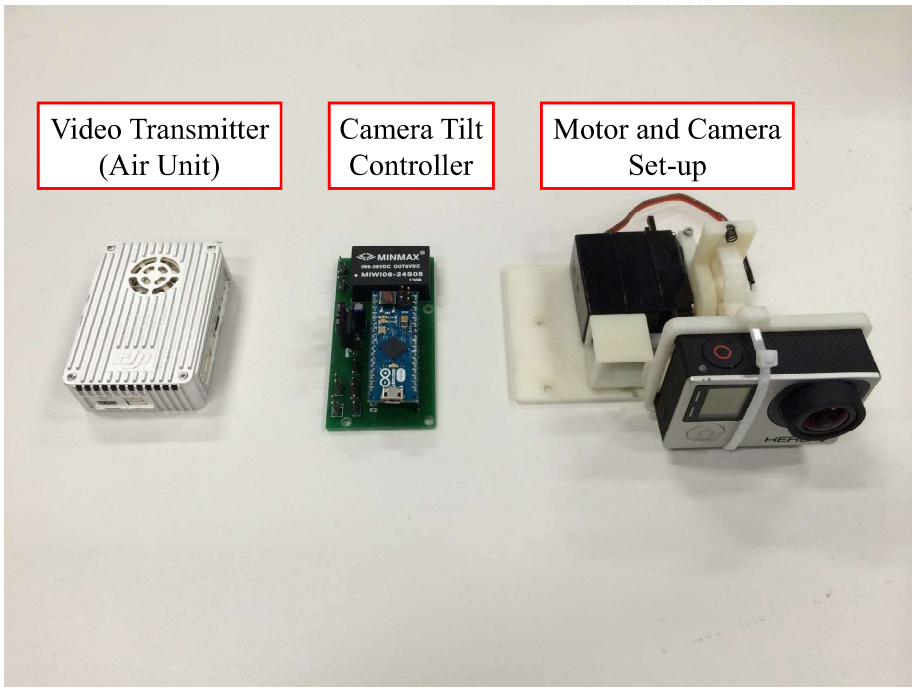

Figure 2.36: Air unit of the visual system.

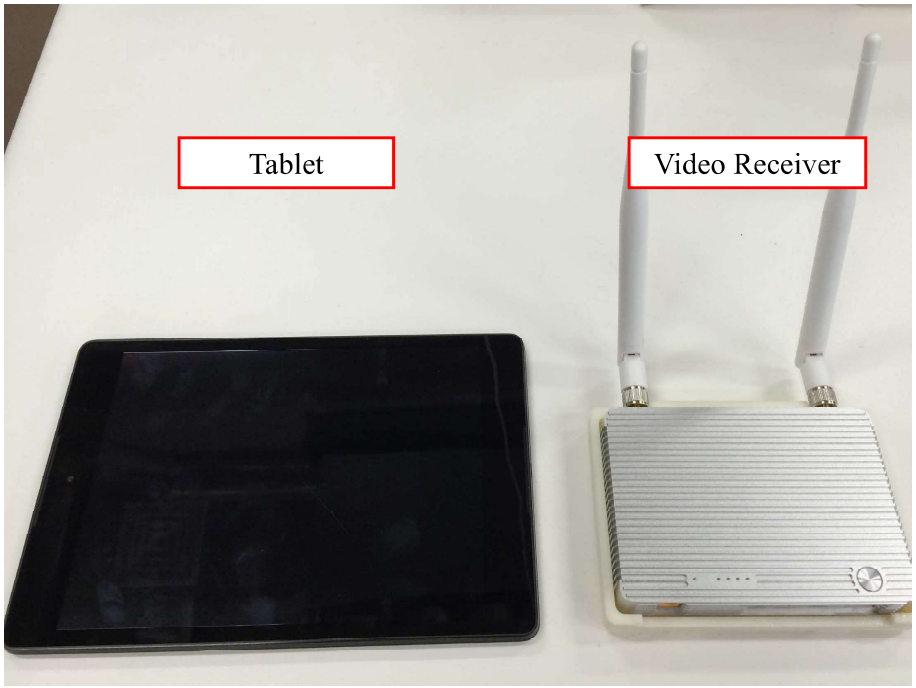

Figure 2.37: Ground unit of the visual system.

2.6.3 Test Flight Replicating Actual Bridge Conditions

The performance of the PRSS UAV was verified prior to actual bridge inspection by implementing a simulated (laboratory-based) bridge inspection, as shown in Fig. 2.38. The set-up had limited spaces and was made of a rigid structure to mimic a bridge. The tool used to record all necessary data for the evaluation such as flight attitude, speed, and duration was a motion capture system using VICON TRACKER software. Five motion capture markers were installed in the UAV and set as an motion capture object to obtain the data. Likewise, image test materials were attached to different positions on the structure to check the performance of the visual system and quality of captured images. The image test material was carefully designed to produce actual line widths from 0.1 to 2.0 mm. Fig. 2.39 shows an image of the PRSS UAV in the bridge mock-up structure during the test flight.

The raw data acquired from the motion capture system were used for post-processing, extracting useful data for analysis. The recorded average flight duration of several test flights was 5.7 min. The average speed of the PRSS UAV was 0.65 m/s. The main purpose of the test flight was to obtain data during collisions with the mock-up structure. Different kinds of collision can happen during actual bridge inspection however, analyzing common conditions will give a better understanding of the PRSS UAV's performance. One type of collision is a horizontal head-on collision with the structure, and a severe collision might occur in this way. Such a severe collision could happen when the PRSS UAV is attempting to get close to the structure in the presence of erratic wind and it abruptly increases its flight speed. Hence, testing the UAV up to its maximum flight speed will give better

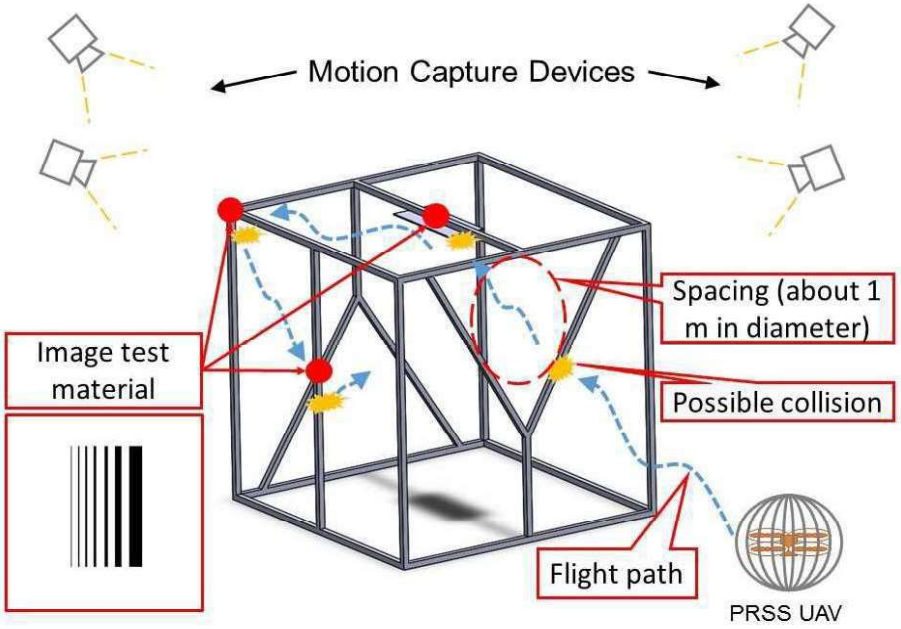

Figure 2.38: Mock-up structure simulating the actual bridge structure.

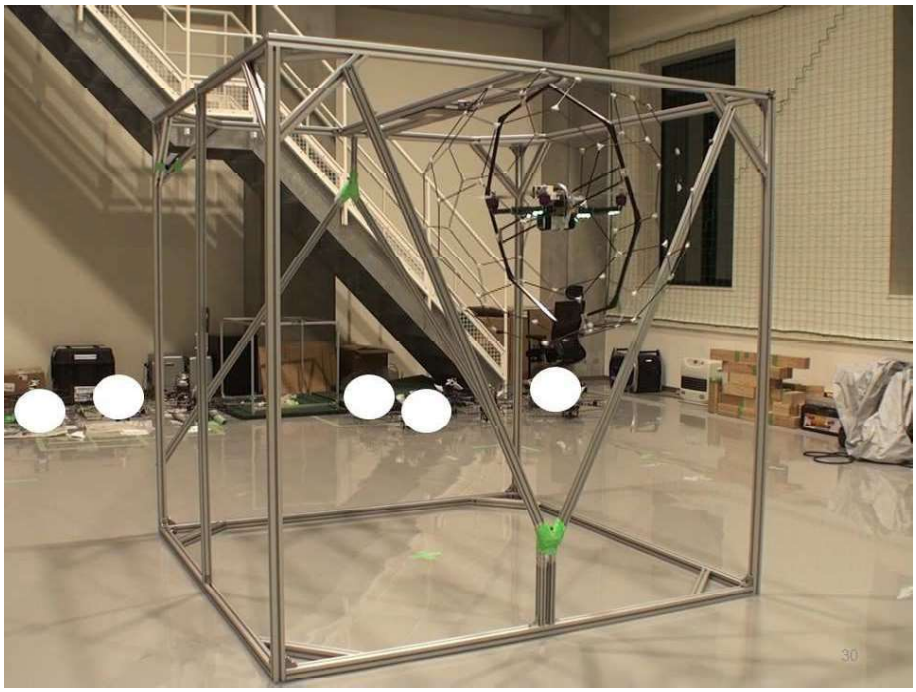

Figure 2.39: An example of an actual test flight (right).

insight about how collision affects the system.

Figs. 2.40 and 2.41 shows the flight attitude at different speeds ranging from 0.7 m/s to 1.4 m/s (close to maximum flight speed). Region A is the flight attitude as it approaches the structure and region B shows the flight attitude shortly after the collision with the structure. All region B data show that horizontal collision causes a slight disturbance with a maximum deviation of 6.5 degrees at 1.4 m/s. Subsequently, a quick recovery to normal flight attitude was possible at all three speeds.

Other possible collisions may happen at average speeds, such as crossing the mock-up structure and vertical head-on collisions. In the crossing scenario, the PRSS UAV collides with the edge(s) of the structure causing disturbances but continuously crossing the structure. In Fig. 2.42, region B has a deviation of about 2.5 degrees maximum after the collision at 0.7 m/s and it recovers quickly about 1 s. Another scenario is a vertical head-on collision. This condition frequently happens when images are taken vertically such as image of the bottom side of the floor slab and main girder. Fig. 2.43 shows one of the flight attitudes during a collision with the top surface as it moves vertically at 0.6 m/s. The collision causes a disturbance in the roll and pitch; however, the effect is insignificant with a deviation of fewer than 2 degrees. The UAV then makes a quick recovery.

All three scenarios, indicates that the UAV is stable. The spherical shell absorbs the effect of collision by a random 3 degree-of-freedom rotation. The insignificant disturbance validates the advantages of using a passive rotating spherical shell.

In the course of the test flight, the visual system was able to vary its camera angle from 0 to 90 degrees. The combination of camera tilt and yaw rotation of the UAV

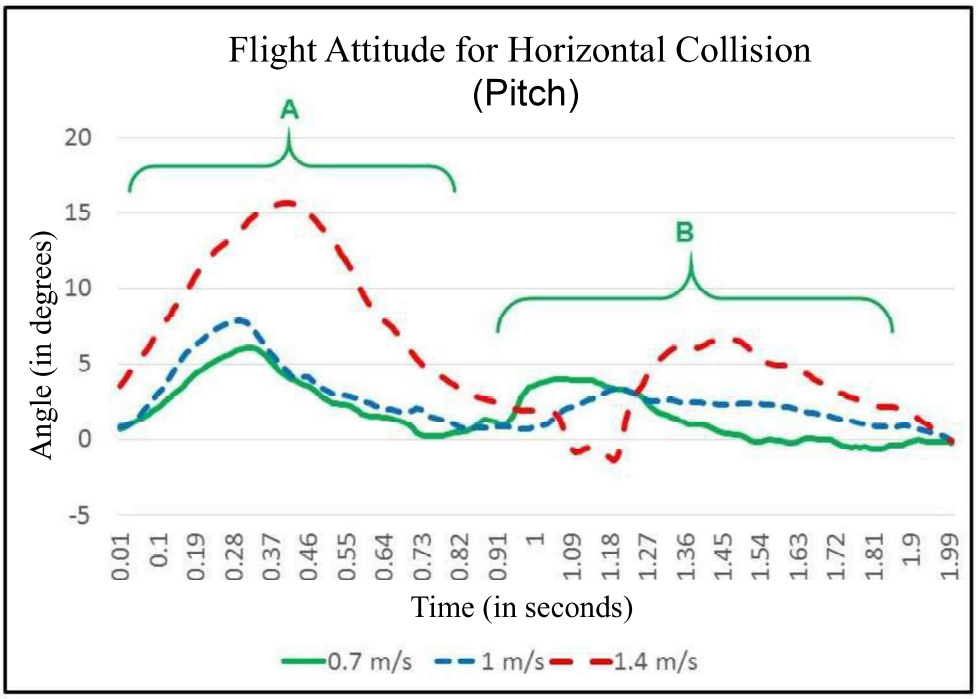

Figure 2.40: Flight attitude (pitch) on horizontal collision at different flight speeds.

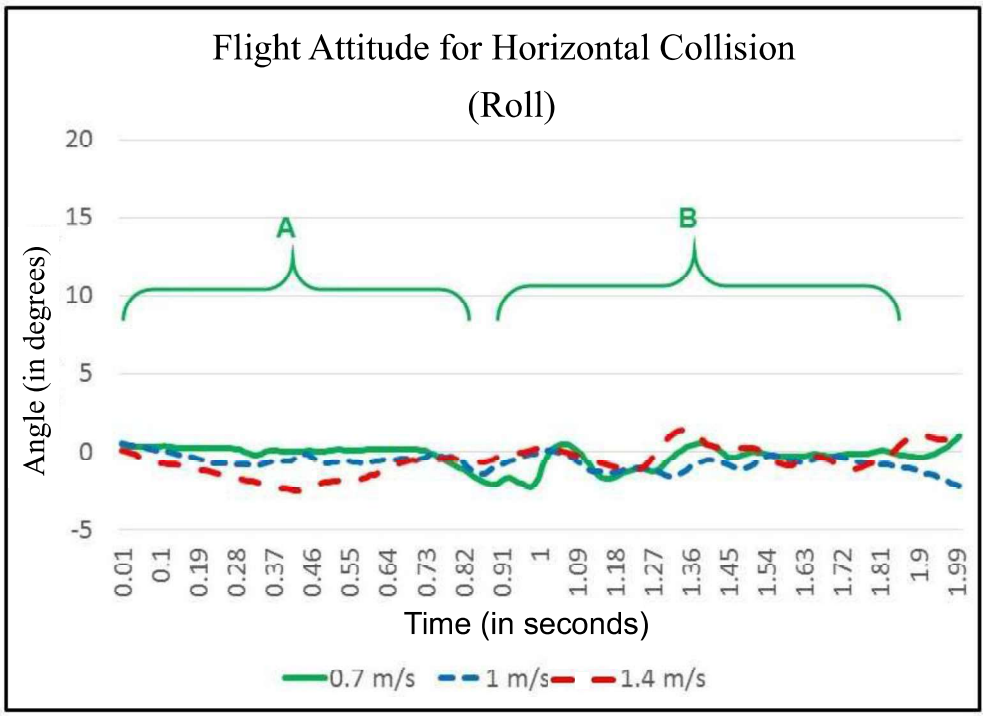

Figure 2.41: Flight attitude (roll) on horizontal collision at different flight speeds.

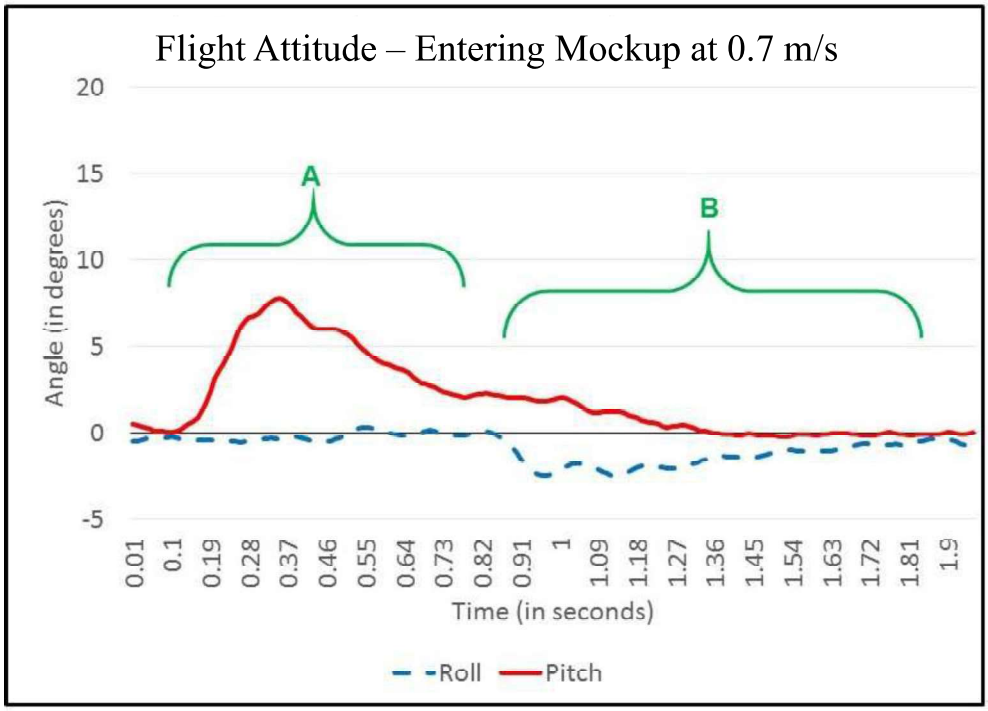

Figure 2.42: Flight attitude when the UAV crosses a structure at 0.7 m/s.

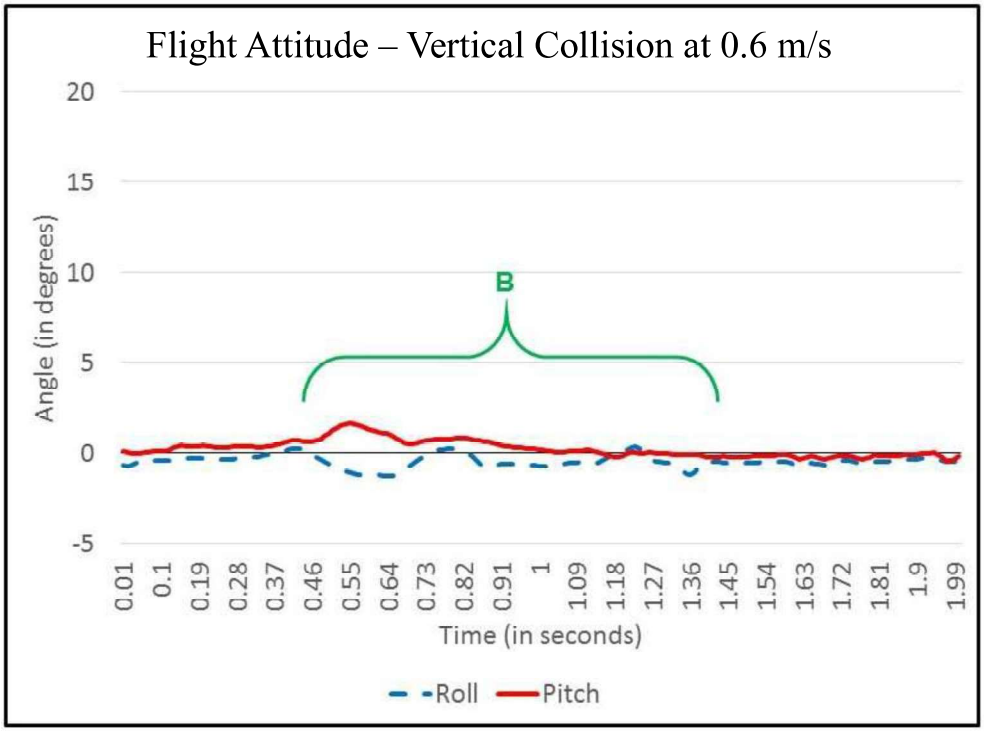

Figure 2.43: Flight attitude during vertical collision shows no significant disturbance at 0.6 m/s

produces a full overhead view of the mock-up. As a result, images of the three image test material positions were easily taken. Likewise, the camera was successful at detecting the minimum line width of 0.1 mm at a camera distance of 0.5 m. Fig. 2.44, 2.45, and 2.46 show the captured images at different camera tilt angles. In addition, a preliminary test was conducted for the speed of the camera that will enable the clear capture of 0.1 mm line widths at a distance of 0.5 m. For the GOPRO Hero 4 camera, the maximum movement speed is equivalent to 0.3 m/s.

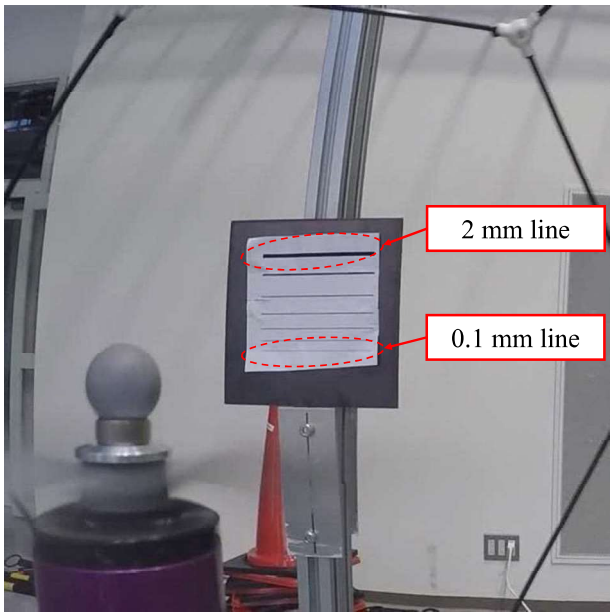

Figure 2.44: Captured images at 0 degree camera tilt using the image test material.

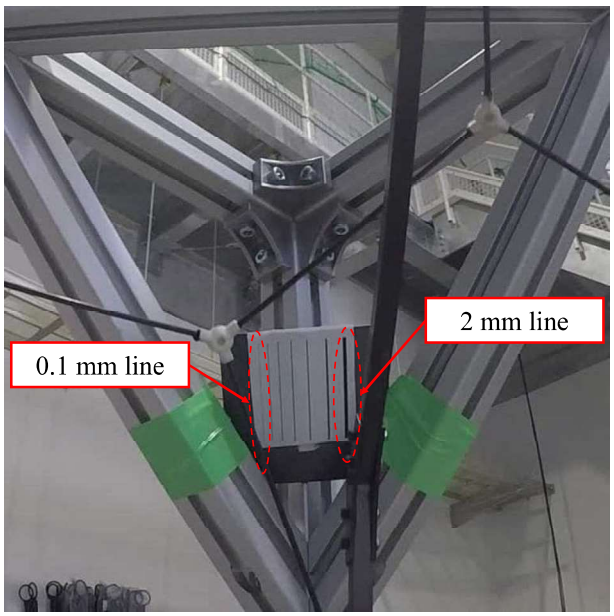

Figure 2.45: Captured images at 45 degree camera tilt using the image test material.

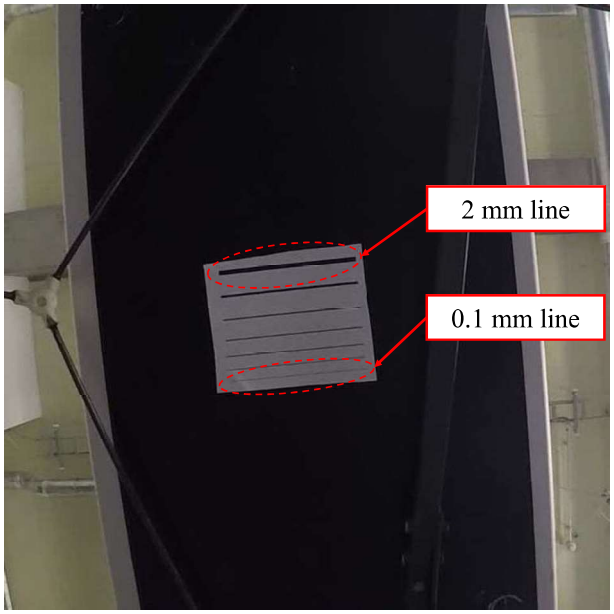

Figure 2.46: Captured images at 90 degree camera tilt using the image test material.

2.6.4 Actual Experiment: Accessing the Complex Part of the Bridge

The bridge experiments were performed in two different sites: the National Institute for Land and Infrastructure Management (NILIM)-Tsukuba and a part of the Kaminoyama Highway in Japan. Primarily, the experiment is focused on evaluating the performance of the PRSS UAV on accessing the complex structure. The first inspection was conducted at the NILIM bridge in Tsukuba, Japan. This steel girder bridge is similar to old bridges that require repair and maintenance. The bridge has many steel braces including k-type bracing in each section as shown in Fig. 2.47. Numerous flights were conducted and then collected several images on the different part of the bridge.

For the entire inspection, which consisted of several flights, the PRSS UAV successfully demonstrated its abilities, such as passing through limited spaces and movement/roll in contact with both smooth and uneven surfaces. Fig. 2.48 shows the sequence and how it passes through the k-type steel bracing without any fear of collision as it moves to another section of the bridge. Figs. 2.49 and 2.50 show movement (rolling) in contact with the floor slab (a smooth surface) and main girder web plate (an uneven surface), respectively. Several times, the PRSS UAV also experienced severe collisions, especially when there were wind gusts, but it was able to handle the impact and maintained its normal flight attitude. The recorded maximum wind gust speed was 9.9 m/s. Although the wind gust disturbed the flight, especially during take-off, the PRSS UAV was able to manage the disturbance and continue performing its task. The average flight duration was about 4.5 min which was slightly shorter than the test flights.

As for the observation, the conditions at the actual bridge such as the presence of

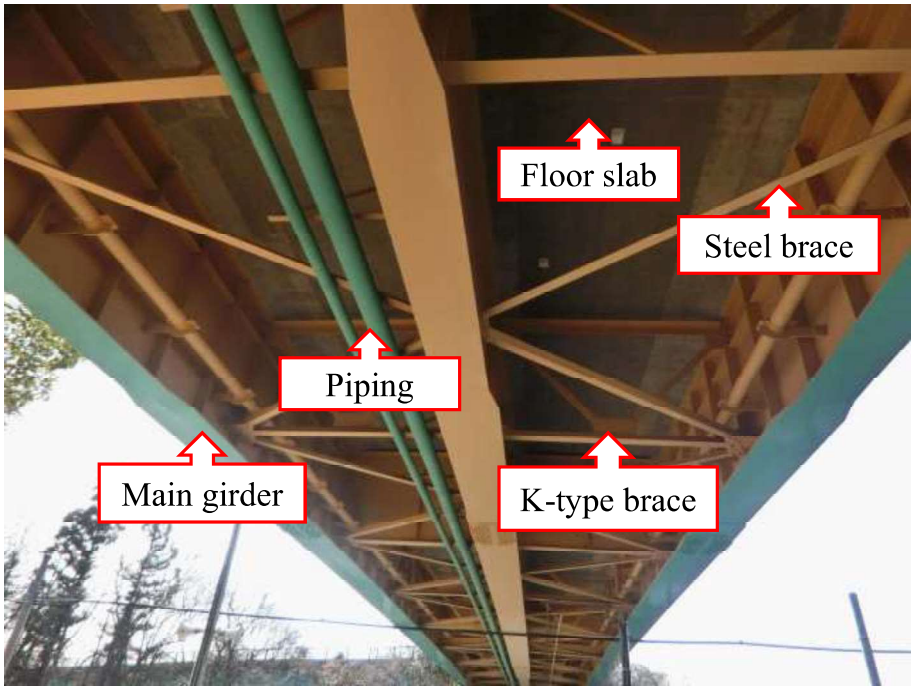

Figure 2.47: Steel girder bridge with a large number of steel bracing including k-type bracing in the crossbeam.

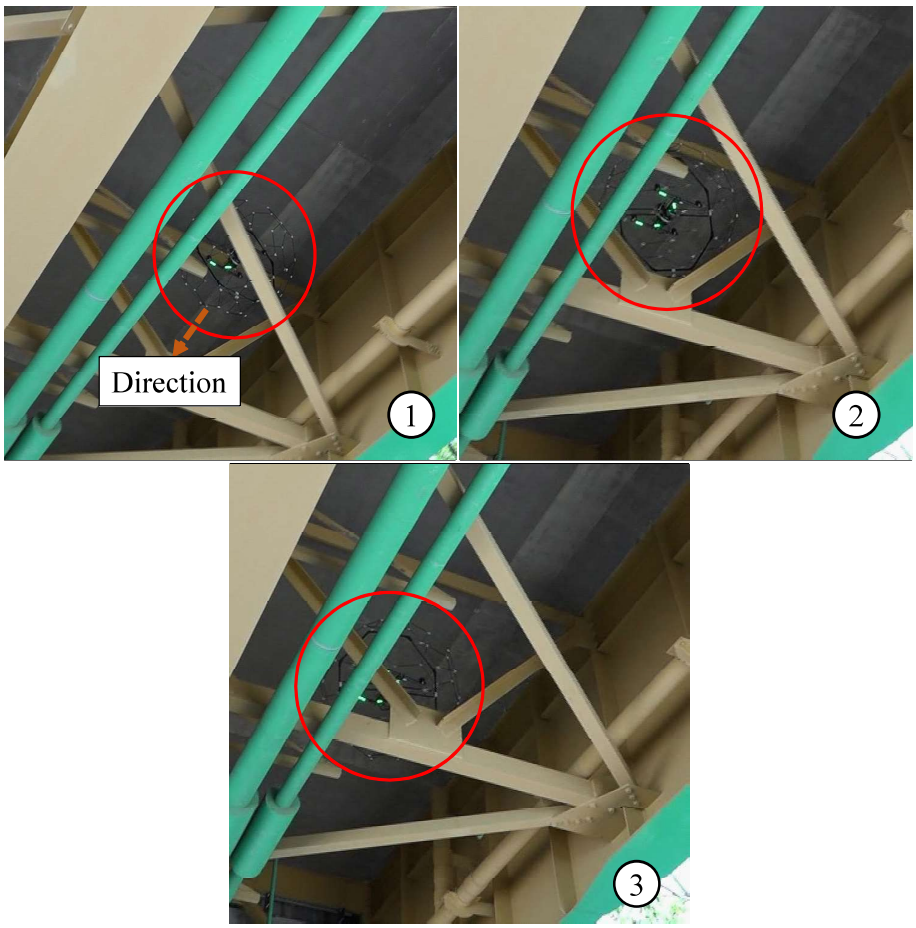

Figure 2.48: Crossing the steel k-type brace underneath the bridge.

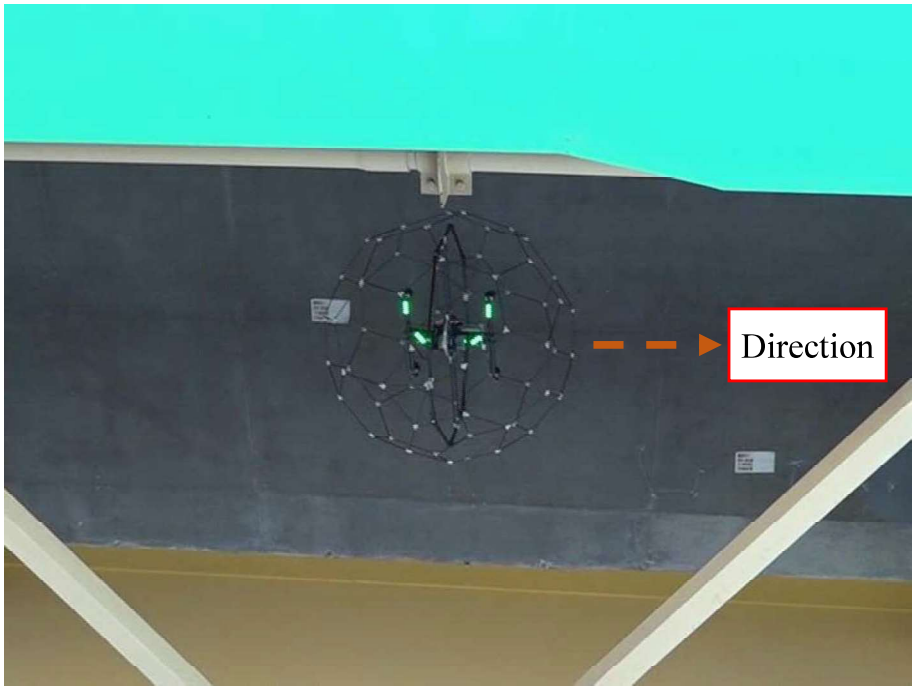

Figure 2.49: Image of the PRSS UAV as it moves while in contact with the floor slab.

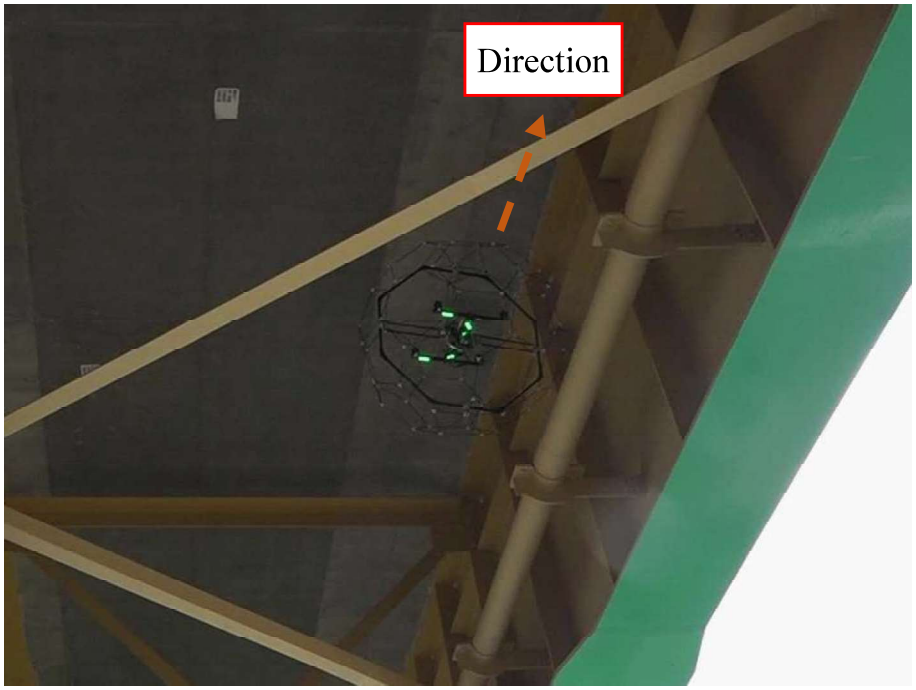

Figure 2.50: Image of the PRSS UAV as it moves while in contact with the main girder web-plate.

erratic wind gusts significantly affected the flight endurance of the system. The possible cause is that the UAV tended to draw more power to compensate for the disturbances. The large inspection area of the bridge also required us to perform several flights because of the limited flight time. Nevertheless, the ability to quickly replace the battery alleviates this problem. Another important observation is that even though the UAV is protected by the spherical shell, small pointed parts of the bridge can enter the interior of the spherical shell and may hit the propeller. All of these observations provide us with more information for improving the system.

2.6.5 Acquiring Images on Critical Parts of the Bridge

The visual system successfully provided images from different camera positions. A vertical view as the PRSS UAV enters the bridge with a 90-degree camera tilt is shown in Fig. 2.51, labelled 90-degree tilt. The horizontal view underneath the bridge with a 0-degree camera tilt while shows the corner view with a 45-degrees camera tilt are shown in Fig. 2.51 labelled 0-degree tilt and 45-degree tilt, respectively.

Several images on different parts of the bridge were taken, especially on the parts where damage frequently exists. We primarily took images of the main girder, where corrosion and cracks usually occur. Fig. 2.52 illustrates images of various parts of the main girder that include images of the girder web plate and tensile bolts (inside and outside) of the girder connecting the web plates.

Images of the main floor slab (inside the bridge) were also obtained, as shown in Fig. 2.53, where cracks normally develop as well as in the floor slab overhang (outside part of the bridge). Other images were taken of the bridge shoe and corners as shown in Fig. 2.54. As the PRSS UAV move, it affects the quality of the images because of the limited capability of the camera to capture images in motion and . The installation of a camera that can capture high-speed motion images but is lightweight and small in size is desirable. However, for now, such cameras are not easily available on the market.

Another experiment was performed at a part of Kaminoyama highway at Kaminoyama-shi, Japan. This type of bridge is a steel girder bridge with channel type bracing, as shown in Fig. 2.55. In the same manner, we verified its performance and acquired clear and close images of various parts of the bridge. But we focused on testing the quality of images the system can capture using official image test material provided by the highway management professionals.

Fig. 2.56 (right) shows the first image test located at the floor slab where camera positioned at a 90 degree tilt while Fig. 2.56 (left) shows the image captured by the camera. It reveals a clear image of 0.1 mm to 2.0 mm line marks.

The weakness of the image quality evaluation, however, is we use an image test material. It expected that an image quality of a real damage such as cracks is more difficult

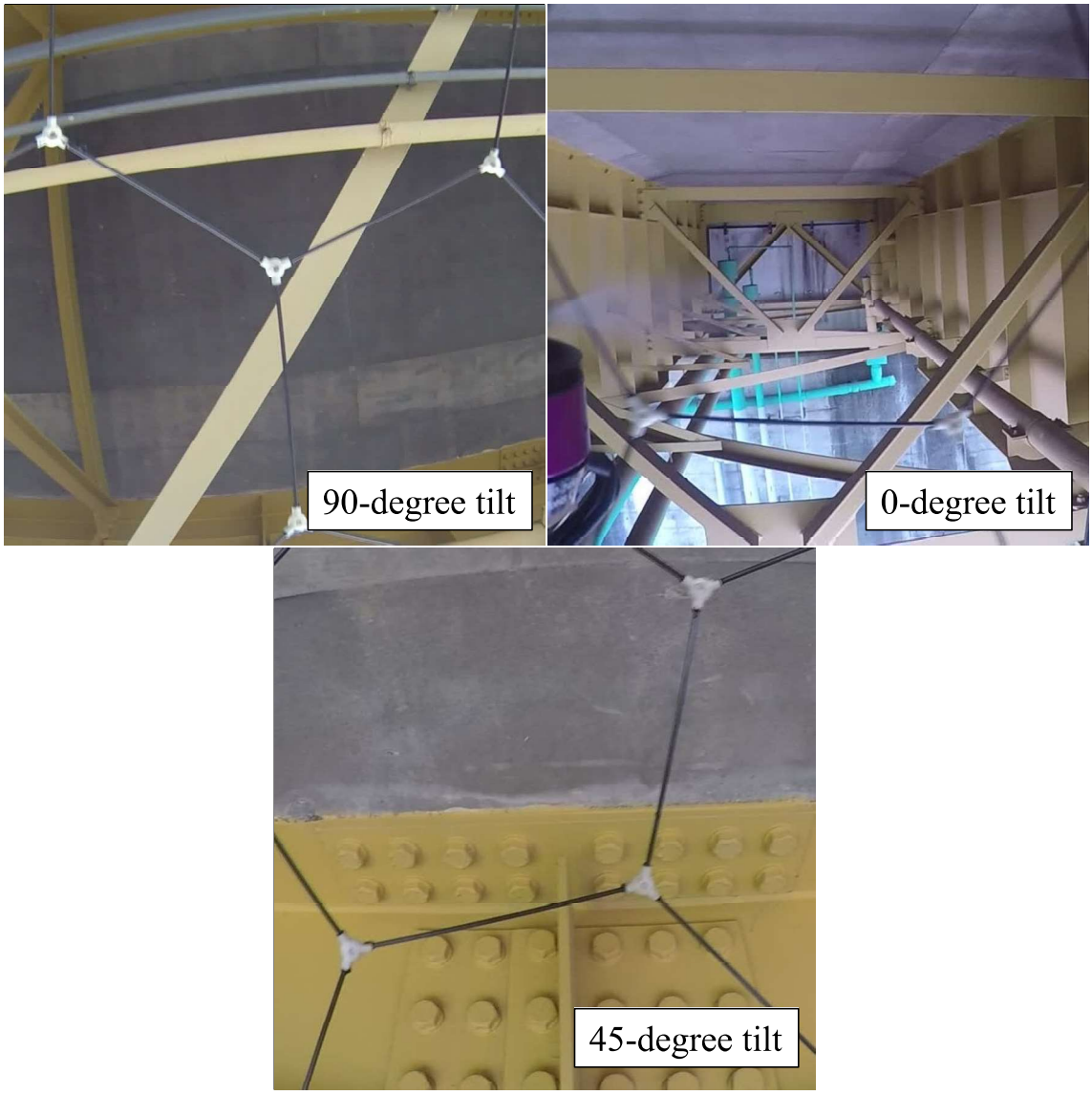

Figure 2.51: Images from different camera angles.

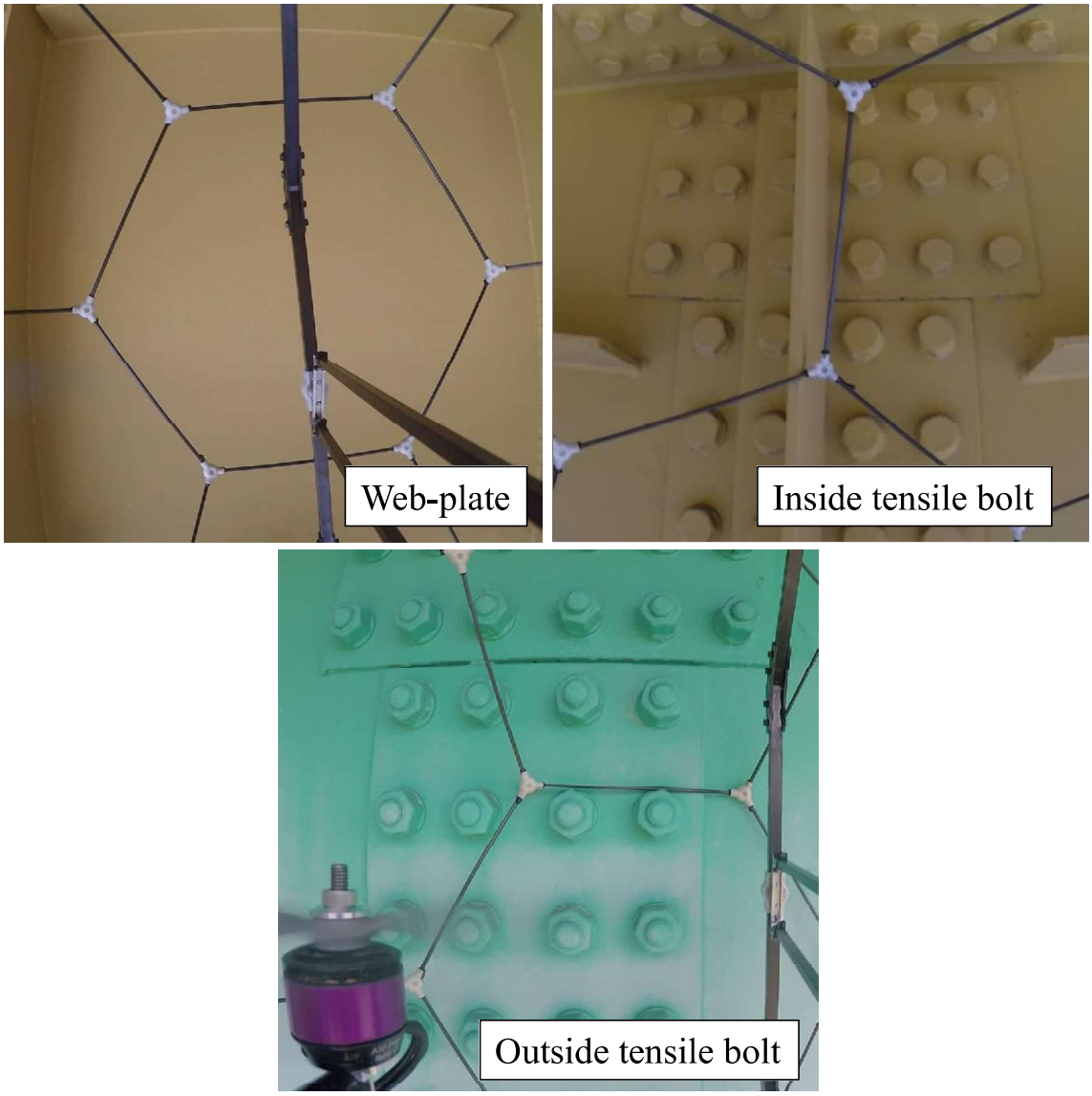

Figure 2.52: Images on different parts of the main girder including the web-plate, and tensile bolts in and outside the bridge.

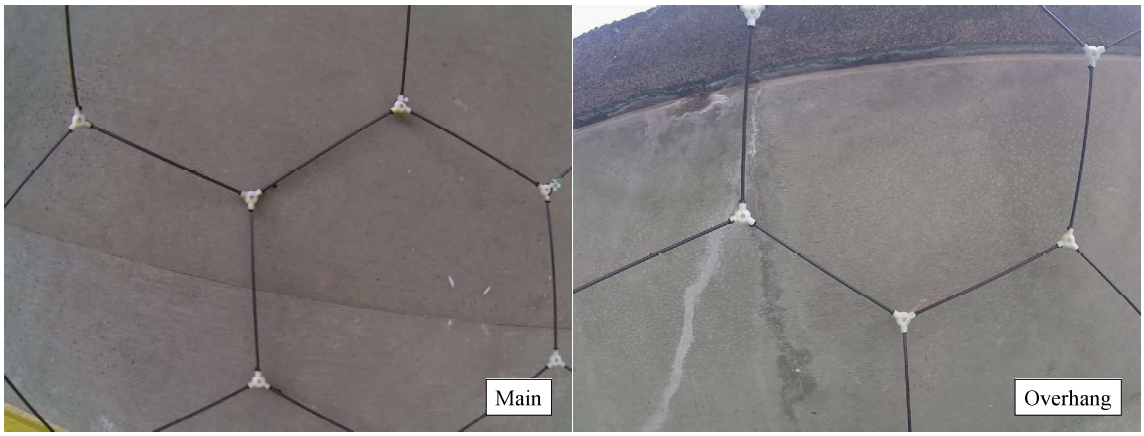

Figure 2.53: Images of the floor slab main and overhang where cracks normally develop.

Figure 2.54: Images of the bridge shoe and bridge corner.

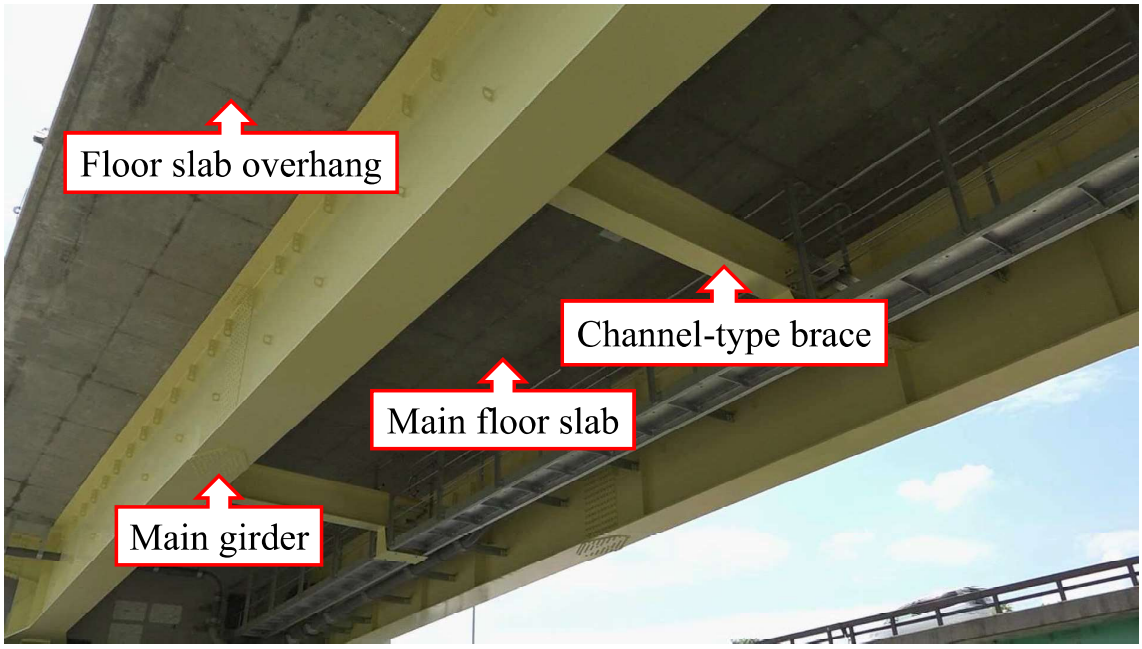

Figure 2.55: Steel girder bridge with channel-type bracing.

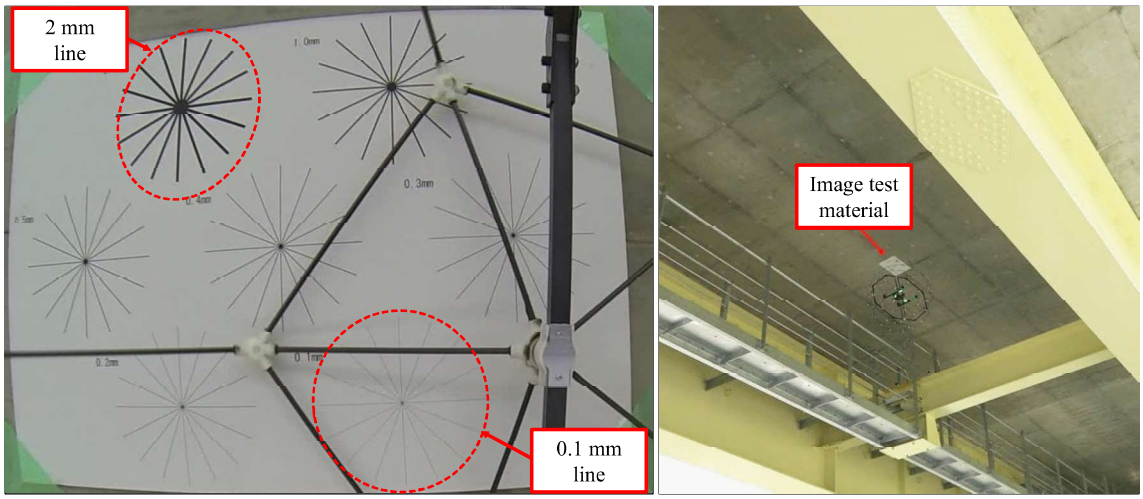

Figure 2.56: Captured images of test material attached to the floor slab of the bridge (left) and image of the PRSS UAV moving close to the test material (right).

to recognize using the current camera for a 0.1 mm width. So, it cannot be completely claimed that the system can perfectly capture 0.1 mm cracks, but instead it provides information on how to improve the image quality. The movement of UAV carrying the camera adds up to the problem of image quality. Likewise, the external illumination under the bridge may not be good all the time. These points are crucial to consider when working with the visual system to be used in the future. Currently, these issues are being worked out by the project collaborator who manufactured renowned state-of-art photographic equipment to build a camera that has the following features: high-speed, lightweight, and capable of capturing a good quality image under poor illumination.

2.6.6 Comparison with the Previous System

To compare the performance of the new and old system, both will be evaluated based on available payload, flight time and flight in the presence of wind.

In the actual bridge inspection, the system requires extra payload for the visual system. An appropriate visual system should be able to carry one camera plus extra components for full overhead view movement of the camera and a video transmitter for real-time monitoring. The estimated weight of each component needed for visual inspection is 100 g for the camera, 100 g for the video transmitter, and 100 g for the extra component. Thus, the estimated total weight needed for the visual inspection is 300 g.

As listed in Table 2.8, the old system has only 120 g extra payload. It can carry a camera but cannot carry additional components such as video transmitter and another component. In previous paper [32], it is also revealed that the total weight of the old system used in visual inspection of the bridge is 1956 g consisting of the UAV, gimbal system, spherical shell and one GoPro camera. With a 2000 g maximum take-off weight that means it cannot carry additional components. On the other hand, the new system

Figure 2.57: Actual flight of old system at Ushigeo Bridge in Sendai.

Table 2.10: Comparison of flight time for old and new system on actual experiment

Flight No.	Duration (MM:SS)	
	Old system	New system
1	02:00	4:58
2	01:50	4:10
3	01:30	4:50
4	00:55	4:30
5	03:55	4:18
Average	02:02	4:33

has an extra payload of 503 g. Therefore, it can carry all the components mentioned above to have an appropriate visual system. Likewise, the remaining payload (203 g) can be used to increase flight time of the UAV by changing a much higher battery rating.

Next is to compare the flight time based on the actual experiment. For the old system, the experiment was conducted at Ushigeo Bridge in Sendai. The actual flight of the old system is shown in Fig. 2.57. For the new system, the data will be obtained from the experiment conducted at NILIM Bridge in Tsukuba. Table 2.10 shows the flight duration for five flights and the average flight duration of the old and new system. The average flight duration of the new system is more than twice the duration of the old system. The flight duration of the new system can still be extended for few minutes as it was previously mentioned that there is still 203 g extra payload. However, it is recommended in the future work to extend the flight time as much as possible about 20-30 minutes. This is to allow one flight for the inspection of the entire bridge. For now, extending the flight time is too difficult because of many constraints involved in design process like especially the weight and size of the spherical shell.

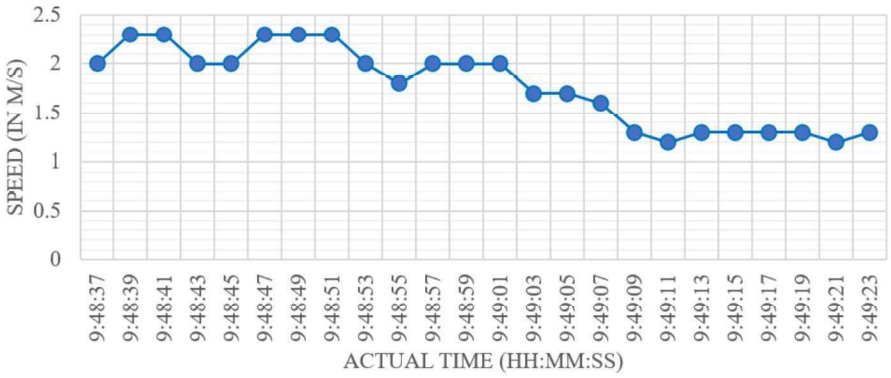

Figure 2.58: Wind speed during the actual flight experiment of the old system.

Lastly is the comparison of actual flight experiment in the presence of wind. Because the old system has not included the aerodynamic design as part of the design strategy [32], it is not mainly intended for the condition with strong wind reaching up to 8 m/s. Thus, the experiment of the old system was conducted only in no wind or low wind condition. Fig. 2.58 shows the wind speed of the old system during the actual flight experiment. The maximum wind speed reaches up to 2.3 m/s which is considered as low wind speed. Such wind speed is still possible for the old system to conduct the flight. Meanwhile, the new system that was designed with aerodynamic consideration was able to fly more than 8 m/s wind gust. In one of the actual flight, the wind gustiness reaches up to 9.1 m/s as shown in Fig. 2.59.

Thus, it showed that the new system has improved its payload capacity, flight time, and capability to fly in the presence of strong wind as compared to the old system.

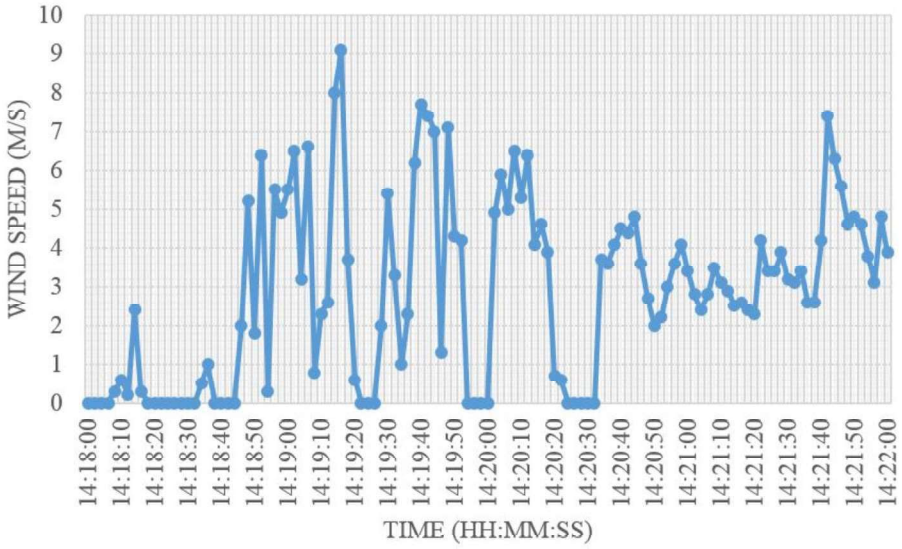

Figure 2.59: Wind speed during the actual flight experiment of the new system.

Table 2.11: Third party evaluation result.

QUESTIONS	MB	B	F	P	MP	NA
Quality of acquired image: General	0	4	2	0	0	1
Quality of acquired image: Damage	0	3	4	0	0	0
Quality of acquired image: Crack	0	4	3	0	0	0
Does not require scaffolding	2	4	1	0	0	0
Safety: Ground unit	1	5	1	0	0	0
Safety: Air unit	1	5	1	0	0	0
Robustness to external illumination	0	1	5	0	0	1
Completely inspect critical parts efficiently	1	2	2	1	0	1
Easy transport and deployment	1	3	2	0	0	1
Flight stability	2	2	2	0	0	1
Performance against wind up to 10 m/s	0	5	2	0	0	0
Flight time	0	1	2	3	1	0
Data transmission	0	2	3	1	0	1
Noise	1	5	1	0	0	0
Improvement required prior to deployment	None	Few		Many		NA
	0	4		1		2

2.6.7 Evaluation of Highway Management Professionals

Seven third-party human evaluators who are highway management professionals in Japan, where bridge inspection is one of their task, were used to obtain statistically significant evaluation results. The evaluation scheme requirements are similar to the NGRSI requirements for visual inspection robots. The evaluation shown in Table 2.11 compares the proposed system against the conventional method of inspection performed by the human inspector. There are six responses which are MB - MUCH BETTER, B - BETTER, F - FAIR, P - POOR, MP - MUCH POORER, and NA - NO ANSWER. The positive response category consists of MB, B, and F, while the other answers are considered negative response.

About 88 % of the responses are positive, and about 47 % of the responses indicate that the new system is better than the conventional method. Likewise, the respondents were convinced of the quality of the acquired images and all answered with a positive response except for one no answer. Items such as "safety", and "no scaffold during the inspection", "performance against the wind", and "noise" obtained positive responses. Moreover, the items "robustness to external illumination", "ease of transport and deployment", and "flight stability" obtained positive response except for one no answer.

Five respondents also positively agreed that it can completely inspect critical parts of the bridge while one each rated it poor or gave no answer. The lowest score is about the flight time. The third party suggested that the inspection flight should be longer because of the large search area of the bridge. A flight time of 10 min or more would be

a better inspection duration. In general, four respondents agreed that the system needs few improvements prior to deployment while one responded it needs a lot of improvement, and two did not answer.

2.7 Chapter Conclusions

In this Chapter, the improvement of the flight performance of the existing system focusing on increasing the flight capability, reducing the weight, and minimizing the effect of air drag was presented. The flight capability of the new system increased by 40 % based on the maximum take-off weight rating from 2000 g to 2800 g. It also improved the weight of the spherical shell, decreasing by 23.56 % from 416 g to 318 g. The improvement on the performance of the new system also shows a positive outcome by means of thrust-to-weight T/W ratio. The calculated T/W ratios are 1.06 and 1.22 for existing and new system, respectively. It can be recalled that the higher the T/W ratio, normally greater than 1.0, the better the performance of the system. The new spherical shell structure and components also show that it is effective in reducing the drag force. Both the CFD simulation and wind tunnel testing confirmed the positive outcome of the evaluation which reduces the total drag force by 34.74 %. The new system ability to fly even in the presence of wind was verified in an actual field test experiencing a wind gustiness up to more than 8 m/s.

Meanwhile, the visual inspection of the bridge as a case study was successfully implemented. A simulated bridge inspection verified the advantage of passive rotating spherical shell showing no significant disturbance on the UAV's flight attitude and showing the performance of the system to capture images on the different section. Before the actual deployment, the bridge conditions and requirements were also determined. The system was also able to operate in erratic wind gusts reaching up to more than 9 m/s. The image test revealed that the visual system could detect 0.1 mm lines at a distance of about 0.5 m (from the center to the outside of the spherical shell). Both the simulated bridge inspection (laboratory-based) and the actual experiment at the Kaminoyama highway confirmed this result. The camera tilt from 0 to 90 degrees and the UAV yaw rotation provides a full overhead view that makes it possible to acquire images of any part of the bridge. With this coverage, the visual system was able to obtain images from different areas in the actual bridge experiment. The images include a part of the main girder, floor slabs, and bridge shoe, and bridge corner. The use of the UAV with passive rotating spherical shell along with a visual system has shown to be effective for close visual bridge inspection by satisfying the essential requirements set by the NGRSI requirements. Given the actual bridge inspection mission, it was able to verify the improvement of the new system compared to the old system. It showed that the new system satisfied the payload requirement for the visual system. It also showed higher flight time than the old system.

Likewise, it was able to fly on strong wind compared to the old system. Subsequently, the majority of the third party evaluator agreed that the system has many positive outcomes and only requires a few improvements before its final deployment.

Limitation of the Study

The aerial vehicle used for the entire study is a quadcopter or four rotor-type UAV. Although another type of UAV can be implemented such hexacopter and VTOL drone, the quadcopter is considered a good choice for this study for several reasons such as easily available in the market, small size, has stable hovering, and can be easily and precisely controlled. Still, in general, the selection of aerial vehicle depends on the specific mission. Moreover, the UAV used an off-the-shelf controller. This means that there is no supplementary control strategy added in the UAV controller. The stability of the entire UAV system relies mainly on the added three degree-of-freedom gimbal mechanism in the case of unavoidable collision or disturbance. The reduction of weight mentioned in this Chapter only covers the change made in the spherical shell. Any weight changes on the UAV such as motor and propeller are not accounted. However, those disregarded change in weight still reflects on the overall weight of the system. The reduction of the drag force is as well focused only on the spherical shell. Consideration of aerodynamic effect on the body of the quadcopter and gimbal mechanism is a good area for future works. In the case of the bridge inspection in the bridge, the mission only covers acquiring images from the different part of the bridge. The evaluation of any found damages in the bridge such as cracks and rusts are to be implemented in the future work.

Future Work

The primary challenge to be addressed in the future work is to further improve the payload by increasing the flight capability and reducing the weight of the system while constantly satisfying the parameters, requirements, and constraints. Resolving the payload issue is essential for the further increase of flight endurance, the possible addition of other components need for visual exploration such camera stabilization system, and addressing the other issues caused by a limited payload. Air drag can be further minimized by applying aerodynamic design not only for the spherical shell but the other main components of the system such as the main UAV and gimbal mechanism. Further work on image processing to satisfy the remaining NGRSI requirements remains to be done. It is recommended that an image processing on the raw data to remove the main part of the spherical shell that blocks the camera view should be implemented. The system also requires intensive image processing to recognize damage against a complex background.

Chapter 3

UAV for Physical Interaction in a Complex Environment

3.1 Introduction

In recent years, many researchers and developers in academia and industry have broadened the task of the UAV from primary role of remote sensing to a more interesting role, the aerial interaction with the environment. Peschel started to investigate the potential for physical object manipulation by a small unmanned aerial system (UAS) and identify the five associated human-robot interaction (HRI) research challenges [80]. Up to now, several developments related to aerial interaction have already been presented that include pick and place operation [81], grasping task [82] [83], a design of manipulator [84] and adhesion mechanisms [85]. It is expected that in a few years from now, more studies involving aerial interaction will come out solving the different issues and completely offer a reliable platform. Similar to visual exploration, the use of UAV will, in the near future, offer a safe, low-cost and quick action for physical interaction with the environment.

In disaster robotics, the aerial interaction will a huge impact, and it will be helpful during calamities. The future role of aerial interaction is to keep human out of danger while performing disaster mitigation task like manipulating valves or emergency devices while situated at a distance from the site. Recent examples of the need for robots to manipulate the environment include robot submersibles inserting a tube and regulators into the damaged drill pipes at the 2010 Deepwater Horizon spill in the Gulf of Mexico and the use of robots to attempt to turn valves in the 2011 Fukushima Daiichi nuclear emergency [34]. For now, mobile ground robots have acceptable capabilities to do both visual and physical interaction task in the harsh environment. One main disadvantage though of a mobile ground robot which happened during the actual mission in exploring Fukushima Daiichi power plant is that it was not able to climb stairs because of the blockage [4]. It

is clear that the disadvantage of the mobile ground robots over the flying robots is the mobility.

Moreover, many individual types of research of the UAV today including the studies as mentioned earlier are helpful in slowly bringing a good hint for the future of aerial interaction in the harsh environment. For example, the series of the development of the aerial system intended for physical interaction with the environment that is done by the same group of researcher [86] [87] [88] gives an idea for the future interaction of the UAV. Likewise, the introduction of a passive rotating spherical shell by two independent group which protects the UAV while keeping it stable during a collision with obstacles [5] [6] is a valuable input. However, the passive rotating spherical shell mechanism has a conflicted feature between visual exploration and physical interaction. For visual exploration, the passive rotation of spherical shell does not completely affect the required image. The raw image taken by the camera can be subjected to an image processing to remove the passive rotating shell of the UAV such as studied by Okada et. al [89]. However, in the case of physical interaction, the passive rotating spherical shell will eventually cause a self-collision and will compromise the stability of the UAV. Any attempt to access the outside of the shell will disturb the passive rotation of the spherical shell. The unknown and random speed and direction of rotation of the spherical shell make it harder to predict when to access outside the shell. Ideally, any manipulating system should have the freedom to access outside the shell at any moment and duration. One way to address the problem without discarding the idea of passive rotating spherical shell mechanism, considering its immense advantages for a complex environment application, is to cut the spherical shell into two hemispherical shells. As a result, it will provide a gap for the manipulator to access outside the shell without affecting the passive rotation. Also, the protection offered by the spherical shell is maintained and at least retained certain freedom of passive rotation enough to secure good stability for the UAV.

Two Rotating Hemispherical Shells

The concept of two rotating hemispherical shells can be traced back on Omni-ball mechanism presented by Tadakuma et. al [90]. Although the Omni-ball mechanism is intended for omnidirectional movement in a ground/surface, however, the structure of mechanism can be expanded for the mechanism of the UAV. The core section structure of the Omni-ball is shown in Fig. 3.1. It has two hemispherical shells that rotate passively, and in the center of it lays the active rotational axis. Each passive rotational axis is independent, which implies independent rotation of the two hemispherical shells. An actuator in the active rotational axis is added for the movement of the omnidirectional vehicle as its main application. In the case of rotation of the two hemispherical shells for the UAV, all

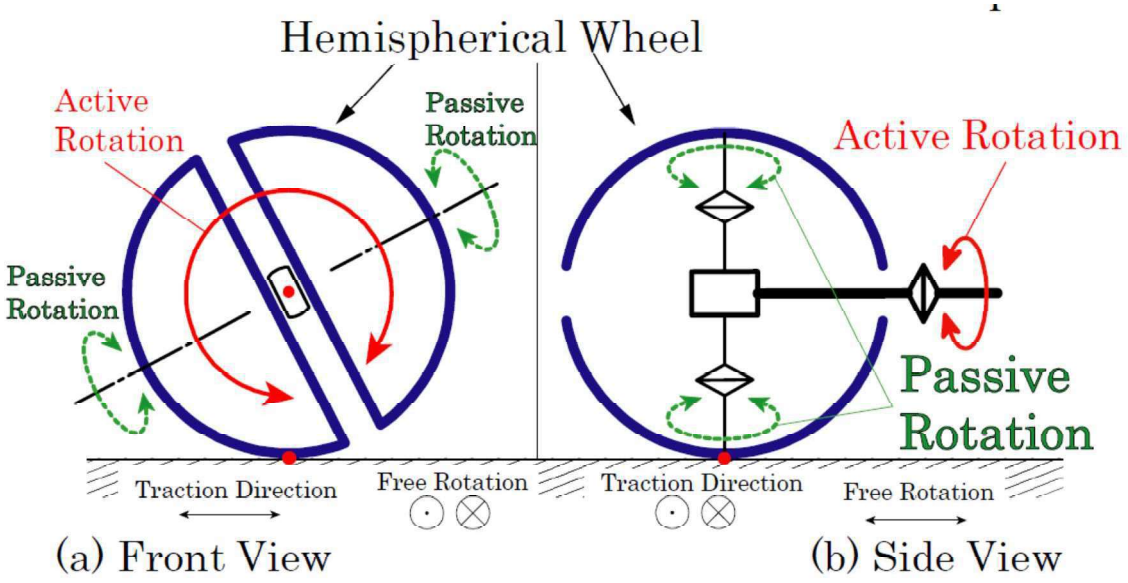

Figure 3.1: Basic structure of the Omni-ball [Source: Tadakuma, 2007].

rotations in different axes will be configured as passive. The drawback of Omni-ball that was mentioned is that mechanism has one singular point only when the plane containing all three axes of this wheel becomes perpendicular to the ground. In such state, the hemispherical wheel cannot rotate passively. This is valuable information because it can also occur on the mechanism introduced for the UAV.

Physical Interaction Configuration by Small UAVs

The three different configurations of physical object interaction were presented by Peschel [80] based on the various grasping research already been reported. They are the ventral, frontal, and dorsal configuration. The configurations are illustrated in Fig. 3.2 and described by Peschel as follows:

1. Ventral Interaction - The most common location of physical interaction is below the UAV, on the ventral side of the lower frontal plane. In this description, two frontal planes (lower and upper) are designated to form a region where no physical interaction would be recommended (i.e., across and between the rotor blades). The space of ventral interaction forms a hemisphere below the lowest part of the rotor blades, and takes into account the limitations of range due if landing supports are present. The ventral side of the UAV is where camera payloads are typically mounted as this is the most stable location of the vehicle. Research related to ventral interaction for small UAVs has addressed agile load transportation, mobile manipulators, grasping in flight, and multi-vehicle grasping. The main limitation to ventral interaction is the air turbulence always present below the rotor blades,

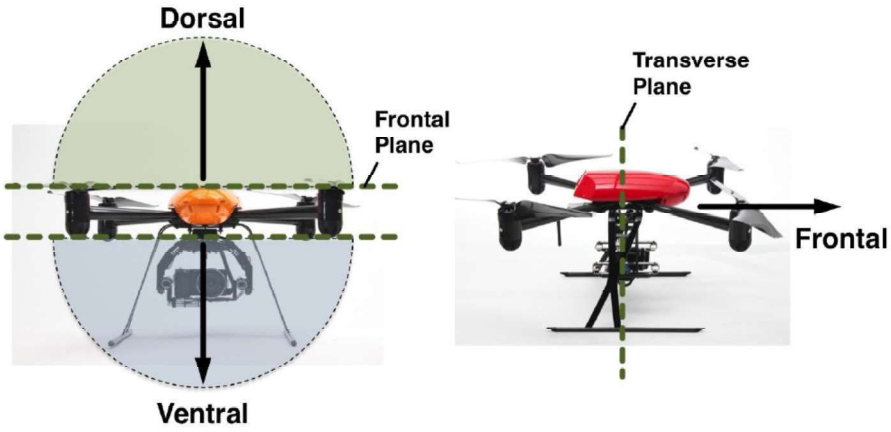

Figure 3.2: Illustation of three possible physical interaction configurations [Source: Peschel, 2012].

which could perturb the object of interest in an unpredictable manner. Small UAS missions involving ventral interaction would include dropping and retrieving physical objects such as micro ground robots and instruments (e.g.,micro penetrometers).

2. Dorsal Interaction - The least studied location of physical interaction is above the UAV, on the dorsal side of the upper frontal plane. The dorsal interaction space forms a hemisphere above the upper part of the rotor blades, and does not possess any limitation of range. Camera payloads are not usually mounted on the dorsal side of a UAV as downward views would be obstructed. Research related to dorsal interaction for small UAVs is limited and has focused mainly on platform stability. Two main limitations exist for dorsal interaction: i) air suction effects will be present that could disturb the object of interest in unpredictable ways, and ii) activities will be occurring above the rotor blades, representing a potential hazard to the vehicle. Possible applications by small UAS involving dorsal interaction include placing and retrieving objects such as wireless sensors on the underside of a bridge, and moving or manipulating environmental objects such as tree canopy foliage.

3. Frontal Interaction - A special case of ventral interaction is frontal interaction, which is anterior to the transverse plane of the UAV. Frontal interaction is from a fixed position and relies on the vehicle for movement to manipulate of objects. Some small UAV designs have fixed forward facing cameras that cannot be controlled; therefore, frontal interaction for a physical object is the only available option without adding additional cameras to the platform. Research related to small UAV frontal interaction has also focused on platform stability, as this configuration tends to be the most stable. The obvious limitation for frontal interaction is the fixed presence in the frontal plane, prohibiting the range of motion present in ventral and dorsal inter-

action. Potential small UAS applications for frontal interaction would be a similar to dorsal interaction, such as sensor and object movement, but this would involve more coarse manipulation (pushing and pulling) rather than fine manipulation (e.g., an arm-based grasper with several degrees of freedom).

Proposal

In this study, a new approach is proposed for UAV with a passive rotating spherical shell to allow physical interaction while retaining the protection and good stability for the UAV. The main idea is to divide the spherical shell into two hemispherical shells to allow any manipulator to access outside the shell freely. The first step is to determine the unaffected gap. It is expected that the whole gap as the result of the cutting of the spherical shell will not all be useful. Finding out the unaffected gap will determine what kind of configuration and size of the manipulator is possible for physical interaction. The new approach will retain the protection of the UAV through the spherical shell. Regarding passive rotation, one DOF on either pitch and yaw axis will be withdrawn as a consequence for dividing the spherical shell. Hence, it is necessary to understand the behavior of the new mechanism on how it reacts to the various kind of disturbances. On the other hand, the cutting of the spherical shell will have a consequence on the rigidity of the system. The cutting will cause deformation and deflection. Thus, analyzing the main cause of the problem will give insight for the appropriate solution. Finally, an experimental prototype will be developed to verify the performance and capabilities of the new system.

Another proposal is the implementation of physical interaction using UAV with two passive rotating hemispherical shells. Nod-destructive impact hammer testing is the proposed application. This operation is necessary to determine damage structures that are not visible on the outer surface, for example, hollow space in the concrete wall due to deterioration. It is assumed that the target environment is too cluttered for an ordinary UAV like a complex-structured bridge or partially damaged building. Thus, the idea is to attach the hammering device into the proposed UAV with two passive rotating hemispherical shells. The first step is to develop a general concept and design of the system. The expected configuration for hammer testing is normal to vertical wall or structure. Hence, it is considered to develop a hammering system positioned at the frontal part of the UAV. The challenge is to maintain a stable hovering position of the UAV while performing a hammer testing so it can provide useful data from the sensors, such as impact force and sound, needed for further evaluation. The primary problem is as the UAV come closer (expected to tilt in pitch axis as it moves forward) to the vertical wall or structure, it may get sucked up because of the low pressure above the UAV. The idea is to add a horizontal actuator to push the UAV horizontally without tilting to avoid the problem; this method

has been introduced by Albers et. al [91]. Hence, the aim is to implement a control strategy to keep the UAV and hammering device normal to the wall or structure. Finally, an experimental prototype will be developed to verify the performance of the system.

Outline

In this Chapter, it discusses two main topics: the proposal of UAV with a passive rotating hemispherical shell and the hammering test using the proposed system. The objectives of this Chapter are enumerated in Chapter 3.2. Furthermore, Chapter 3.3 and 3.4 discusses the general concept, rotation analysis of hemispherical shells, analysis during an interaction, structural analysis, and mechanical design, and the development of experimental prototype and test flight of the proposed system. Chapter 3.6 discusses the background of the hammering test, general concept, design, and analysis of hammering system, development of the prototype, and flight experiment. Chapter 3.7 concludes and summarizes the result of development and test flights of the proposed systems.

3.2 Objectives of this Chapter

The main objectives of this chapter are:

1. To introduce a new passive rotating shell mechanism for the UAV that will allow physical interaction.
2. To implement a hammer test as physical interaction application using the UAV with two passive rotating spherical shell.

The first objective can be realized by cutting the spherical shell creating two hemispherical shells that will provide a gap for physical interaction while retaining the essential features of the former system. The first specific aim is to analyze the gap and check the significant part of the gap unaffected by the rotation of two hemispherical shells. By this means, the configuration of physical interaction can be determined. Second is to analyze the passive rotation of the two hemispherical shells during disturbances. It is expected that the reactions of the new mechanism caused by external disturbances are different from the previous system. The latter system will have rotation freedom on two axes, but the hemispherical shells can rotate independently while the former has 3 DOF rotation of spherical shell. Thus, it is necessary to check its reactions in various condition. The third aim is to analyze and design the structure of the system. As already mentioned, the cutting of the spherical shell will weaken the new structure. Thus, it is necessary to check and develop a new structural support. The final aim is to develop a working experimental prototype to test the performance of the new system.

The second main objective mainly focused on the application of physical interaction using the two passive rotating hemispherical shells. The first aim is to develop a general concept for the new mechanism with a hammering system as a physical manipulator. The hammering system mentioned in here will be used to test the strength of the structure specifically concrete. Second is to analyze and design a proper hammering system for the new mechanism. This includes the hammering device, the holder and platform for the hammering device, and additional components to complete the system. The third aim is to implement a control strategy, especially during hammering. It is expected, during hammering, a reaction force will occur that will likely cause the UAV's movement away from the target structure. Thus, an additional actuator is required to counter the said reaction force. Also, keeping the UAV close to the target structure will enable the system to acquire consistent data. Lastly, an experimental prototype will be developed to verify the performance of hammering system attached in the UAV with the new mechanism.

3.3 Significance of the Study

There is two main significance of the study in this Chapter. First, the proposed mechanism will open new tracks for another researcher to focus. It will start the research on the use of the UAV with passive rotating shells for physical interaction in the complex and harsh environment. This is particularly significant as initial studies in the field of disaster robotics field. For example in the future in can be used for grasping of a sample in a damaged structure or switching valves in damage nuclear plant. It will also open up a new possibility of another great research track which is the power tethering while the UAV is protected and kept stable. Second, the proposed specific application of physical interaction using the newly proposed mechanism which is the hammer testing is as well used in the field of disaster robotics. The hammering system along with the UAV with two passive rotating hemispherical shells can be used to check a partially damaged infrastructure or building. For example, the condition of a partially collapsed building can be checked first before the rescuer going into the building.

3.4 Related Literature

For the past few years, the use of UAV has been extended from visual exploration to interaction with the environment. Various studies in the different area have been started that contributes to the development of physical interaction using UAV such as pick and place operation, grasping task, manipulator design and adhesion mechanism. For pick and place operation, Lindsey et al. developed grippers attached to the bottom of each quadrotor enable them to pick up, transport and assemble the structural elements [81]. For grasping task, Pounds et al. demonstrates a helicopter UAV that grasps an object

while in flight. It mainly presented the platform's underactuated gripper and its contribution to aircraft stability while grasping [82]. Another flying robot equipped with an upward directed hand on top of a quadrotor airframe was presented which is intended to realize an aerial manipulation task at high altitude, considering a workspace above the robot [83]. For the design of manipulator, Wuthier, et al. presented a novel four degree-of-freedom aerial manipulator allowing a multirotor UAV to interact with the environment physically [84]. For adhesion mechanism of UAV, a method by which a micro air vehicle (MAV) can hover without activating the power using magnetic adhesion and winch mechanisms with the objective of extending the flight duration [85]. These individual studies only show a positive development in the area of physical interaction using UAV. However, these studies can only be utilized in an open space and not in a complex environment. This is because the UAV being employed by the most researcher has no enough protection to deal with disturbances in a complex environment.

On the other hand, the passive rotating spherical shell mechanism has been the main subject in the previous Chapter. It showed the two main advantages: the protection of the UAV using spherical shell and the 3 DOF passive rotation using gimbal mechanism, which allowed it to be utilized in a complex environment for exploration. Those advantages have been stated by two independent group of researcher who introduced the mechanism for the UAV [6] [5]. However, the UAV with a passive rotating spherical shell can only be used fully for visual exploration. It was figured out that such system will make it too difficult to perform physical interaction for one main reason: there is no free access to outside of the spherical shell. An image processing to estimate the position of the spherical shell at random speed and direction such as proposed by Okada et. al [89] has been started. However, the primary problem is that it may require high-speed manipulator to interact outside the spherical shell without hitting it physically. Disturbing the passive rotation of spherical shell will compromise its stability and probably will cause the UAV to fall. As of now, there is no study on high-speed manipulator suitable for physical interaction using UAV is present in the academia as well as in industry. At this point, a UAV with a passive rotating spherical shell cannot be used yet for physical interaction. One possible option is to cut the spherical shell to provide gap while retaining, at least 2 DOF passive rotation.

The concept of cutting the whole sphere can be traced back on Omni-ball proposed by Tadakuma et. al [90] [92]. It has two hemispherical shells that rotate passively, however, the inner axis is for active rotational movement. The concept of Omni-ball mechanism was only implemented as spherical wheels for the omnidirectional ground vehicle, and no research has done yet for such mechanism to be used for the UAV. The related studies of physical interaction, the concept of passive rotating spherical mechanism, and the idea of Omni-ball will be combined to come up with a new mechanism as proposed in this Chapter.

3.5 UAV with Two Passive Rotating Hemispherical Shells

3.5.1 General Concept

The general concept of the system is shown in Fig. 3.3. The system mainly comprises a UAV and two hemispherical shells. It has two (2) axes of passive rotation and independent rotations of the two hemispherical shells. For a normal (lateral) posture such as that shown in Fig. 3.3, it provides rotation about the pitch and roll axes. The separation of the hemispherical shells through the removal of a certain portion of it to create a space between them opens up the possibility of access outside the shell. However, all the gap created by the separation is not usable for physical interaction and power tethering, because of the rotation of the shell.

If we analyze the gap further when the two hemispherical shells rotate in different directions (either roll, pitch or both axes) as shown in Fig. 3.4, it is noticeable that portions of it are unaffected by such rotation(s). These unaffected gaps are the essential part of the system for achieving physical interaction and power tethering capability. Ideally, these unaffected gaps maintain a constant area A_g equivalent to Eq. 3.1. The size of the unaffected gap can be adjusted depending on the required size for a certain application (for example, depending on the size of the end-effector of the manipulation system).

$$A_g = \pi \frac{g^2}{4} \tag{3.1}$$

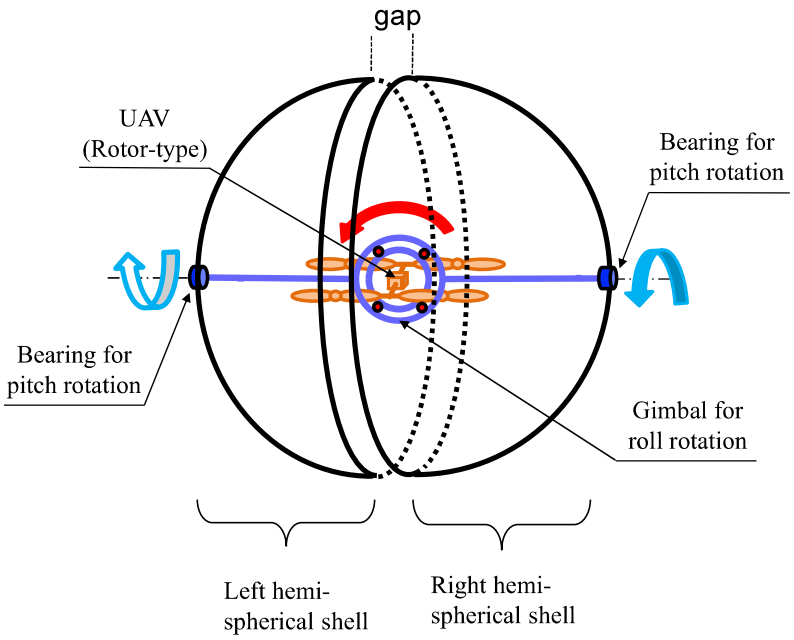

Figure 3.3: General concept of UAV with two passive rotating hemispherical shells.

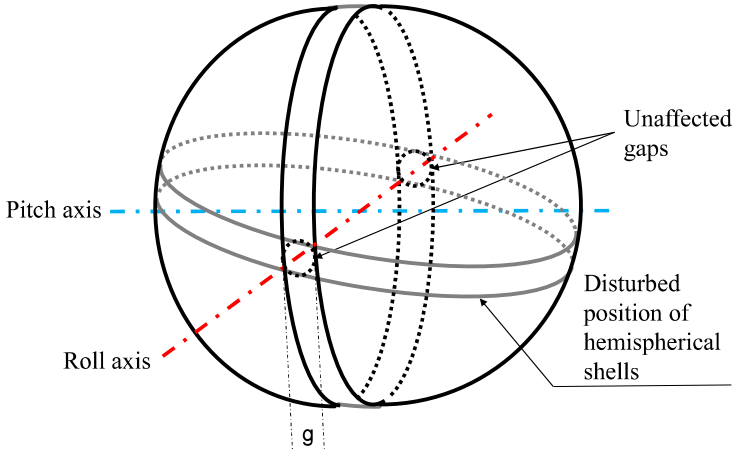

Figure 3.4: Significant gap unaffected by rotation of hemispherical shells.

The proposed system will have two postures: the lateral (normal) posture and the upright posture. The lateral posture of the hemispherical shells is shown in Fig. 3.5 (a). The center of gravity (COG) of the two hemispherical shells positioned at the left and right, both with equal weight W_{HS}, maintains the system in such a posture during flight unless there is a disturbance in the roll axis. This posture allows rotation about the pitch and roll axes. Next, when the whole shell is disturbed causing a roll rotation (see Fig. 3.5(b)) and stops at the position shown in Fig. 3.5(c) , it will attain an upright posture. The COGs of the two hemispherical shells are positioned at the center of the body frame of the UAV, which is also in a balanced condition. This posture allows rotation about the roll and yaw axes.

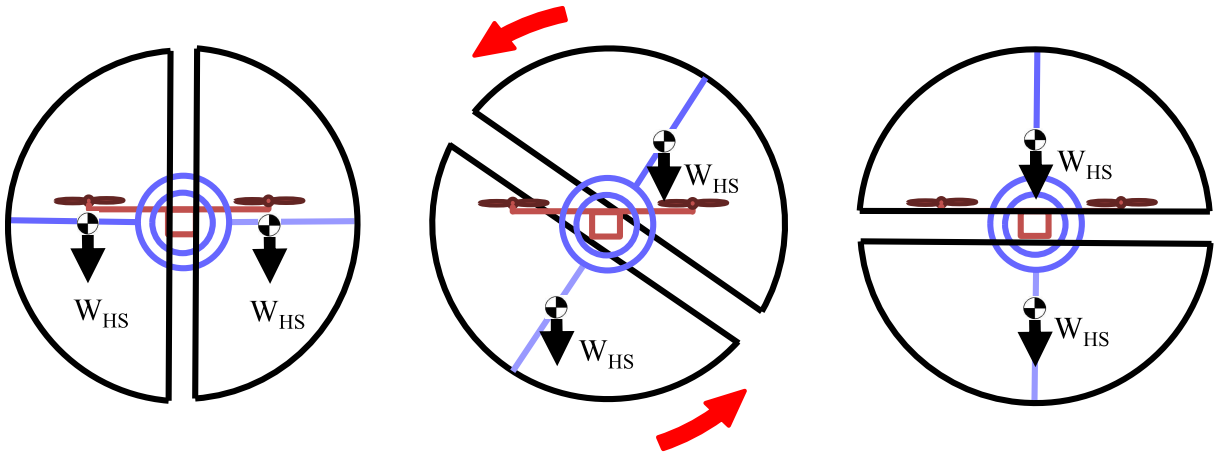

(a) Lateral posture (b) Disturbed position (c) Upright posture

Figure 3.5: Postures of hemispherical shells (HS) with corresponding center of gravity's orientation.

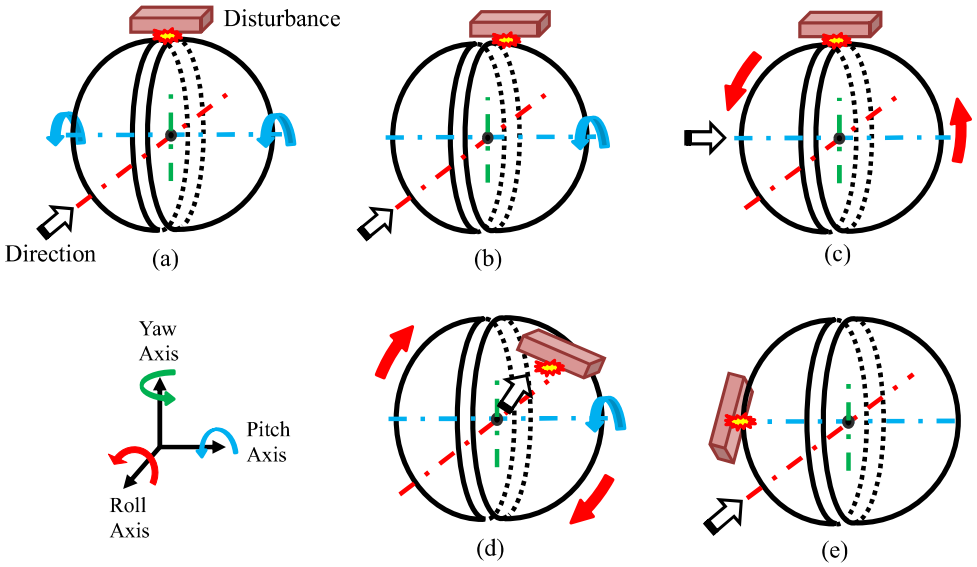

Figure 3.6: Motion of two hemispherical shells during disturbances.

3.5.2 Rotation Analysis of the Hemispherical Shells

It is expected that during a flight, the system may experience disturbance(s) as it makes contact with or collides with obstacles. As a result, the two hemispherical shells will react with different modes of rotation for different conditions. Fig. 3.6 shows the motion of the two hemispherical shells for different scenarios. Fig. 3.6(a) illustrates the motion when both hemispherical shells rotate together in the same direction about the pitch axis as it hits an obstacle when the system moves parallel to the roll axis. With a similar flight direction but only one hemispherical shell is disturbed, the motion for one hemispherical shell is shown in Fig. 3.6(b). On the other hand, if the flight direction is parallel to the pitch axis and the disturbance is as shown in Fig. 3.6(c), the two hemispherical shells will rotate as one about the roll axis. Fig. 3.6(d) illustrates a combined motion of two hemispherical shells as the system moves in the combined direction hitting one hemispherical shell. This condition will frequently occur. Meanwhile, Fig. 3.6(e) shows no rotation for both the hemispherical shells; the obstacle is parallel to the yaw axis of rotation. In this condition, the attitude of the UAV about the yaw axis is affected. A control strategy can be added to reject the disturbance and move away from the obstacle.

3.5.3 Analysis for Physical Interaction

The manipulation system is rigidly positioned in the front side of the UAV through its body frame. It can move along the roll (longitudinal) axis, where it cannot obstruct the rotation of the two hemispherical shells, as shown in Fig. 3.7. Therefore, the expected kinematics of the manipulator are translation and rotation along the pitch axis. One possible mechanism given the translational movement of the manipulator is an extend-retract

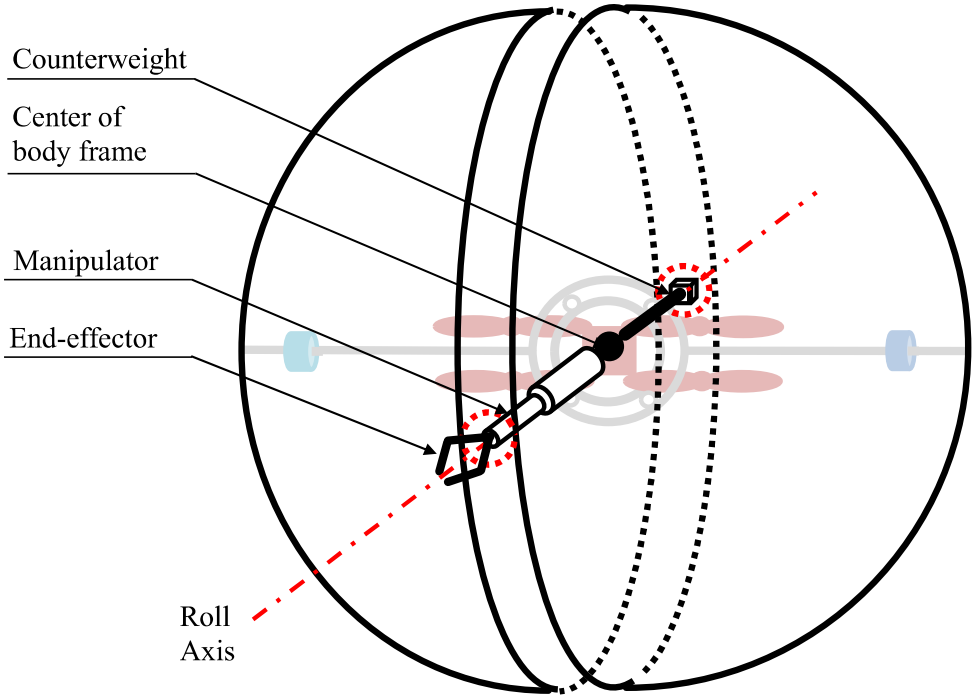

Figure 3.7: Positioning of manipulation system along roll axis.

mechanism. It is important to avoid unnecessary physical contact of the manipulation system (especially its exposed end-effector) with the environment whenever it is not in use.

The position of manipulation system is intended to facilitate horizontal manipulation. Problems are expected to occur especially when the end-effector is in contact (interact) with the target environment. However, several studies have already been proposed to tackle horizontal interaction with the environment. Scholten et al. [86] proposed an interaction control for the underactuated quadrotor equipped with a manipulator where the impedance and the PI controller are used to control the end-effector during free-flight and contact mode, respectively. It shows that the controller can track a reference force in the environment and reject the disturbances while keeping the end-effector in its position. A passivity-based control strategy to handle both the case in which the end-effector is in contact with or not in contact with the environment is also proposed [87]. Furthermore, a mechatronic design of a robotic manipulator [88] that can perform both trajectory tracking in free flight and physical interaction, and can even be used with the existing onboard control architecture is introduced. Another problem is that a quadrotor-type UAV may get sucked against the wall because of the low pressure above it, which can lead to a crash. Albers et al. introduced a method for horizontal manipulation where an actuator is added to the system to generate forces during physical contact while the UAV stays horizontal [91].

For the grasping task, the object grabbed becomes a payload and such an object will

cause load imbalance and shift the center of gravity of the system. The quadrotor-type UAV has the capability to adapt the payload offset or load imbalance and can maintain a horizontal flight attitude even with unbalanced loads [93]. Pounds et al. studied the stability of a quadrotor with the added payload and presented stability bounds within which the changing mass-inertia parameters of the system due to the acquired object will not destabilize with a standard flight controller. However, it is also expected that a robust control strategy will be implemented to deal with the possible instability during load imbalances while the system collides with obstacles.

3.5.4 Structural Analysis and Mechanical Design

Cutting the spherical shell into two hemispherical shells make the structure weak, causing deformation at the base, especially when it is subjected to a load. This requires a tough but lightweight support at the base of the hemispherical shell to minimize deformation. The proposed structure of the hemispherical shell is shown in Fig. 3.8. The shaft holder set is used to connect the shaft and the hemispherical shell.

Separation of the hemispherical shells will also cause deflection during take-off or landing and flight. Without any appropriate supports and relying solely on a single

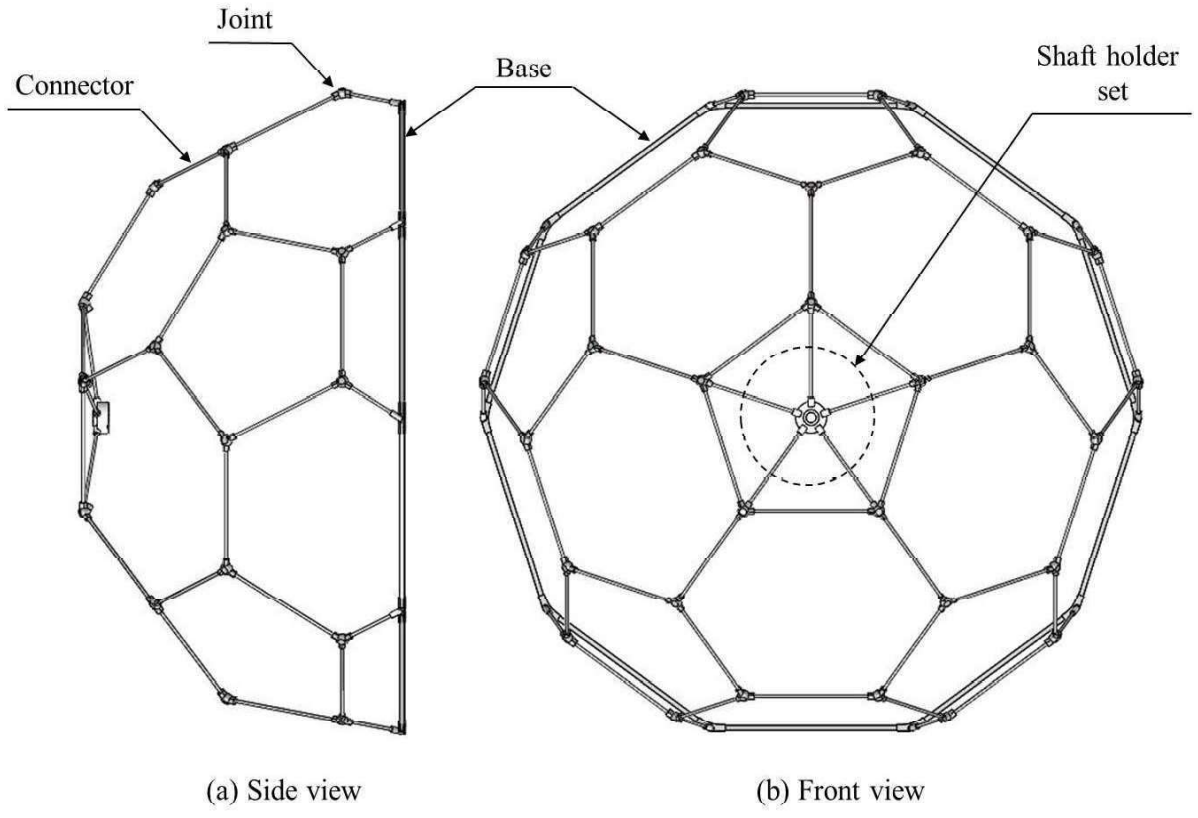

Figure 3.8: Hemispherical shell structure.

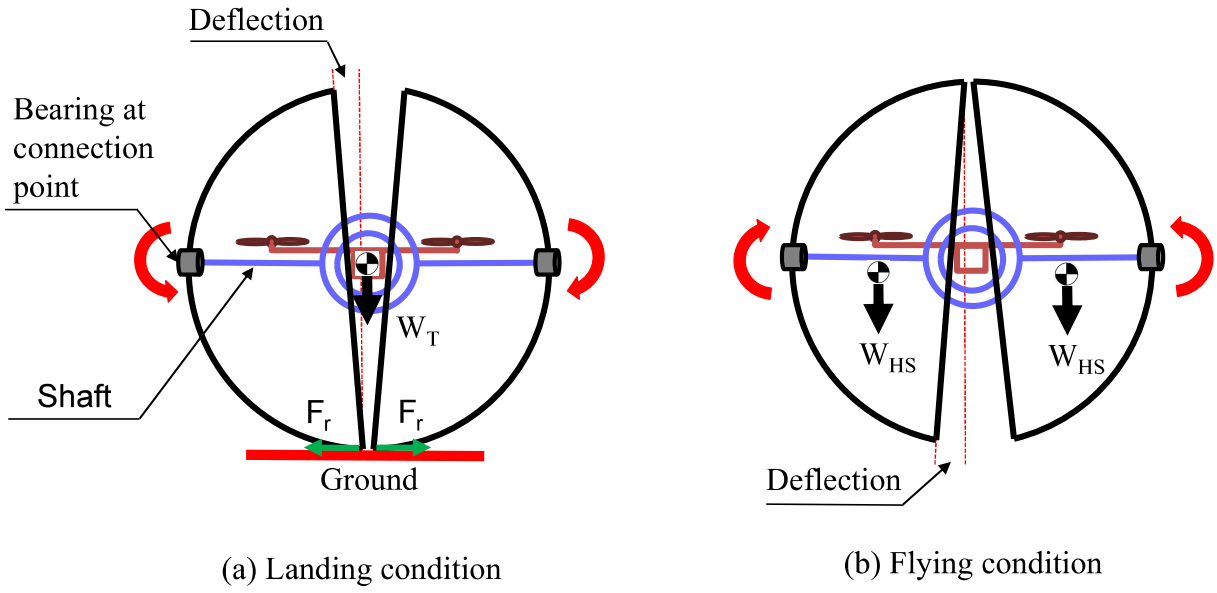

(a) Landing condition

(b) Flying condition

Figure 3.9: Deflection of hemispherical shell (HS) due to weak support.

bearing, the hemispherical shells are expected to deflect as shown in Fig. 3.9. The total deflection is contributed from the bearing's internal clearance and the deflection due to its own weight. During the landing position, the two hemispherical shells act as support structures to the rest of the system with weight W_T. With no other support and small frictional forces (F_r) at the bottom of the hemispherical shell, the moment at the connection point leads to a deflection as shown in Fig. 3.9 (a). In the flying condition, the hemispherical shells become the load, with each having weight W_{HS}.

Similarly, deflection will occur during flight as shown in Fig. 3.9 (b). It is necessary to minimize the deflection during flight to avoid the following problems: (a) the two hemispherical shells may hit each other, which will affect their passive rotation; (b) the deflection may affect the size of the unaffected gap; (c) too much deflection might cause contact with the propeller. In addition, a collision during flight will worsen the problem if the deflection is not minimized. On the other hand, although landing/take-off condition is expected to caused more deflection since W_T is greater than W_{HS}, the problem can be avoided by adding a special landing pad as a support or utilized the upright posture of the shell since it has a good standing posture without causing deflection.

One way to solve the deflection problem is to add trusses along with a secondary bearing as shown in Fig. 3.10. The trusses keeps the secondary bearing in line with the primary bearing (locking up their position), thus avoiding the deflection caused by the internal clearance of a single bearing. Furthermore, the secondary bearing and trusses will counter the moment caused by W_{HS} (during flight) or W_T (during landing). Five trusses and one bearing on each hemispherical shell can be installed given the inner structure of the hemispherical shell.

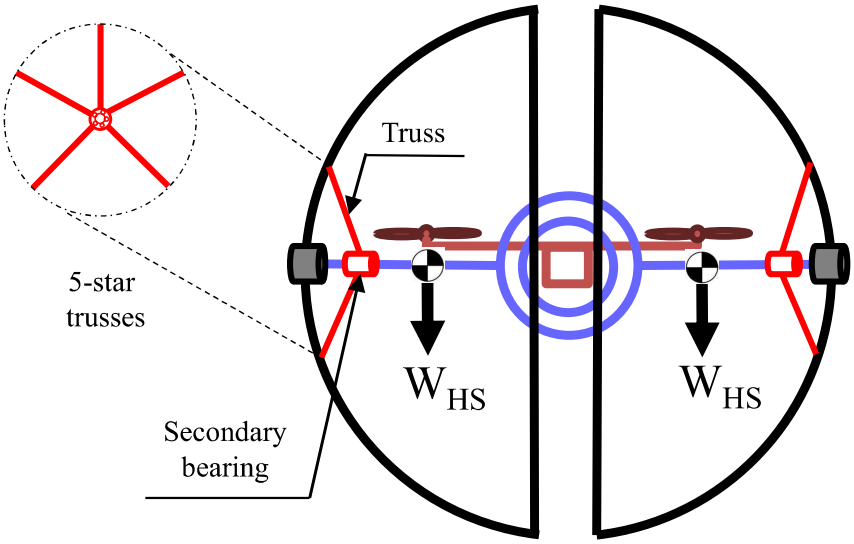

Figure 3.10: Proposed trusses and secondary bearing to minimize deflection of hemispherical shell (HS).

The truss force F_A and stress σ_A can be calculated for the selection of material. By symmetry and letting a single truss carry all the reaction force, a simplified two-dimensional force body diagram can be analyzed as shown in Fig. 3.11. The maximum deflection occurs during the landing/take-off condition, and thus the loading on this condition is used. A force of 12.2 N (maximum load) located 408.5 mm from the main bearing (pt. B) is applied. Taking the moment (+CCW) at point B,

$$M_B = -F_A sin(35) \times 0.0755 + (12.22 \times 0.4085) = 0 \tag{3.2}$$

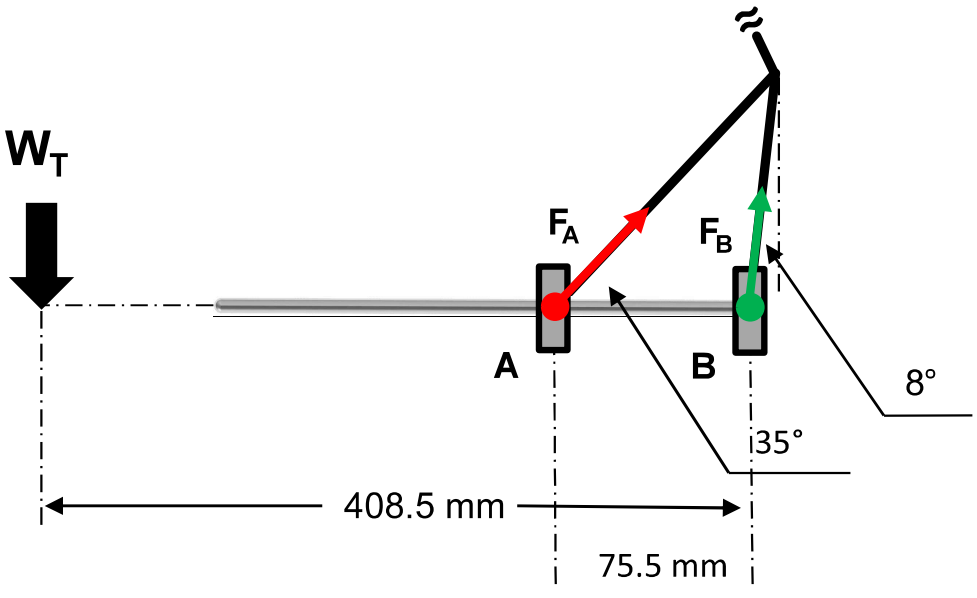

Figure 3.11: Calculation of the reaction force on the truss.

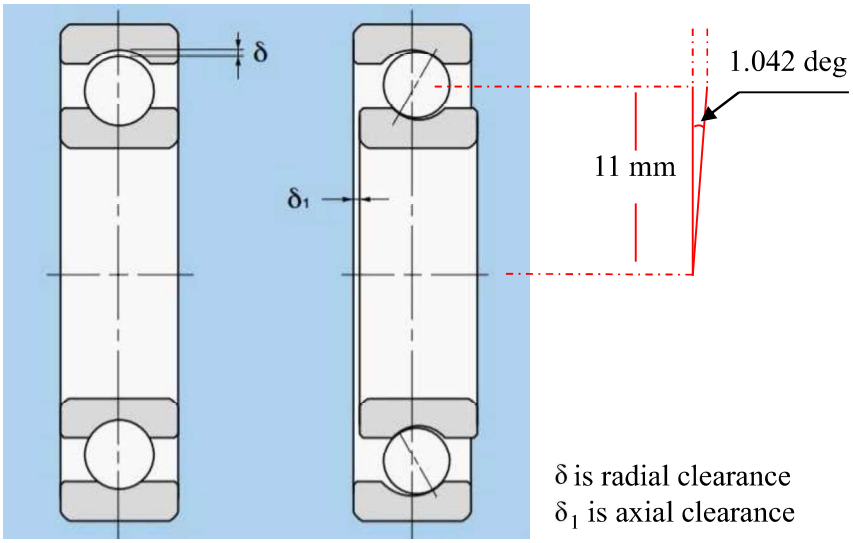

Figure 3.12: Estimated deflection of bearing due to internal clearance.

$$F_A = 115.27\ N \tag{3.3}$$

The stress σ_A is F_A over the cross-sectional area of the truss, where a 3.5-mm-diameter carbon rod is used. The stress σ_A is equal to 11.98 MPa. The typical yield strength σ_Y of carbon material is approximately 200 MPa. Because σ_A is much less than σ_Y , the 3.5-mm-diameter carbon rod is completely safe to use.

The deflection of the bearing due to the internal clearance δ_{BIC} can be determined using the bearing's specification. Fig. 3.12 shows the estimated deflection angle θ of the 6201zz radial bearing on the basis of the bearing's datasheet. With respect to the hemispherical shell, this deflection is $r\theta$, where r is the radius of the shell. Thus, δ_{BIC} is equal to 7.65 mm.

A static simulation is also performed to determine the deflection caused by the weights W_{HS} and W_T with corresponding values of 2.1 N and 12.2 N, respectively. By symmetry, the simulation is simplified by using only one hemispherical shell. The shaft is considered a fixed support. Fig. 3.13 shows one of the simulation results. The overall results of the simulation are shown in Table 3.1.

Table 3.1: Deflections for different conditions

Mode	Type	δ_W (mm)
Flight	With trusses	1.37
Flight	Without trusses	2.33
Landing/Take-off	With trusses	16.2
Landing/Take-off	Without trusses	33.84

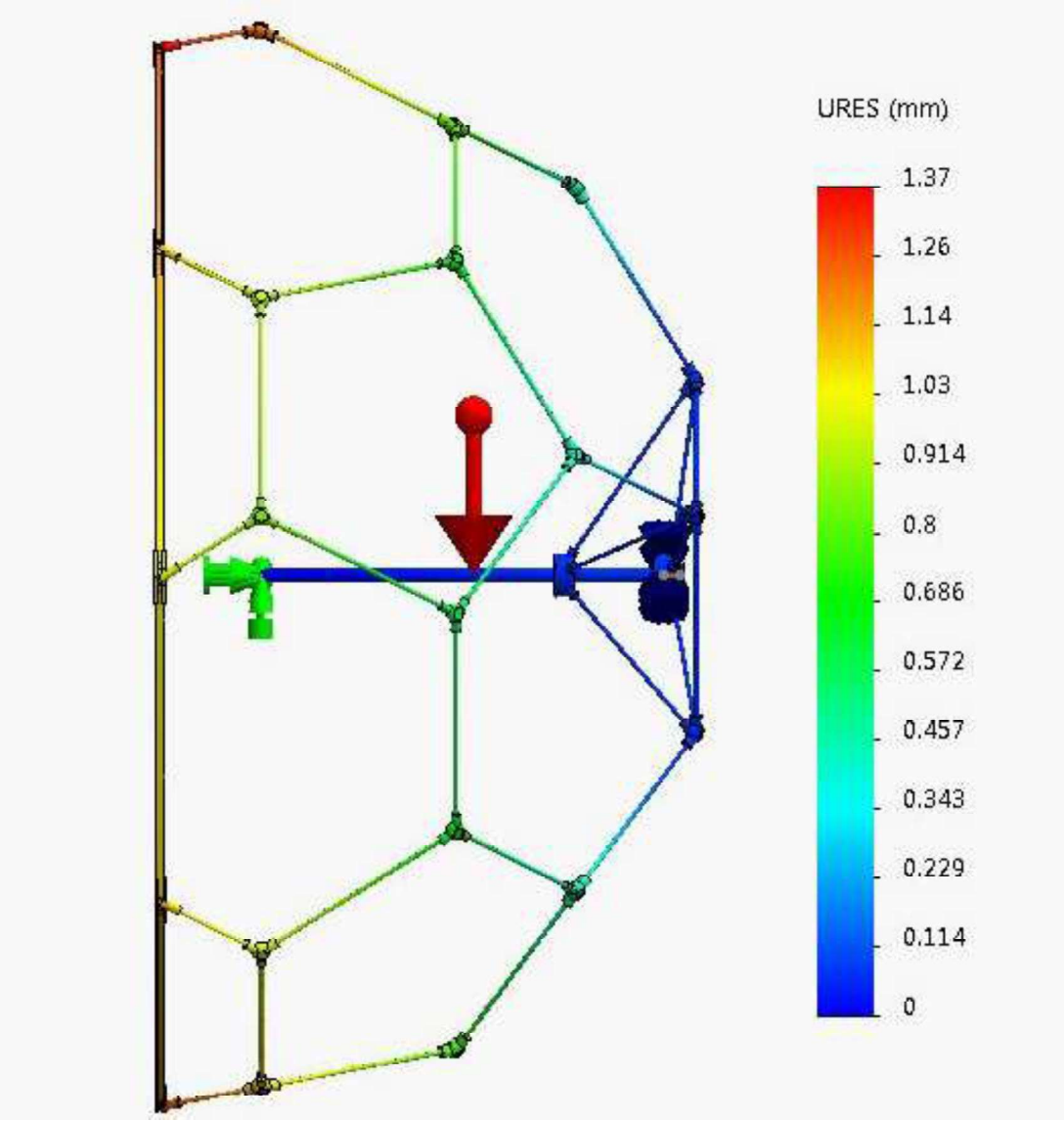

Figure 3.13: Simulation to determine the deflection caused by HS's own weight.

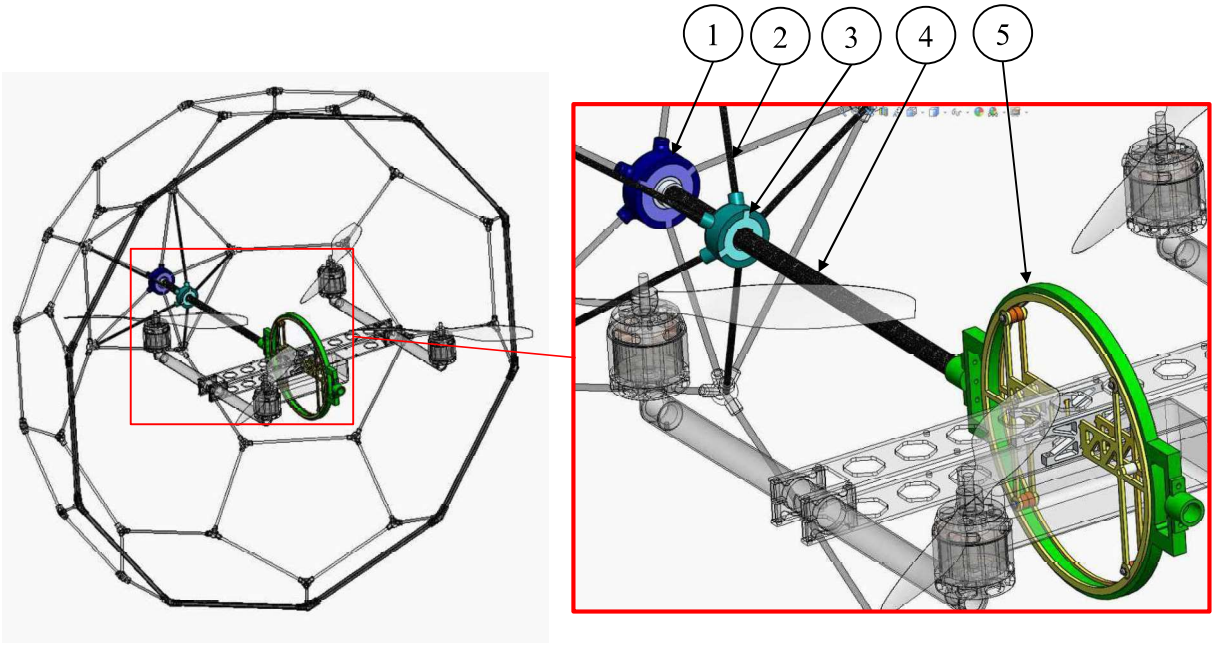

(a) Internal mechanical structure (b) Closeup view

Figure 3.14: Internal mechanical structure of proposed system.

Fig. 3.14 shows the internal mechanical structure of the proposed system for rotation and support of hemispherical shell. The components and its function are as follows:

1. The main bearing set is used for rotation of the hemispherical shell in the pitch axis.
2. The trusses are to support the hemispherical shell and prevent deflection.
3. the secondary bearing set serves as the base for the trusses while it allows rotation.
4. The shaft is used to hold and connect the hemispherical shells to the main part.
5. The roll gimbal set is for rotation of the hemispherical shell about the roll axis.

3.5.5 Experimental Prototype and Test Flight

Fig. 3.15 shows the fabricated prototype. The system weighs 2300 g including the battery, and its spherical shell diameter is 850 mm. The gap g is 50 mm in diameter. The components and specifications are as follows: (1) The joint is made from 3D-printed ABS plastic material and weighs 1.9 grams each. (2) The connector is a 3.5 mm carbon rod with a weight density of 11 g/m. (3) The center frame is made of 10 pieces of ($\phi_o = 6$ mm) square carbon pipe forming a regular decagon. (4) The UAV is a quadrotor-type with an overall diameter of 730 mm and a maximum take-off weight of 2.8 kg. It uses a 2700 mAH (milli ampere-hour) battery. (5) The roll gimbal set consists of ($\phi_o = 8$ mm)

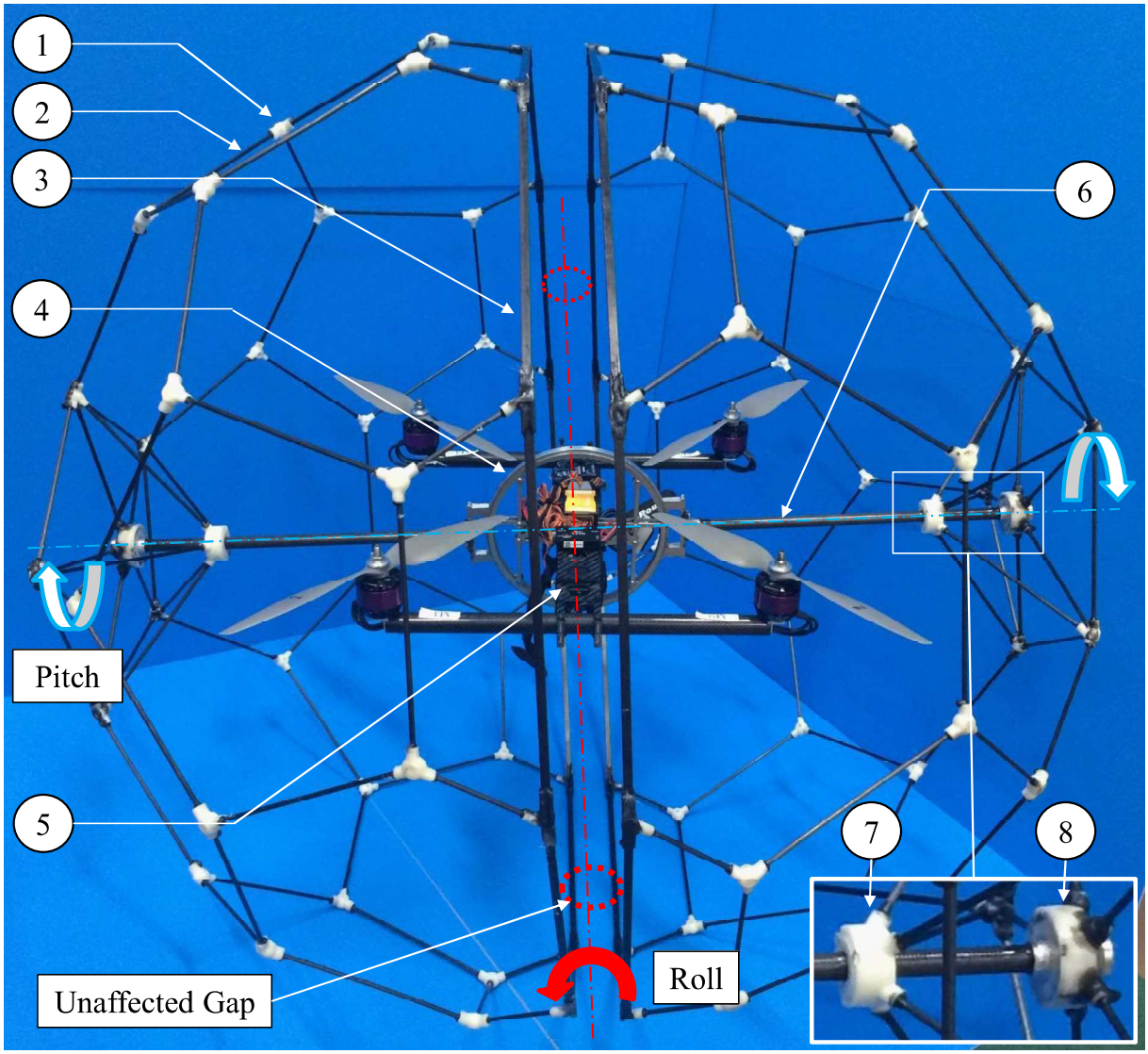

Figure 3.15: Experimental prototype.

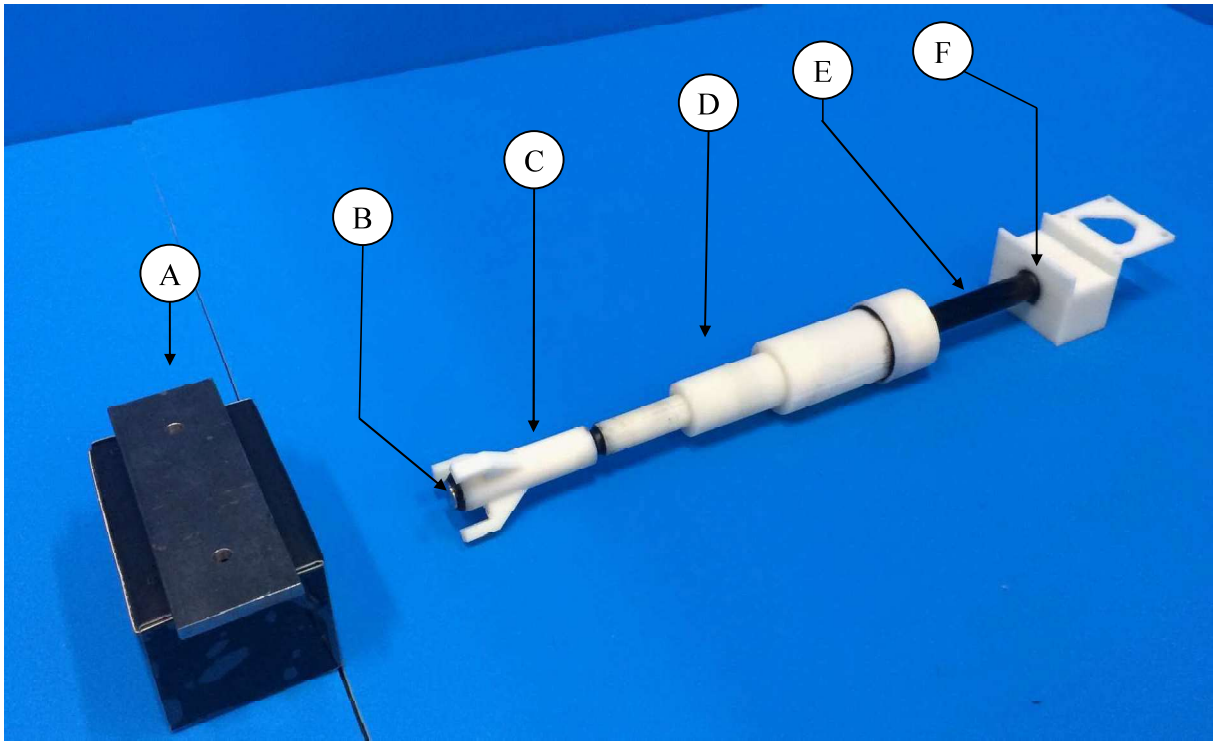

Figure 3.16: Simple manipulation system model with sample object to grabbed.

bearing set and a gimbal aluminum frame. (6) Shaft is made of a tough ($\phi_o = 11$ mm and $\phi_i = 9$ mm) specialized carbon pipe material. (7) The secondary bearing set contains an ($\phi_o = 24$ mm and $\phi_i = 12$ mm) angular contact bearing. (8) The primary bearing set contains a ($\phi_o = 32$ mm and $\phi_i = 12$ mm) radial bearing.

Fig. 3.16 shows the manipulation system (MS) model weighing 61 g. A (B) magnet is attached in (C) the end-effector to mimic simple grabbing of (A) a sample object weighing 103 g. The (D) manipulator is modeled by two rotation and two translation kinematics. However, no movements will be performed in our experiment. A (E) shaft is added just to extend the manipulator and is connected to (F) the MS-to-UAV holder.

The first flight experiment mimics the system to fly into a complex structure and then perform the physical interaction. Fig 3.17.1, shows the initial position where the UAV, obstacle, and object to grabbed are labeled as A, B, and C, respectively. A manipulation system model has already been attached in the system in preparation for the grasping task. Fig 3.17.2 and 3.17.3 show the system colliding with the obstacle at the side and top, respectively. Fig. 3.18 shows the flight attitude of the UAV during a collision with obstacles at a flight speed of 0.72 m/s. The disturbance to the UAV is insignificant and it is able to recover quickly. Fig 3.17.4 shows the reaction of the two hemispherical shells after the collision where they passively rotate because of the disturbance. The type of motion after the collision is more as in Fig. 3.6(d), where one hemispherical shell rotates about the pitch axis while both of them rotate about the roll axis. Fig 3.17.5 shows the

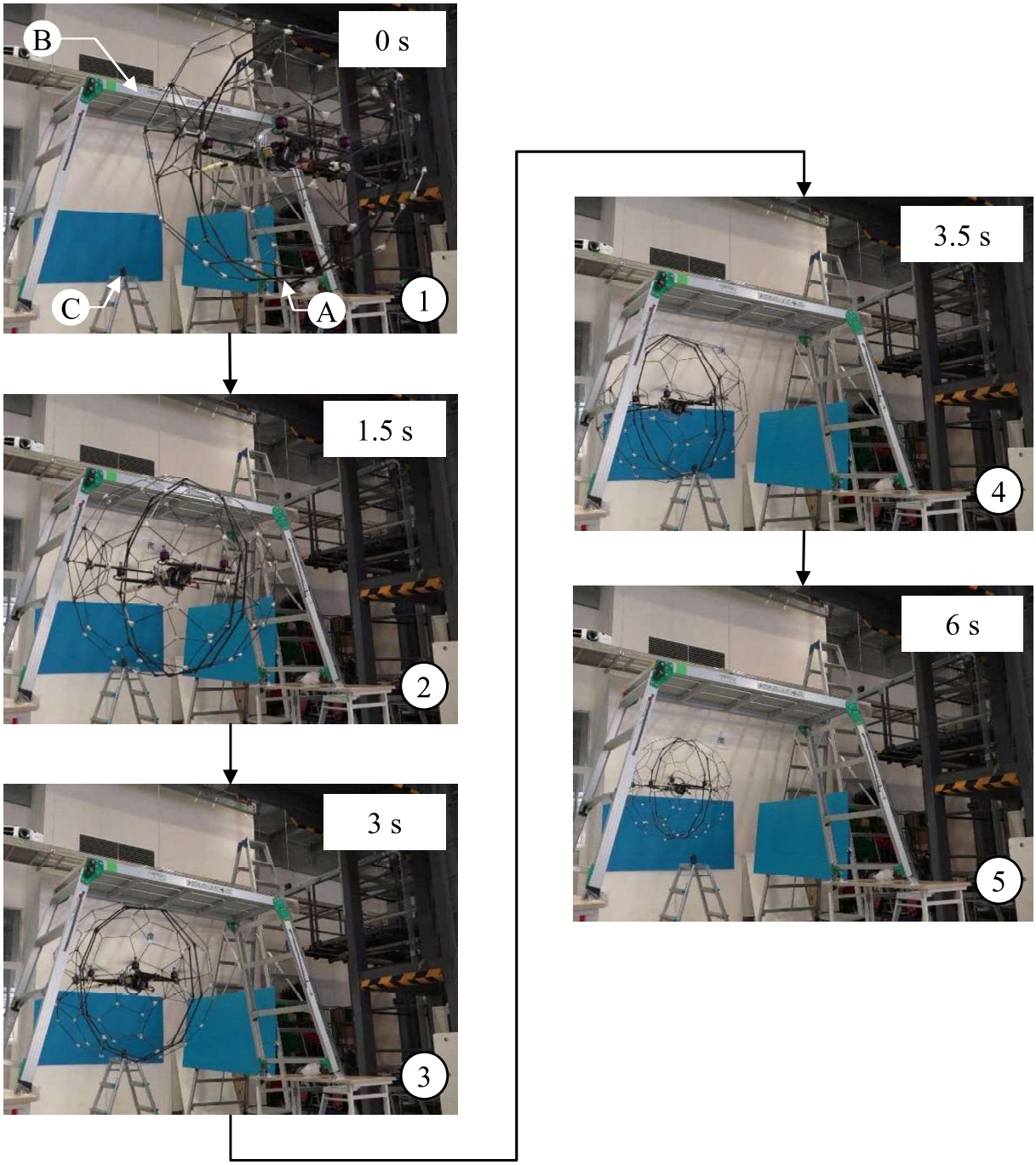

Figure 3.17: Sequence of images for the system with manipulation system model as it crosses the obstacle. Labels A, B, and C are the system, obstacle, and object to be grabbed, respectively.

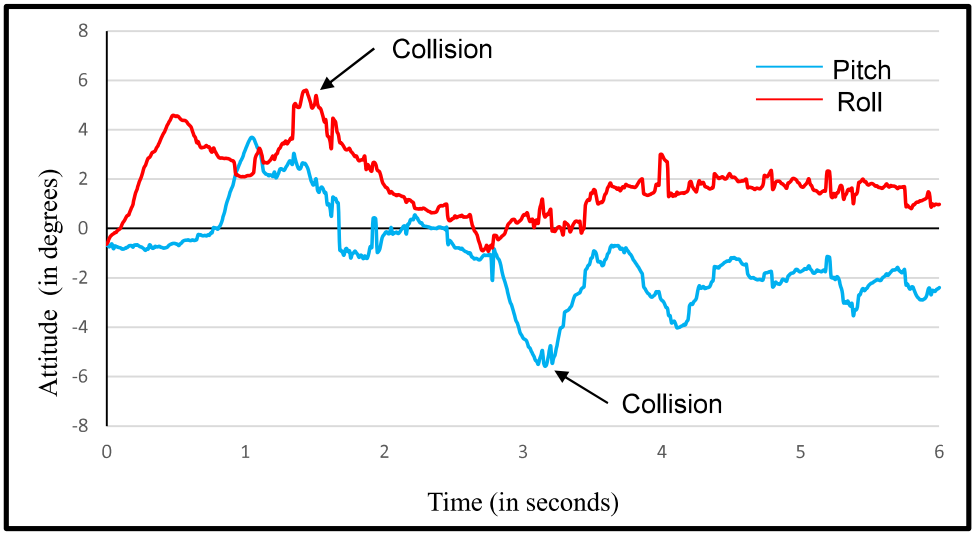

Figure 3.18: Flight attitude of the UAV during collisions with obstacle taken using motion capture system.

complete recovery of the UAV and its movement towards the target object. Fig 3.19.1 shows the system approaching the target object after it crosses the obstacle. Fig 3.19.2 shows the system start to grab the (metallic) object through its manipulation system model where a magnet is attached. Fig 3.19.3 shows the system holding the object and leaving.

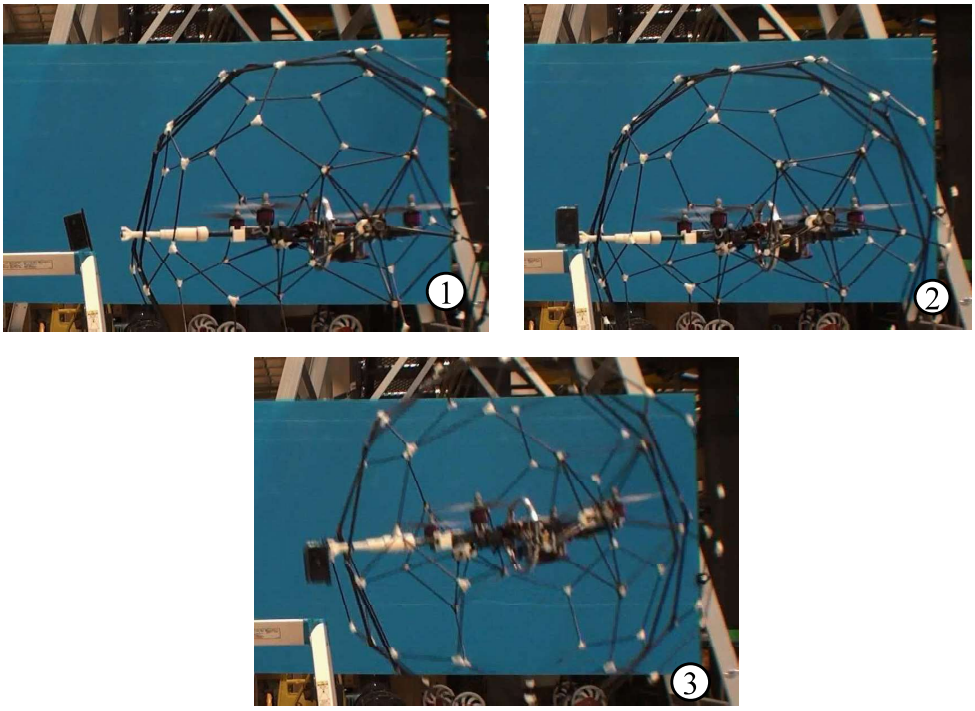

Figure 3.19: Sequence of images for simple grabbing task using the manipulation system model.

3.6 Hammer Test (HT) Using UAV with Two Passive Rotating Hemispherical Shells

3.6.1 Background of HT, Initial work and the Issues

A hammer testing is a non-destructive inspection technique to assess the concrete structure's inner compressive strength by lightly hitting the surface of the concrete with a special hammer device. Checking the inner condition of deteriorated concrete-made infrastructures such as bridges and tunnels is so important to foresee critical problems that can lead to an accident or collapsed of infrastructure. Unable to do so will have a negative impact as it can cause fatalities or affect the economy when the infrastructure is damaged. For instance, a concrete flaking happened in 1999 in a Shinkansen tunnel of West Japan Railway. A 226 kg concrete mass had fallen and hit the Shinkansen train running in the tunnel [94] which halt the train operation for some time. Also, the Sasago tunnel ceiling collapse on the Chou Expressway in 2012 which killed nine people and two people injured [1]. About what has been discussed in the previous Chapter about the visual inspection of old bridges (above 50 years) in Japan, another task is to check the internal condition of bridges through hammer test. Similarly, the traditional hammer test is performed manually by a human inspector which they need to use scaffolding to reach the target. As previously mentioned, this task is unsafe for the human inspector, requires more time and the installation of the scaffoldings are expensive.

Today, UAVs are being used to facilitate human inspector in infrastructure inspection to provide safe, fast and inexpensive operation. Yano initiated the study of hammer test of the structure using multi-copter [95] [96]. The study focused on testing the condition of the tiles on the vertical wall. The general concept of the initial work is to attach the hammering device on the frontal side of the quadrotor UAV as shown in Fig. 3.20. The hammering device will constantly hit the structure while the UAV is in contact with the wall. A roller is also attached to assist the UAV as it hovers up and down. Subsequently, the sound produced by the hammer is being recorded for post-processing. The variation of sound determines the healthy and unhealthy tiles. However, this work has limitation and flaws. First, the interaction with the wall relies mainly on the UAV's controller. To move closer and keep its distance from the wall it needs to tilt on pitch axis constantly. The tilting of the UAV, however, incite risk of falling as the low pressure above the UAV caused it to get sucked up by the wall, this problem is mentioned in Chapter 3.5. Second, the initial work is intended only for an open space wall and cannot be applied to a complex infrastructure like the bridge. This is because there is no enough protection to keep the UAV stable at the moment it will get contact with the obstacle. Lastly, the attached hammering device may not be robust enough to perform the task as well

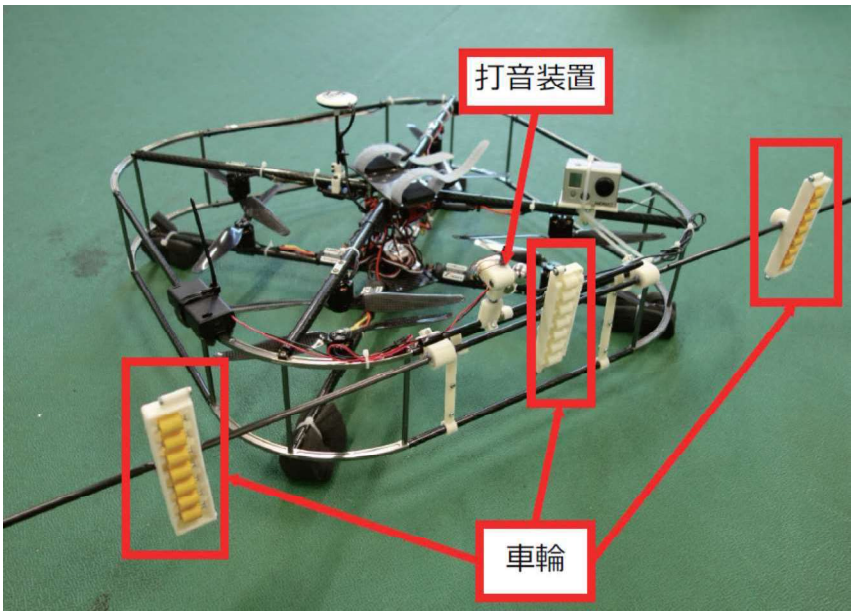

Figure 3.20: Initial study of hammering test of structure using multicopter, Source: Yano, 2014.

as acquire useful data. The initial work presented a hammering device using knocking technique. The striking force introduced in the former study may not be enough to test a concrete structure, if we based the striking force applied by a human on manual inspection.

This section will present solutions to the limitation as mentioned above and flaws. It is intended to develop a new system that can provide a good hammering action and allows the system to be used in the complex-structured environment. At the same time, it is also the intention to implement the new concept of two passive rotating hemispherical shells for the UAV mentioned in Chapter 3.5. This study, however, will focus only on the development of mechanism. The acquisition of sensor data and post-processing to determine the health and unhealthy structure is not part of the scope of the study. This part is being worked out by project collaborator.

3.6.2 General Concept

Fig. 3.21 shows the general concept of hammer test using UAV with two passive rotating hemispherical shells. All components are installed within the two hemispherical shells to ensure they are protected against any obstacles. The hammering device is positioned along the roll axis of rotation and on the frontal side of the UAV and placed near the border of the protective shell through extension arm. The hammering action is controlled by the controller unit which receives command from the RC transmitter. This controller is separate from controller unit of the UAV. The hammer guide is added to facilitate the hammer and keep the distance between the structure and the hammer (end-effector). In

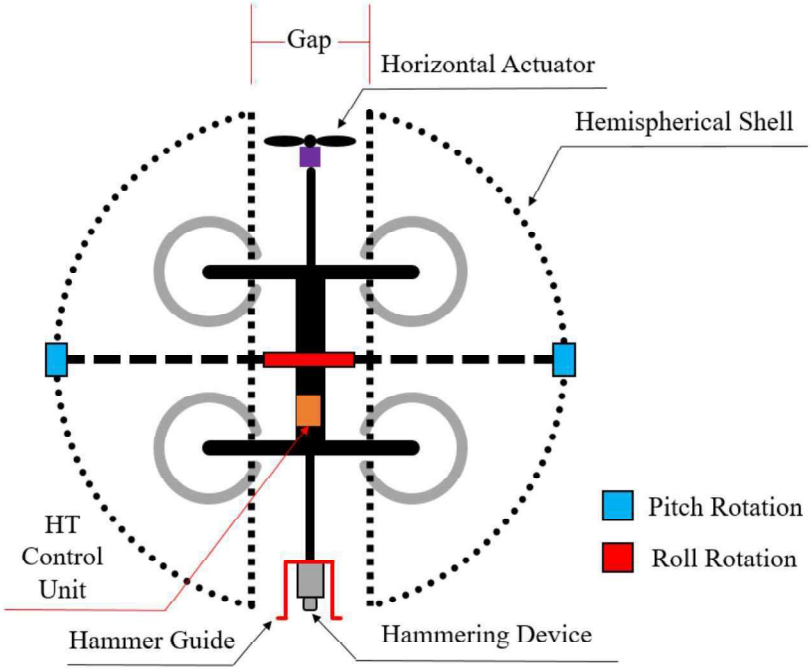

Figure 3.21: Proposed hammer test using UAV with two passive rotating hemispherical shells.

such way, an effective striking force can be obtained. To avoid tilting of the UAV just to move closer and in contact with the vertical structure or wall, a horizontal actuator (HA) is implemented. This horizontal actuator will generate enough thrusting force that will allow the UAV to move forward without tilting. Another advantage of not tilted is that the hammering device (rigidly attached to the UAV) will be perpendicular to the vertical structure or wall which is the ideal position for hammering. This horizontal actuator is also controlled by the mentioned controller unit for activation. The size of separation of hemispherical shells or so-called gap is selected based on the diameter of the horizontal actuator's propeller. A clearance is added to ensure it will not affect the air flow when the propeller rotates. Also, the horizontal actuator is placed opposite to the hammering device (still lies on roll axis of rotation) to serve as a counterweight.

3.6.3 Hammer Test System: Design and Analysis

Fig. 3.22 shows the block diagram of the complete hammer test system. The hammer test system comprises the hammering device, horizontal actuator, micro-controller unit (MCU), data storage, and RC transmitter. The controller unit activates the solenoid through circuit driver to strike the hammer. The command comes from the human operator on the ground through RC receiver. The controller unit also receives analog data from a piezoelectric sensor and small microphone for every strike and store them into the SD card. However, these collections and storing of data will not be implemented in this study.

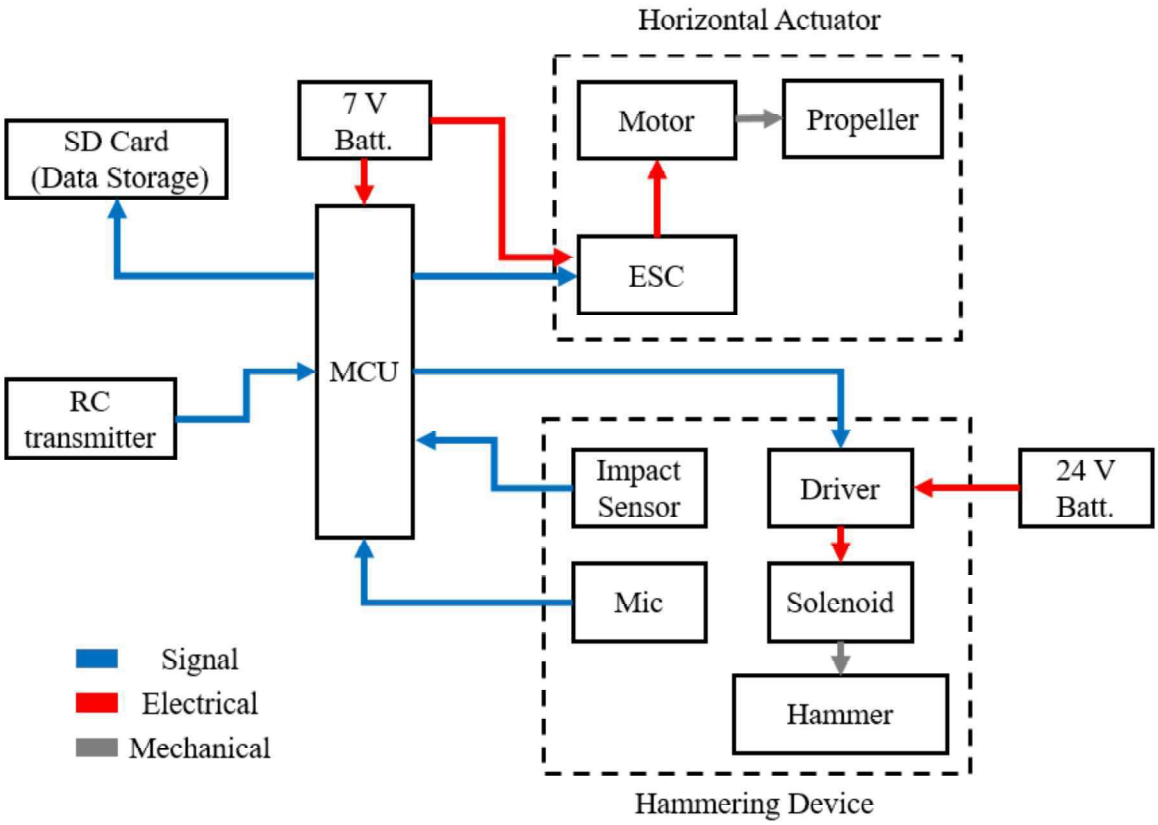

Figure 3.22: Block diagram of the proposed hammering system.

The controller unit also activates the motor through electronic speed controller (ESC) of the horizontal propeller during hammering to keep its distance from the vertical structure or wall. The present hammering device is a prefabricated system manufactured by collaborating company as shown in Fig. 3.23. It also includes other optional components such as Bluetooth and vibration sensor but will not be implemented in this study as well. The simple concept of hammering lies on the solenoid. Once activated, the solenoid pushes the plunger where the hammer is attached at the end. Then, the plunger retracts and pulls back by the spring. The solenoid takes power from UAV's battery. Meanwhile, the controller unit and other small components are supplied by the small secondary battery.

The hammering device needs to be configured to have enough striking force especially to keep a fixed distance between the hammer and wall. The task of the horizontal actuator is to push the UAV horizontally to the wall. However, the problem will be on how to control the horizontal actuator. Keeping a fixed distance using distance sensor is difficult to obtain and impractical. Also, as the hammer hits the structure with force F_H, it has a reaction force F_R that will tend to push the UAV away from the wall. A simple solution is to add a fixed space and apply a force T_{HA} by the horizontal actuator to keep pushing the UAV to the wall as shown in Fig. 3.24. A preliminary test was conducted to deter-

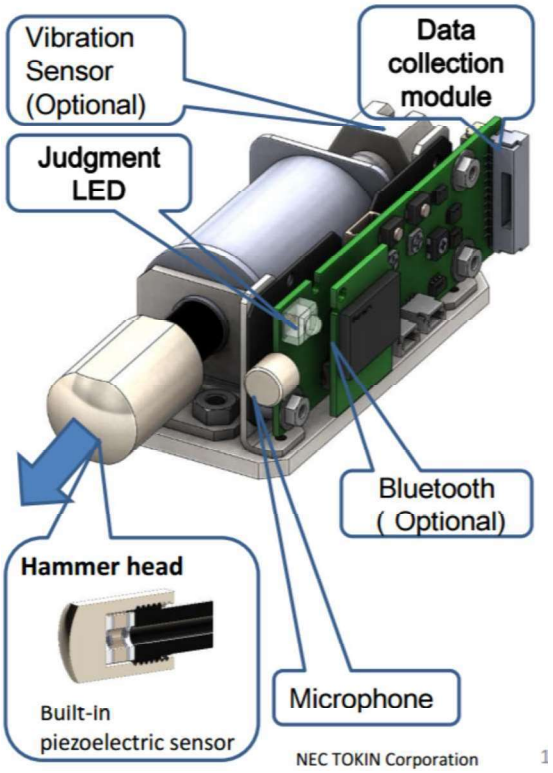

Figure 3.23: Hammering device provided by external company.

mine the distance that produced an effective striking force and sound of the prefabricated hammering device. Fig. 3.25 shows the result of striking power versus distance. The strike of the hammer is evaluated from a distance of 1.25 mm to 10 mm. As expected, the closest distance produces the highest striking force. However, the sound it produced weakens as it goes farther from the wall. The 5 mm distance is set as a baseline for an optimal striking force and sound. Since there is no specific requirement for striking force and sound yet, a 5 mm clearance is assumed acceptable.

The hammer guide will not only provide fixed space but it will also regularly in contact with the structure wherever the hammer moves. The hammer guide should be smooth as possible to avoid excessive frictional force and free to move on the surface. If excessive friction is present, the stability of the UAV might be affected since the hammer guide, or the hammering device as a whole is rigidly connected to the UAV. The idea is to install rollers as shown in Fig. 3.26.

On the other hand, the horizontal actuator only requires little thrust to continually push the UAV to the wall. In such case, a small brushless motor (capable of carrying up to 200 g) [97] and 5 inch propeller [98] is used. A preliminary test set a 0.2 m/s^2 as appropriate acceleration for a UAV with a mass of 2.8 kg. This requires a 0.56 N

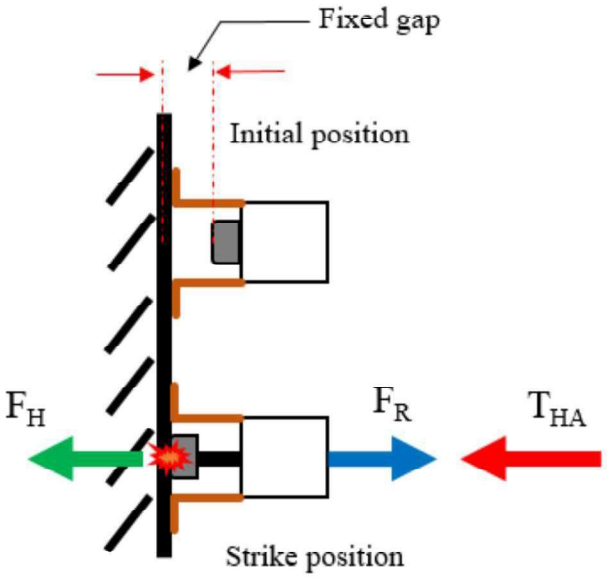

Figure 3.24: Concept of fixed space to provide appropriate striking.

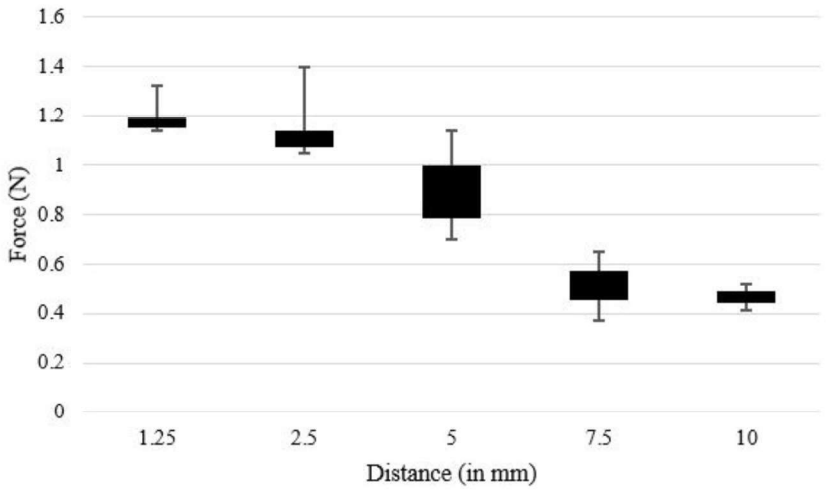

Figure 3.25: Striking force versus distance.

of thrust for the horizontal actuator. Based on the selected propeller performance data [99], an 8000 revolution per minute (RPM) of propeller rotation is enough to produce more than the required thrust. This rotational speed is translated into a pulse (PWM) by controller unit as understood by the electronic speed controller (ESC). The test was conducted to achieve an 8000 RPM by adjusting the pulse in the controller unit and then check the actual rotational speed by digital tachometer as shown in Fig. 3.27. An aerodynamic simulation was also conducted to verify the airflow of the horizontal propeller not to interfere the airflow of the UAV. The horizontal actuator's propeller is expected to suck the air near the main propellers. The horizontal actuator's propeller is placed approximately 75 mm from the tip of the rear propellers of the UAV. The simulation result shows no interference since the change of the velocity of the main propellers are negligible ($\Delta V_{max} = 0.65$ %). The visual result also verified the numerical values as it shows a clear division of airflow (encircled) between the main propeller and horizontal actuator's propeller as shown in Fig. 3.28.

3.6.4 System Prototype and Flight Experiment

Fig. 3.29 shows the UAV with two passive rotating hemispherical shells attached with hammering system. The hammering system weighs 325 grams. The list and short details of the components of the hammering system are as follows: (1) Horizontal actuator comprises of small brushless motor, electronic speed controller and 5 inch propeller, (2) Horizontal actuator extension arm and holder which connects the actuator to the main body of the UAV, (3) Controller unit is a microcontroller board based on the ATmega32U4 which handles all the control, receive and send tasks, (4) Hammering device extension arm and holder connects the device to the main body of the UAV, (5) Hammering device comprises of solenoid, solenoid driver, and hammer as end-effector, (6) Hammering device platform and guide serve as holder for hammering device, guide during hammering task,

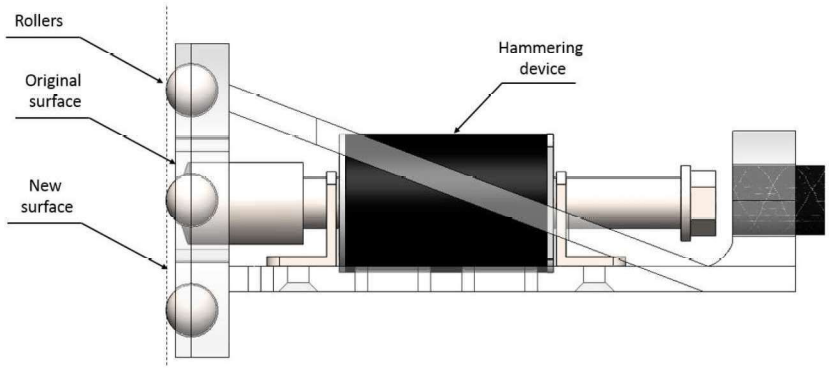

Figure 3.26: Rollers to avoid excessive friction on the surface.

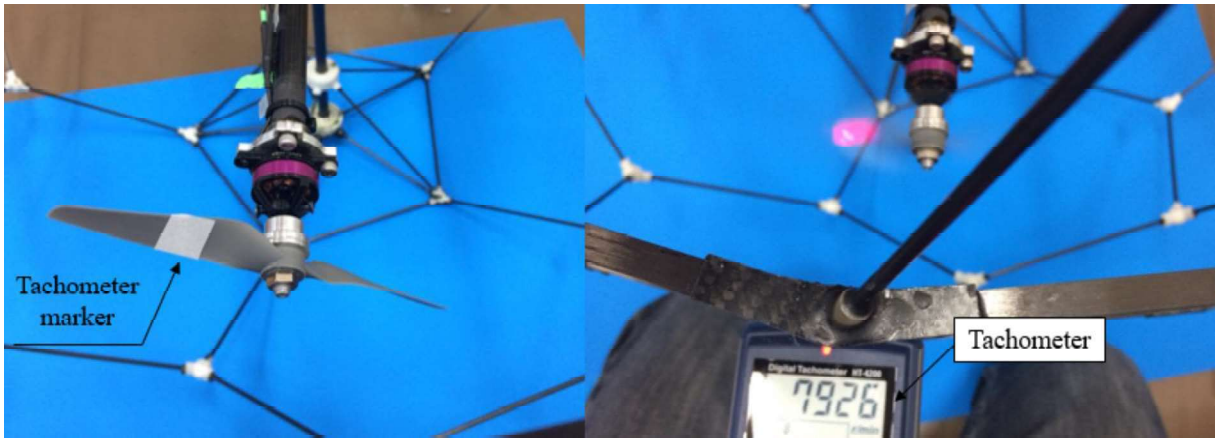

Figure 3.27: Checking the RPM of horizontal actuator through digital tachometer.

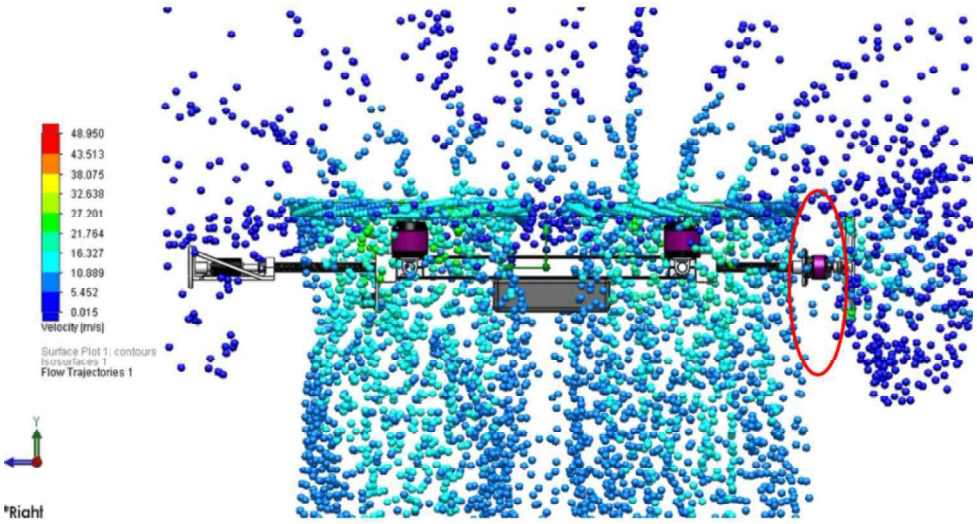

Figure 3.28: Aerodynamic simulation to verify the noninterference of horizontal actuator's airflow.

and responsible for maintaining the distance between the hammer and target structure or wall.

The primary goal of the flight experiment is to verify the hammering action of the UAV with two passive rotating hemispherical shells attached with hammering system. The experiment is intended to show the performance of hammering system by adding the horizontal actuator and hammer guide rollers. Subsequently, it aims to check if the hammering device can maintain its distance to the wall for a long time. Fig. 3.30 shows an actual flight experiment. A simple set-up is implemented by placing a dummy wall where the hammering device can interact. The UAV is kept tracked by the motion capture system for further analysis of its position and attitude during hammering. The pre-fabricated hammering device manufactured by collaborating company can process (sense, receive and store) data approximately 5 seconds. For the system to acquire useful data, it is important that it can strike and subsequently record the data for at least three successive attempts

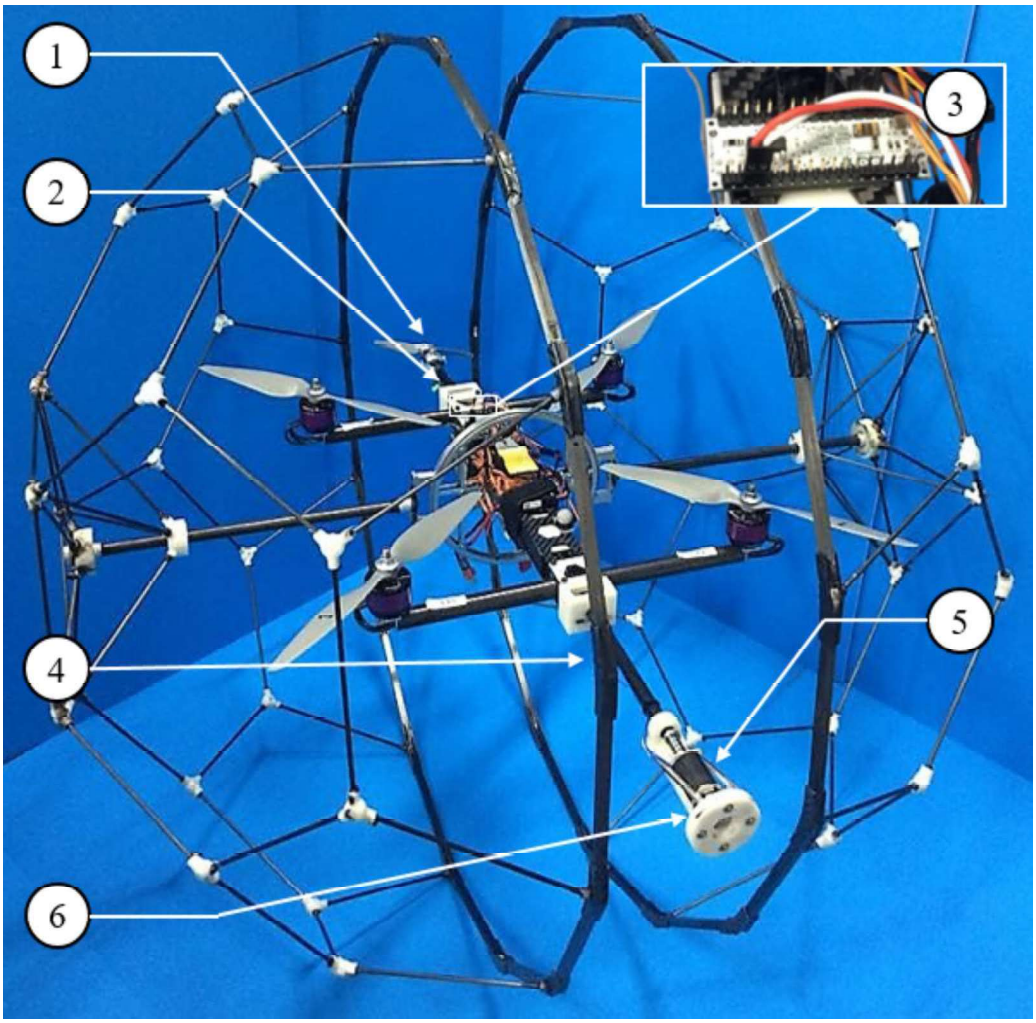

Figure 3.29: UAV with two passive rotating hemispherical shells attached with hammering system.

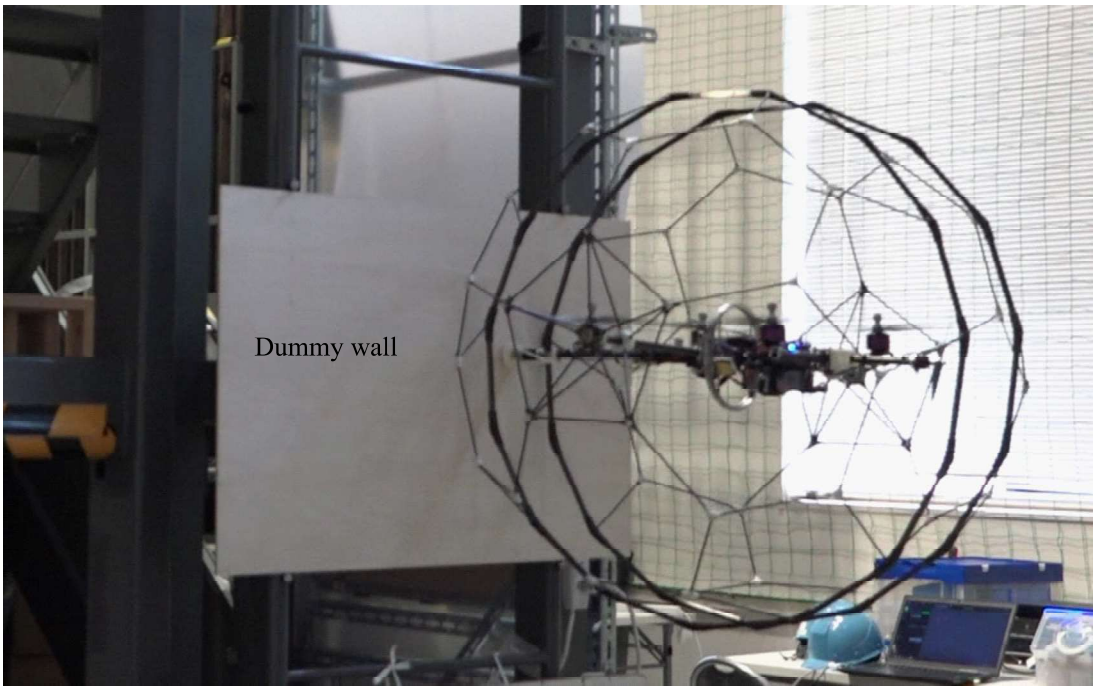

Figure 3.30: Flight experiment of UAV with two passive rotating hemispherical shells attached with hammering system.

in the same area of interest for short time duration. Failing to perform the procedure may result to delay of the inspection process.

The first experiment involves hammering without the horizontal actuator. For several attempts, the system can only stay an average of 4 seconds. The primary reason is that the reaction force during the strike tends to push the UAV away from the wall. For instance, a 75-second continuous hammering action as shown in Fig. 3.31, approaches the wall four times. It initially comes close to the wall and strike, but after few seconds it started to move far away from the wall. The full distance graph is shown at the top portion of Fig. 3.31. Likewise, it was not able to stay close to the wall. The closest attempts as shown in the bottom graph of Fig. 3.31 are encircled in red dash line. The average striking distance is 5 mm while the maximum limit before it fails to hit the structure is 10 mm. These distances are indicated with the green and blue dash line in Fig. 3.31 for average striking distance and maximum limit, respectively. In the graph, it barely able to reach the 5 mm distance. For instance, Fig. 3.32 which is the second encircled region from the right was able to stay about 3 seconds and then try again for 2 seconds before it completely moves away from the wall. The rest of the encircled region stayed within the 5 to 10 mm distance for few seconds and left. This hammering action is poor, and definitely, it cannot obtain useful data.

Meanwhile, the outcome of the absence of horizontal actuator is completely different

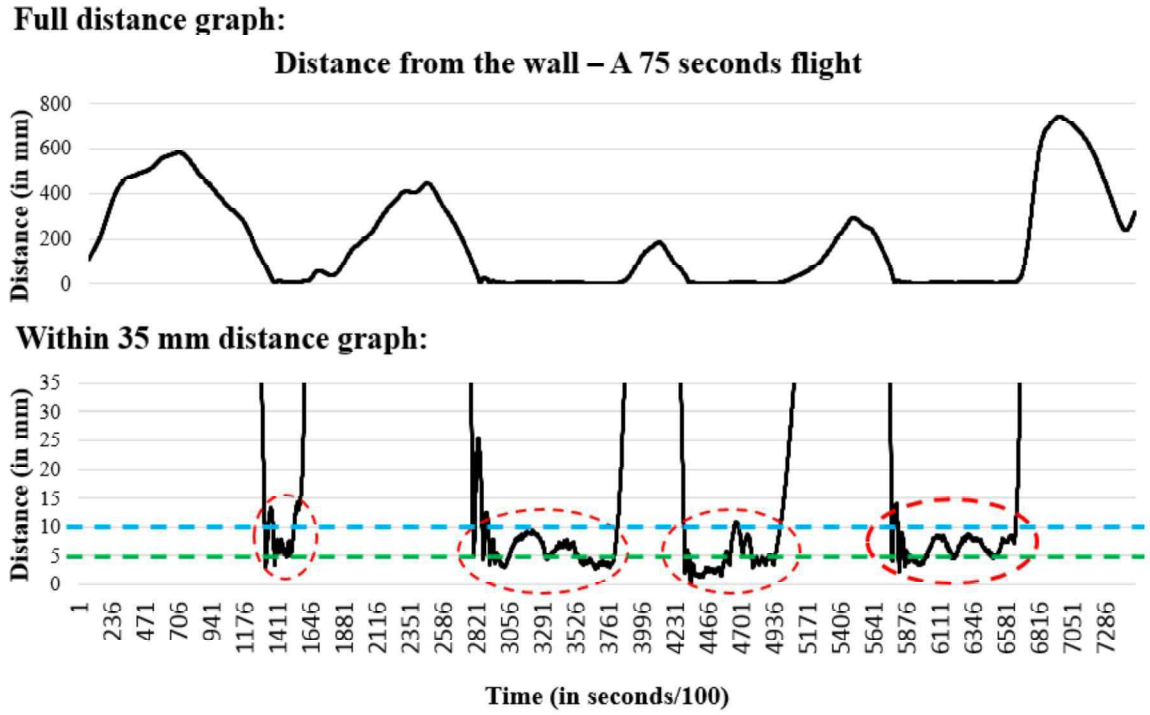

Figure 3.31: A 75-second hammering action without horizontal actuator.

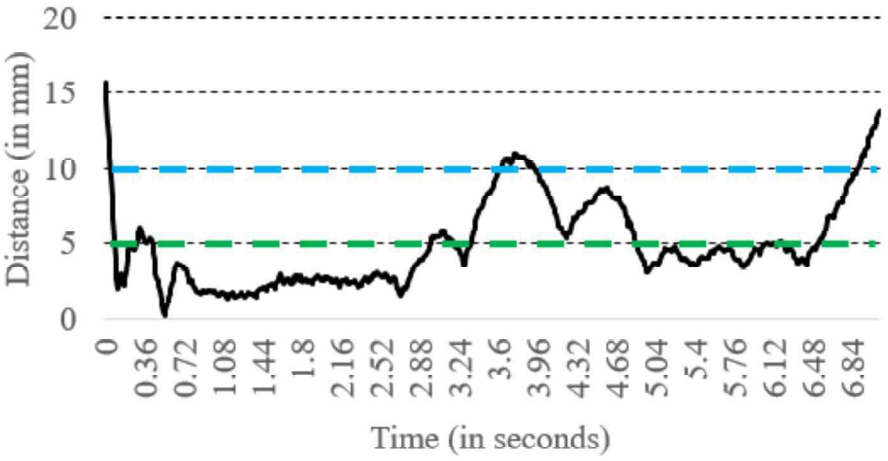

Figure 3.32: Closest distance from the wall for without horizontal actuator.

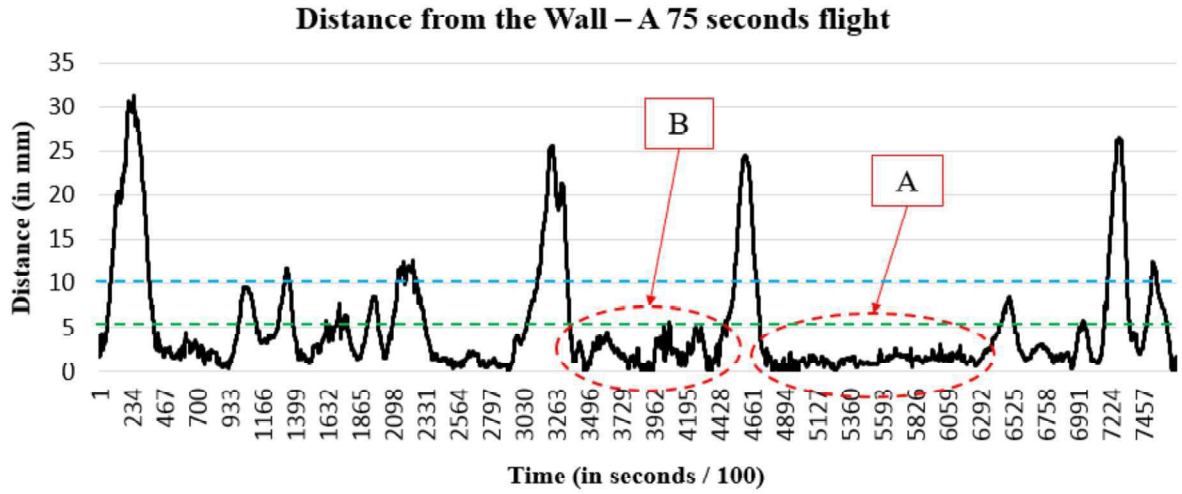

Figure 3.33: A 75-second hammering action with horizontal actuator activated.

when they are being installed as part of the hammering system. The second experiment is by implementing the horizontal actuator. In most trials, the UAV was able to stay longer and closer to the wall. For a 75-second continuous hammering action with horizontal actuator activated, the UAV can stay much longer and closer to the wall as shown in Fig.3.33. It stayed within 35 mm distance for 75 seconds time duration. It also showed the two longest stayed time within the 5 mm distance from the wall, 12 seconds for encircled region B and 20 seconds for encircled region A. The 20-second region is magnified in Fig. 3.34. A 20-second duration and within 5 mm closeness to the wall could offer useful data in a single flight. During the experiment, the hammering device has maintained perpendicular to the surface. This is the advantage of the horizontal actuator that helps in preventing the UAV to tilt or rotate in yaw axis by pushing the UAV to the wall. Such appropriate hammering posture is illustrated in Fig. 3.35.

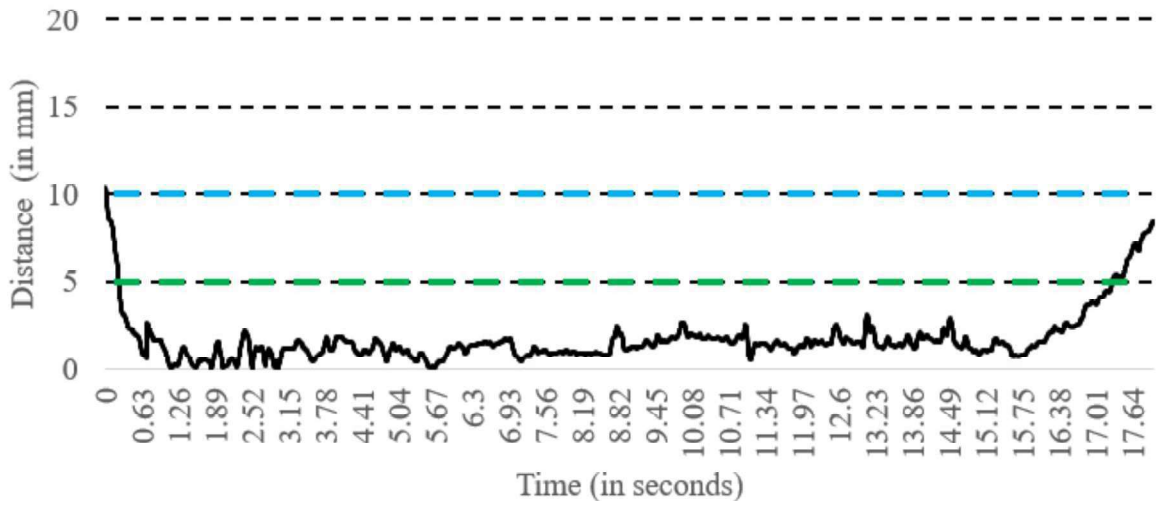

Figure 3.34: Closest distance from the wall with the horizontal actuator activated.

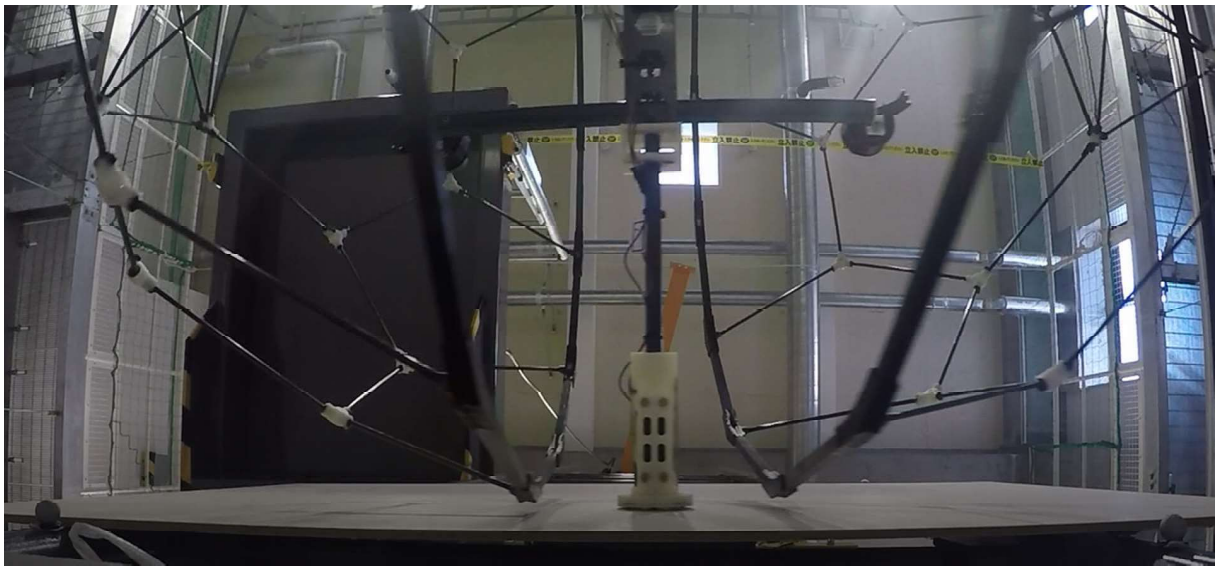

Figure 3.35: Appropriate hammering posture as a result of adding horizontal actuator.

3.7 Chapter Conclusion

In this Chapter, a new concept of two passive rotating hemispherical shells was introduced. The concept, general applications, and design of the proposed system have been presented. The performance of the system with regards to physical interaction and power tethering capabilities was initially verified in our test flights. The characteristics of the passive rotating spherical shell mechanism of protecting the UAV and ensuring good stability have been kept. The concept of two separated hemispherical shells to provide a gap proved effective. The gap size can also be adjusted depending on the requirement. Significant gaps along the longitudinal axis of the UAV (front and back) were found that are not affected by the rotation of the two hemispherical shells and indicate a convenient position for manipulation and good access for the power cable. The weak structure of two hemispherical shells as a result of separating them is resolved by adding a tough but lightweight base to minimize deformation and adding trusses and a secondary bearing to minimize the deflection. The flight experiment verified the systems capability of entering a complex space and then performing manipulations, which is vital for a real-world mission such as exploration in disaster sites.

Moreover, a combined implementation of UAV with two passive rotating spherical shells and the hammer test which creates a new specific system for physical interaction in the complex environment was presented. The idea emerged from the problems of the initial work of hammer test using the UAV. The utilization of protective shell and passive rotation so it can be used in a complex environment and the application of horizontal actuator to provide good hammering action was implemented. A general concept of hammering system was proposed and showed the complete system design. The horizontal actuator was used to help in bringing the hammering device to the wall and keeping an appropriate hammering posture while the UAV is in a stable attitude. The idea of hammer guide was also introduced to have effective striking of the hammer. Ball rollers were also added to aid the movement of the hammering device throughout the surface of a wall. The components of horizontal actuator were properly selected to come up with enough thrusting force. Also, the position of the horizontal actuator was checked using flow simulation so that its airflow cannot interfere the airflow of the UAV. The conducted flight experiment confirmed that the UAV with two passive rotating spherical shells is appropriate for physical interaction. The experiment also verified the performance of the proposed hammer test system. It showed that by implementing a horizontal actuator and hammer guide can result in an appropriate hammering posture and action.

Limitation of the Study

The study of UAV with two passive rotating hemispherical shells introduced in this paper is not yet adequate to conclude a system can be used in the actual field. It requires

additional study especially verifying the systems flight stability. In Chapter 3.5, an actual manipulation through grabbing of an object was introduced. However, the effect of the shifting of the COG or load imbalances was considered negligible. The object used is considered as lightweight enough to be handled by the controller. A study to minimize or avoid a serious stability issue in a situation where the manipulation system or power cable guide which is directly connected to the UAV is subjected to disturbance is not included in this paper.

Moreover, the experiment of UAV with two passive rotating hemispherical shells attached with hammer test system is an initial step for a real mission. For the meantime, the experiment was conducted indoor. Also, the acquisition of sensor data and post-processing to determine the condition of the structure have not yet implemented. Likewise, no control strategy is implemented to deal with a severe disturbance caused by interaction with structure. Lastly, the conducted experiment is performed only by a single operator as an initial step to test the performance of the system.

Future Work

A further study on the stability of the UAV with the two passive rotating hemispherical shells is the primary interest in the future work. It is planned that a more intensive experiment will be conducted to test the stability of the system against the different type of disturbances and the attachment of manipulation system and mechanism for power tethering. An actual experiment in the infrastructure or disaster-stricken area like in the bridge is expected to be conducted to verify the capability of the proposed system further. Meanwhile, a further study on the proposed application: the hammer test using the UAV with the two passive rotating hemispherical shells to improve the system so it can be used in an actual mission.

Chapter 4

General Conclusions

This work has established two different type of UAV with spherical shell and gimbal mechanism that allows visual and physical exploration in a complex environment such as in infrastructure and disaster site. They are the UAV with a passive rotating spherical shell for visual exploration and the UAV with two passive rotating hemispherical shells for physical interaction. The main approach is to develop a UAV for visual exploration to be used for an actual mission in a complex environment is by optimization of three primary forces acting on the UAV: the thrust force, weight and external force. The existing system which is developed by former researcher [6] serve as the reference of the optimization technique as it already mentioned necessary parameters to allow a UAV with a passive rotating spherical shell to be used in a complex environment. Subsequently, the visual inspection of the bridge serves as the actual mission that verifies the effectiveness of the approach.

Meanwhile, the primary approach to develop a novel UAV for physical interaction in a complex environment is by separating the spherical shell into two hemispherical shells to provide a gap for physical interaction. The good part about the new system is that the essential components of the earlier system such as the spherical shell and the gimbal system were retained to ensure protection against any obstacle and for better stability of the UAV. The hammer test using the UAV with two passive rotating hemispherical shells serve as the real application to demonstrate the capability of the new concept. Likewise, the hammer test using the UAV with two passive rotating hemispherical shells presented in this study is a novel approach that would allow the UAV to perform hammer test in a complex environment, particularly in infrastructure.

Through these approaches, the challenges in exploring the actual complex environment have been partially addressed. Firstly, the proposed approach on optimization of the UAV with a passive rotating spherical shell for visual exploration on a complex environment offers a robust solution that resulted in the success of the actual mission. With the proposed method, the problem of limited payload, limited flight time and unable to fly on a harsh wind condition have been addressed. The effectiveness of the proposed approach has

been validated through an actual mission in a complex environment, the visual inspection of the bridge. The robust design of UAV with a passive rotating spherical shell allows us to obtain necessary information in the bridge like the images on the various part of the bridge. Second, the proposed UAV with two passive rotating hemispherical shells offer a new solution to physical interaction in a complex environment. With the proposed method, it is possible for the UAV to install manipulation system while the spherical shell protects it and have a better stability with the aid of the gimbal. An initial experiment verified the capability of the new mechanism such as able to fly along the obstacle without significant disturbance and able to manipulate without disturbing the rotation of the two hemispherical shells.

4.1 Individual Contributions

4.1.1 Optimization of Existing UAV with a Passive Rotating Spherical Shell

The first contribution was the improvement on the performance of the existing UAV with a passive rotating spherical shell by maximizing the flight capability, minimizing the weight, and minimizing the drag force as presented in Chapter 2.5. The novel idea is primarily on the design of the spherical shell component and appropriate selection of spherical shell structure. The joint as the spherical shell component aimed to minimize the drag force by implementing aerodynamic shape while keeping the strength and weight. The shell structure was reselected which resulted in the decrease of the weight of the spherical shell. The motors and propellers of the UAV were reselected to achieve the maximum thrust, thus increasing the payload, without compromising the size of the spherical shell. In general, the flight capability, payload, and ability to fly in high wind improved well for the new system as compared to the old system. The improvement of the new system was verified on the mission requirements for visual inspection of the bridge.

4.1.2 Close Visual Bridge Inspection using the UAV with a Passive Rotating Spherical Shell

The second contribution was the actual mission in the bridge by close visual inspection using the improved UAV with a passive rotating spherical shell as presented in Chapter 2.6. Before the actual mission, the study of bridge condition and requirements was conducted. Through this study, the required diameter of the spherical shell was determined based on the structure of the bridges exist all over Japan. Likewise, the location of damage occur-

rence enabled the system to develop an appropriate visual system to capture all necessary images. In preparation for the actual mission in the bridge, a test experiment replicating the actual bridge conditions was conducted. The experiment enabled us to look beforehand on the actual situation such as the state when it hit with the structure in a different position and if the visual system can capture the image test material imitating tiny cracks placed in various angles. The two separate location with unique bridge structure of actual mission verified the performance of the system. Crossing over the narrow bridge braces, rolling on the floor slab, and moving while in contact with the uneven surface of girder were successfully performed. Various images were successfully obtained from the different part of the bridge such as in web-plate, tensile bolts, main and overhand floor slab, bridge shoes, and bridge corners. Aside from self-evaluation, a third party company expert on bridge management evaluated the performance of the system such as quality of acquired images, safety, flight stability, performance against the wind, and so on. The majority of the evaluation responses were positive. The evaluators agreed the system needs only a few improvements before its actual deployment.

4.1.3 UAV with Two Passive Rotating Hemispherical Shells for Physical Interaction on Complex Environment

The third contribution was the concept of UAV with two passive rotating hemispherical shells as presented in Chapter 3.5. The novel idea is primarily on the separation of the spherical shell into two hemispherical shells that allowed physical interaction while the UAV is protected by the spherical shell and retained two axes of gimbal unit for better stability. This concept solved the main flaw of the previous system concerning physical interaction which is unable to access the outside of the spherical shell freely. The study identified the critical gap unaffected by the rotation of the two hemispherical shells. The gap enabled the researcher to determine the physical interaction configuration which is a frontal-type. Although the separation of the spherical shell into two hemispherical shells resulted in issues such as deformation and deflection, those issues were addressed by thorough structural analysis and appropriate mechanical design such as the introduction of trusses to support the hemispherical shell. An experimental prototype was developed, and initial flight experiment was conducted to validate the capability of the new system such as flying over the obstacle and perform a simple manipulation task.

4.1.4 Hammering Test using the UAV with Two Passive Rotating Hemispherical Shells

The fourth contribution was the real application of UAV with two passive rotating hemispherical shells using hammer test as presented in Chapter 3.6. The UAV with two passive rotating hemispherical shells, hammering device, and other necessary sub-system made up the entire UAV system for non-destructive hammering test intended in infrastructure inspection. In this study, an efficient method of hammer test using a UAV was introduced. The combination of hammer guide and horizontal actuator assisted the hammering device to have an effective strike. An initial flight experiment was successfully conducted to test the performance of the hammering system attached in the UAV with two passive rotating hemispherical shells.

4.2 Conclusive Remarks on UAV for Visual Exploration of Infrastructure and Disaster Site

In this study, a UAV system that is suitable for visual exploration of a complex environment such as infrastructure and disaster site has been developed. This study presented the improvement of the UAV with a passive rotating spherical shell so it can be used in the actual mission. It implemented the three important approach for the improvement of the system that includes minimization of weight, minimization of drag force, and maximization of flight capability.

Minimization of weight was introduced to add more payload capacity so it can carry more loading especially for the visual system components such as the cameras and video transmitter. The minimization of system's weight was realized by reducing the weight of the spherical shell. The key idea was the reselection of the spherical shell structure. It was revealed that by selecting the 3V geodesic structure and transform it into fullerene structure by removing some of the connections symmetrically, the weight of spherical shell goes down significantly.

On the other hand, the minimization of drag force was also a novel approach that improves the performance of the system. The key idea was to apply the aerodynamic design of the component of spherical shell specifically on the joints. By the introduction of airfoil shape joints, the drag force reduced as compared to the old system's joint without aerodynamic consideration. Both the computational fluid dynamic (CFD) and wind tunnel verified the positive outcome of the reduction of drag force. CFD evaluation tool has also provided both visual and numerical result which strengthen the outcome. Meanwhile, the real air flow experiment in the prestigious aerospace center in Japan has

provided a more accurate result of the system when subjected to air drag.

Furthermore, the maximization of flight capability was introduced to increase the payload capacity and flight time of the system. The approach was realized by reselection of the UAV's primary components such as motor and propeller. During the reselection process, it was ensured that the weight and size of the spherical shell were not compromised. As an overall evaluation, the system has improved as reflected in the increase of the thrust-to-weight ratio of the system.

A real application of the UAV with a passive rotating spherical shell was implemented. A close visual bridge inspection was presented as the actual mission. The mission requirements set by the Next Generation Robot for Social Infrastructure or NGRSI was used as the reference for our purpose. The three primary objectives were to be able to access narrow part of the complex-structured bridge, to be able to inspect the critical part of the bridge, and acquire clear images. The new system has shown to be effective in accessing the narrow spaces of the bridge as revealed in the actual flight in various bridges. It was successful crossing the limited spacing of the braces under the bridge. Moreover, the installed visual system that provided a full overhead view has been so helpful in inspecting and acquiring images in critical parts of the bridge like the girder and floor slab. Through the test material, it was able to evaluate the system's ability to capture images. However, it is expected that a real damage might be harder to detect than a test material. It is therefore recommended to develop a camera that can capture high-speed motion, high resolution, lightweight and able to acquire image even of poor illumination. On the other hand, the new system was also compared to the old system to verify its improvement based on actual bridge inspection. Finally, the actual bridge experiment was also evaluated by the highway management professionals. They agreed that the system has several positive outcomes and only requires minor improvements.

As a final conclusion, the proposed system in this study has shown to be effective in the visual exploration of infrastructure and disaster site. This study partially addressed the challenges on the design of UAV system that can be well-suited on a real complex environment.

4.3 Conclusive Remarks on UAV for Physical Interaction of Infrastructure and Disaster Site

A UAV system that is suitable for physical of a complex environment has been introduced and developed. The study presented a new concept to allow physical interaction while taking advantage of the idea of passive rotating spherical shell mechanism. This study successfully introduced the concept of separating the spherical shell into two hemispherical

shells while providing a gap and retaining two axes of passive rotation. It is revealed that the gaps unaffected by the passive rotation of the two hemispherical shell are located on the front and back of the UAV. The location of the gap is the appropriate position for intended physical interaction application. The position of the unaffected gap suggested that the physical interaction that is possible is a frontal type interaction. It was also revealed that the possible movement of the manipulator passing through the unaffected gap is push and pull. Rotational motion of the manipulator was also possible.

An analysis of the reaction of the two passive rotating hemispherical shells against any disturbance has been studied. It was revealed that the two passive rotating hemispherical shells have a good reaction to the disturbance depending on the position except for one case where it cannot react. It was considered as the trade-off of having a gap for physical interaction. This case is a challenging problem to be solved by the future researcher of this study. Moreover, the cutting of the spherical shell resulted in a new problem which is the deflection. In this study, a solution was introduced by adding trusses as support to minimize deflection at the connection point of the main shaft and hemispherical shell. Based on the evaluation, it was successfully reduced the deflection more twice of the original value.

An experimental prototype was developed and then conducted a flight test. The first experiment involved flying over the obstacle. It showed that the system was able to react on the disturbance at various conditions. Another test was conducted by performing a simple manipulation task to demonstrate the capability of the new system regarding physical interaction. The capabilities of the new system were successfully verified. However, it requires an additional experiment, especially in the actual field.

A real application of the new concept was also implemented. The hammer test was used as the real application. The system presented the three major components: two passive rotating hemispherical shell mechanism, horizontal actuator, and hammering device. The two passive rotating hemispherical shell mechanism ensured the protection of the system against any disturbances. The horizontal actuator provided appropriate hammering posture to acquire good data during hammering action. The hammering device performed the hammering task by applying non-destructive impact force on the surface using solenoid.

The three main components were successfully integrated into the UAV. An experiment was conducted to verify the performance of the system with or without activating the horizontal actuator. The experiment was focused only on testing the horizontal actuator since the experiment flying over the obstacle has already been performed in previous part. The first test was conducted without activating the horizontal actuator. It showed that in the absence of the horizontal actuator, the UAV cannot stay close and longer on the wall. The primary reason is that while the hammer strikes the wall, there is a reaction force pushing the UAV away from the wall. If the UAV needs to move forward

to counter the reaction force, it needs to tilt. However, tilting near the structure has shown to be risky as the low pressure above near the structure will be sucked up the UAV. The second experiment was conducted by activating the horizontal actuator during the hammering task. It showed the UAV does not require to tilt when approaching the wall. The horizontal actuator will slowly push the UAV towards the wall. Furthermore, the reaction force of the hammering action was compensated by the constant push of the horizontal actuator. As a result, it was able to stay close and longer on the wall.

As a final conclusion, the new concept of passive rotating spherical shell mechanism has shown to be effective for physical interaction on a complex environment. This study partially solved the problem of physical interaction task that is useful for exploration of infrastructure and disaster site.

Bibliography

[1] M. of Land Infrastructure Transport and Tourism. (Accessed: May 2017) Sasago tunnel ceiling collapse on the chuo expressway (sequence of events and countermeasures). 1-2-1.pdf. [Online]. Available: https://www.mlit.go.jp/road/road_e/03key_challenges/

[2] T. R. C. of the Panel on Infrastructure Development. (2014) Recommendations for full-scale maintenance of aging roads. [Online]. Available: http://mlit.go.jp

[3] T. Oshio. (Accessed: May 2017) The declining birthrate in japan. economic-currents69.pdf. [Online]. Available: https://www.kkc.or.jp/english/activities/publications/

[4] K. Nagatani, S. Kiribayashi, Y. Okada, K. Otake, K. Yoshida, S. Tadokoro, T. Nishimura, T. Yoshida, E. Koyanagi, M. Fukushima, and S. Kawatsuma, "Emergency response to the nuclear accident at the fukushima daiichi nuclear power plants using mobile rescue robots," *Journal of Field Robotics*, 2013.

[5] A. Briod, P. Kornatowski, J.-C. Zufferey, and D. Floreano, "A collision resilient flying robot," *Journal of Field Robotics*, 2014.

[6] S. Mizutani, K. Ohno, K. Yanagimura, Y. Okada, E. Takeuchi, K. Ohno, and S. Tadokoro, "Quadrotor with a rotating spherical shell which can fly in the complex structure," in *Robotics and Mechatronics Conference 2014*, ser. ROBOMECH2014, 2014.

[7] "Unmanned aerial vehicle," wikipedia.org/wiki/, accessed: April 2017.

[8] K. Dalamagkidis, *Aviation History and Unmanned Flight*. Springer, 2015.

[9] J. Keane and S. Carr, "A brief history of early unmanned aircraft," APL TECHNICAL DIGEST, 2013.

[10] R. Barnhart, S. Hottman, D. Marshall, and E. Shappee, *Introduction to Unmanned Aircraft Systems*. CRC Press, 2012.

[11] K. Dalamagkidis, *Classification of UAVs.* Springer, 2015.

[12] K. Dalamagkidis, K. Valavanis, and L. Piegl, *On Integrating Unmanned Aircraft Systems into the National Airspace System: Issues, Challenges, Operational Restrictions, Certification, and Recommendations, Intelligent Systems, Control and Automation: Science and Engineering.* Springer, 2012.

[13] J. J. I. on UAVs, "A concept of european regulations for civil unmanned aerial vehicles," Final Report, 2004.

[14] R. Weibel and R. Hansman, "Safety considerations for operation of different classes of uavs in the nas," in *4th Aviation Technology, Integration and Operations Forum*, ser. AIAA, 2004.

[15] R. Austin, *Unmmaned Aircraft Systems: UAV Design, Development and Deployment.* Wiley, 2010.

[16] S. Ghazbi, Y. Aghli, M. Alimohammadi, and A. A. and, "Quadrotors unmanned aerial vehicles: A review," *Internal Journal on Smart Sensing and Intelligent Systems*, vol. 9, March 2016.

[17] J. Magalasang, *Biomimetic Unmanned Aerial System.* Lambert Academic Publishing, 2016.

[18] S. Construction. (2017) Bracing systems. [Online]. Available: http://www.steelconstruction.info/

[19] S. Griffiths, J. Saunders, A. Curtis, T. McLain, and R. Beard, *Advances in Unmanned Aerial Vehicles: State of the Art and the Road to Autonomy.* Springer, 2007.

[20] A. Beyeler, J. Zufferey, and D. Floreano, "Vision-based control of near-obstacle flight," *Journal of Autonomous Robots*, 2009.

[21] S. Ross, N. Melik-Barkhudarov, A. Wendel, D. Dey, A. Bagnell, and M. Hebert, "Learning monocular reactive uav control in cluttered natural environments," in *International Conference on Robotics and Automation*, ser. ICRA, 2013.

[22] J. Israelsen, M. Beall, D. Bareiss, D. Stuart, E. Keeney, and J. Van den berg, "Automatic collision avoidance for manually tele-operated unmanned aerial vehicles," in *International Conference on Robotics and Automation*, ser. ICRA, 2014.

[23] A. Akhtar, S. Waslander, and C. Nielsen, "Fault tolerant path following for a quadrotor," in *EEE Conference on Decision and Control*, 2013.

[24] M. Mueller and R. D'Andrea, "Stability and control of a quadrocopter despite the complete loss of one, two, or three propellers," in *International Conference on Robotics and Automation*, 2014.

[25] ImpactLab. (2011, August) Japanese inventor develops world?s first flying sphere drone. [Online]. Available: http://www.impactlab.net/

[26] S. Hong, J. Shin, S. Ji, K. Baik, and S. Park, "Design, modeling and hovering control of a spherical mav using a non-linear controller based on nested saturations," in *International Conference on Ubiquitous Robots and Ambient Intelligence*, ser. URAI, 2012.

[27] B. Loh and J. Jacob, "Modeling and attitude control analysis of a spherical vtol aerial vehicle," in *AIAA Aerospace Sciences Meeting including the New Horizons Forum and Aerospace Exposition*, 2013.

[28] S. Bose, R. Verma, K. Garuda, A. Tripathi, and S. Clement, "Modeling, analysis and fabrication of a thrust vectoring spherical vtol aerial vehicle," in *IEEE Aerospace Conference*, 2014.

[29] R. Fuller. U.s. patent 2682235. [Online]. Available: http://www.uspto.gov/

[30] R. Krebs and C. Krebs, *Groundbreaking Scientific Experiments, Inventions, and Discoveries of the Ancient World.* Greenwood Press, 2003.

[31] G. Sarton, *A History of Science: Hellenistic Science and Culture in the Last Three Centuries B.C.* Cambridge: Harvard University Press, 1959.

[32] S. Mizuntani, Y. Okada, C. J. Salaan, T. Ishii, K. Ohno, and S. Tadokoro, "Proposal and experimental validation of a design strategy for a uav with a passive rotating spherical shell," in *International Conference on Intelligent Robots and Systems IROS*, 2015, pp. 1271 – 1278.

[33] S. Omari, P. Gohl, M. Burri, M. Achtelik, and R. Siegwart, "Visual industrial inspection using aerial robots," in *3rd International Conference on Applied Robotics for the Power Industry*, 2014.

[34] R. Murphy, *Disaster Robotics.* The MIT Press, 2014.

[35] J. Adams, C. Humphrey, M. Goodrich, J. Cooper, B. Morse, C. Engh, and N. Rasmussen, "Unmanned aerial vehicle wilderness search support," *Journal of Cognitive Engineering and Decision Making*, vol. 3, no. 1, 2009.

[36] M. Goodrich, J. Cooper, J. Adams, C. Humphrey, R. Zeeman, and B. Buss, "Using a mini-uav to support wilderness search and rescue: Practices for human-robot teaming," in *IEEE International Workshop on Safety, Security and Rescue Robotics*, ser. SSRR2007, 2007.

[37] J. Nikolic, M. Burri, J. Rehder, S. Leutenegger, C. Hurzeler, and R. Siegwart, "A uav system for inspection of industrial facilities," in *IEEE Aerospace Conference*, 2013.

[38] O. Menendez, M. Perez, and F. Auat Cheein, "Vision based inspection of transmission lines using unmanned aerial vehicles," in *International Conference on Multisensor Fusion and Integration for Intelligent Systems*, ser. MFI, 2016.

[39] P. Gohl, M. Burri, S. Omari, J. Rehder, J. Nikolic, M. Achtelik, and R. Siegwart, "Towards autonomous mine inspection," in *International Conference on Applied Robotics for the Power Industry*, ser. CARPI, 2014.

[40] M. Burri, J. Nikolic, C. Hurzeler, G. Caprari, and R. Siegwart, "Aerial service robots for visual inspection of thermal power plant boiler systems," in *International Conference on Applied Robotics for the Power Industry*, ser. CARPI, 2012.

[41] D. Meyer, M. Hess, E. Lo, C. Wittich, T. Hutchinson, and F. Kuester, "Uav-based post disaster assessment of cultural heritage sites following the 2014 south napa earthquake," in *Conference on Digital Heritage*, 2015.

[42] J. Henrickson, C. Rogers, H.-H. Lu, J. Valasek, and Y. Shi, "Infrastructure assessment with small unmanned aircraft systems," in *International Conference on Unmanned Aircraft Systems*, ser. ICUAS, 2016.

[43] S. Gruber, H. Kwon, C. Hager, R. Sharma, J. Yoder, and D. Pack, *UAV Handbook: Payload Design of Small UAVs.* Springer, 2015.

[44] S. Brandt, *UAV Handbook: Small UAV Design Development and Sizing.* Springer, 2015.

[45] D. Raymer, *Aircraft Design: A Conceptual Approach.* AIAA, Inc, 1992.

[46] Nasa. (2017) Thrust to weight ratio. [Online]. Available: https://www.grc.nasa.gov/www/k-12/airplane/

[47] M. Sadraey, *Aircraft Performance Analysis.* VDM Verlag Dr. Muller, 2009.

[48] A. K. Kundu, *Aircraft Design.* Cambridge University Press, 2010.

[49] D. Bridges. (2000, dec.) Introduction to computational fluid dynamics with rotorcraft applications. rotorcfd.pdf. [Online]. Available: www.personal.psu.edu/dob104/papers/

[50] A. Sayma, *Computational Fluid Dynamics*. Ventus Publshing ApS, 2009.

[51] D. Kuzmin. Introduction to computational fluid dynamics. lecture1.pdf. [Online]. Available: http://www.mathematik.uni-dortmund.de/~kuzmin/cfdintro/

[52] J. McAlpine. (2004) Computational fluid dynamics or wind tunnel modeling? CFDvsWT.pdf. [Online]. Available: http://www.envirometrics.com/abstracts/

[53] "Wind tunnel," wikipedia.org/wiki/, accessed: March 2017.

[54] K. Valavanis and G. Vachtsevanos, *Handbook of Unmanned Aerial Vehicles*. Springer, 2015.

[55] E. Pastor, J. Lopez, and P. Royo, "Uav payload and mission control hardware/software architecture," in *IEEE Aerospace and Electronic Systems Magazine*, 2007.

[56] W. Semke, R. Shultz, and D. Dvorak, "Utilizing uav payload design by undergraduate researchers for educational and research development," in *International Mechanical Engineering Congress and Exposition*, 2007.

[57] J. Everaerts, N. Lewyckyj, and D. Fransaer, "Pegasus: design of a stratospheric long endurance uav system for remote sensing," in *The International Archives of the Photogrammetry, Remote Sensing and Spatial Information Sciences*, 2004.

[58] K. Stuckel, W. Semke, N. Baer, and R. Shultz, "A high frequency stabilization system for uas imaging payloads," in *Struc. Dyn. 3*, 2004.

[59] J. Benito, G. de Rivera G., J. Garrido, and R. Ponticelli, "Design considerations of a small uav platform carrying medium payloads," in *Conference on Design of Circuits and Integrated Circuits*, ser. DCIS, 2014.

[60] A. Mattar, C. Vaidya, and A. Saraf, "Airfoil selection, optimization and analysis for a solar-powered unmanned aerial vehicles," in *IEEE Aerospace Conference*, 2016.

[61] S. Abdullah, A. Abdullah, M. Shehzad, and M. Khalid, "Aerodynamics of a flying wing uav with backward facing stepped wing profile," in *International Bhurban Conference on Applied Sciences and Technology*, ser. IBCAST, 2017.

[62] L. Velazquez and J. Nozicka, "Low-speed wind tunnel testing for an unmanned aerial vehicle airfoil," in *Colloquium Fluid Dynamics*, 2009.

[63] R. Lim, H. La, Z. Shan, and W. Sheng, "Developing a crack inspection robot for bridge maintenance," in *International Conference on Robotics and Automation ICRA*, 2011.

[64] Q. Liu and Y. Liu, "An approach for auto bridge inspection based on climbing robot," in *International Conference on Robotics and Biomimetics ROBIO*, 2013.

[65] R. Wang and Y. Kawamura, "A magnetic climbing robot for steel bridge inspection," in *Proceedings of the 11th World Congress on Intelligent Control and Automation*, 2014.

[66] T. Ministry of Land, Infrastructure and Tourism. (2014) Next generation social infrastructure robot. [Online]. Available: http://www.mlit.go.jp/

[67] J. Kim, S. Kim, J. Park, and J. Nam, "Development of crack detection system with unmanned aerial vehicles and digital image processing," in *World Congress on Advances in Structural Engineering and Mechanics ASEM*, 2015.

[68] J. Verbeke, D. Hulens, H. Ramon, T. Goedem, and J. De Schutter, "The design and construction of a high endurance hexacopter suited for narrow corridors." in *International Conference on Unmanned Aircraft Systems ICUAS*, 2014.

[69] Y. Cengel and J. Cimbala, *Fluid Mechanics: Fundamentals and Applications*. McGraw-Hill, 2010.

[70] A. Briod and P. Kornatowski. (2013) Gimball: A crash-happy flying robot. [Online]. Available: http://phys.org

[71] Quanser, "Qball-x4 user manual." Quanser Inc, Technical Report 829, 2010.

[72] J. Duell, *Impact Testing of Advanced Composites*. Trafford Publishing, 2004.

[73] B. Wainfan, *Airfoil Selection: Understanding and Choosing Airfoils for Light Aircraft*. Publisher, 2005.

[74] Jaxa. (2013) Wind tunnel facilities. windtunnel.pdf. [Online]. Available: www.aero.jaxa.jp/publication/pamphlets/pdf/

[75] S. Mizutani, "Study on flying robot with passive rotating spherical shell," Master's thesis, Human-Informatics Laboratory, Tohoku University, 2014.

[76] T. Tamakoshi. (2007) Study on the basic survey of highway bridge conditions. [Online]. Available: http://mlit.go.jp

[77] G. Rui and A. Rui, "Civil engineering structures standard design i," Ministry of Land, Infrastructure, Transport and Tourism, Tech. Rep., 2000.

[78] Y. Rui, "Civil engineering structures standard design ii," Ministry of Land, Infrastructure, Transport and Tourism, Tech. Rep., 2000.

[79] Quanser, "Hero 4 black user manual," GOPRO, Tech. Rep., 2015.

[80] J. Peschel, "Towards physical object manipulation by small unmanned aerial systems," in *International Symposium on Safety, Security, and Rescue Robotics*, ser. SSRR, 2012.

[81] Q. Lindsey, D. Mellinger, and V. Kumar, *Construction of Cubic Structures with Quadrotor Teams.* MIT Press, 2012.

[82] P. Pounds, D. Bersak, and A. Dollar, "The yale aerial manipulator: Grasping in flight," in *International Conference on Robotics and Automation*, ser. ICRA, 2011.

[83] S. Shimara, R. Ladig, L. Suphachart, S. Hirai, and K. Shimonomura, "Aerial manipulation for the workspace above the airframe," in *International Conference on Intelligent Robots and Systems*, ser. IROS, 2015.

[84] D. Wuthier, D. Kominiak, C. Kanellakis, G. Andrikopoulos, M. Fumagalli, G. Schipper, and G. Nikolakopoulos, "On the design, modeling and control of a novel compact aerial manipulator," in *Mediterranean Conference on Control and Automation*, ser. MED, 2016.

[85] K. Yanagimura, K. Ohno, Y. Okada, E. Takeuchi, and S. Tadokoro, "Hovering of mav by using magnetic adhesion and winch mechanisms," in *International Conference on Robotics and Automation*, ser. ICRA, 2014.

[86] J. Scholten, M. Fumagalli, S. Stramigioli, and R. Carloni, "Interaction control of an uav endowed with a manipulator," in *International Conference on Robotics and Automation*, ser. ICRA, 2013.

[87] M. Fumagalli, R. Naldi, S. Macchelli, F. Forte, A. Keemink, S. Stramigioli, R. Carloni, and L. Marconi, "Developing an aerial manipulator prototype: Physical interaction with the environment," in *IEEE Robotics and Automation Magazine*, 2014.

[88] M. Fumagalli, S. Stramigioli, and R. Carloni, "Mechatronic design of a robotic manipulator for unmanned aerial vehicles," in *International Conference on Intelligent Robots and Systems*, ser. IROS, 2016.

[89] Y. Okada, T. Ishii, K. Ohno, and S. Tadokoro, "Real-time restoration of aerial inspection images by recognizing and removing passive rotating shell of a uav," in *International Conference on Intelligent Robots and Systems*, ser. IROS, 2016.

[90] K. Tadakuma and R. Tadakuma, "Mechanical design of omni-ball: Spherical wheel for holonomic omnidirectional motion," in *International Conference on Automation Science and Engineering*, 2007.

[91] A. Albers, S. Trautmann, T. Howard, T. Nguyen, M. Frietsch, and C. Sauter, "Semi-autonomous flying robot for physical interaction with environment," in *International Conference on Robotics Automation and Mechatronics*, 2010.

[92] K. Tadakuma, R. Tadakuma, and J. Berengeres, "Development of holonomic omni-directional vehicle with omni-ball: Spherical wheels," in *International Conference on Intelligent Robots and Systems*, ser. IROS, 2007.

[93] P. Pounds, D. Bersak, and A. Dollar, "Stability of small-scale uav helicopters and quadrotors with added payload mass under pid control," *Autonomous Robots*, 2012.

[94] M. Kunishima and Y. Ishihara. (Accessed: April 2017) Concrete flaking in a shinkansen tunnel of west japan co. [Online]. Available: http://www.sozogaku.com/fkd/en

[95] H. Yano, E. Takeuchi, K. Ohno, and S. Tadokoro, "Attempt of hammering test using multicopter," in *The Robotics and Mechatronics Conference*, ser. ROBOMECH, 2014.

[96] H. Yano, "Study on hammering test of structure using multicopter," Master's thesis, Human-Informatics Laboratory, Tohoku University, 2014.

[97] Hacker. (2017) A10-12s brushless motor. [Online]. Available: https://hackermotorusa.com/

[98] APC. (2017) 5 x 5e propeller. [Online]. Available: https://www.apcprop.com/

[99] A. Prop. (Accessed: May 2017) Performance data. PER3 5x5E.dat. [Online]. Available: https://www.apcprop.com/

Acknowledgements

The author wishes to acknowledge the Japan International Cooperation Agency (JICA) through ASEAN University Network/Southeast Asia Engineering Education Development Network (AUN/SEED-Net). The grant has provided the author a major support for the entire duration of the study. The author wishes to acknowledge all the coordinators of AUN/SEED-Net program and JICA, especially to Ms. Eriko Mori.

The author also acknowledges Prof. Satoshi TADOKORO for his acceptance in the TADOLab. The author indeed thank him for his unwavering support in acquiring the scholarship. I express my very great appreciation to my supervisor Asst. Prof. Yoshito OKADA. He is a great and brilliant mentor for this research and has contributed substantial ideas. I thank him for his support and understanding on my situation both student and personal life. I would also like to thank Assoc. Prof. Kenjiro TADAKUMA for his many great ideas. He provided several pieces of advice, especially on mechanical design. Likewise, I would like to thank Assoc. Prof. Kazunori OHNO for his valuable suggestions and recommendations.

I would also like to thank the valuable feedback provided by the committee members from the other laboratories: Assoc. Prof. Keiji NAGATANI, Prof. Takayuki OKATANI, and Prof. Koichi HASHIMOTO had greatly improved the material in this research. I wish to thank them for examining this work.

I thank the past and current member of TADOKORO laboratory who has been good companions since I entered the laboratory in 2014 especially to Fukuda, Yano, Komori, Koura, Kojima, and Abu.

Thank also for the support of the laboratory secretaries Ms. Yuki Saijo, Ms. Mitsuru Takahashi, Ms. Chiaki Ono, and Ms. Azuma Keiko as well as Ms. Takako Kase of the GSIS office for processing all necessary documents.

I would like to thank the past and present members of Heli team and to the rest of the students in Tadokoro laboratory.

I would like to acknowledge the never-ending love and support of my loving wife Vanessa, daughter Caile, and baby Monchou and their prayers.

Special thanks to my parents and siblings.

I would like to thank Kapatiran family especially ate Charity Sato for their friendship while staying here in Japan.

And most of all, great thanks to our God through Jesus Christ.

This work is dedicated to my miracle child Monchou.